DWR-1461

PNE-522
FINAL REPORT

MASTER

Plowshare civil, industrial and scientific uses for nuclear explosives

PROJECT SCHOONER

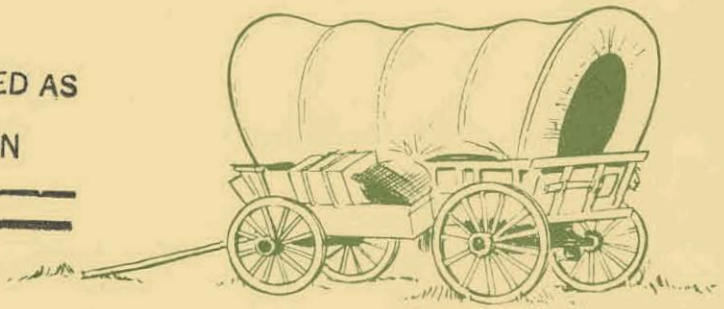

A Contribution to the Analysis of Seismic Data from Cratering and Contained Events

P5881

Environmental Research Corporation
Alexandria, Virginia

ISSUED: JUNE 30, 1970

DISCLAIMER

LEGAL NOTICE

Printed in USA. Price $3.00. Available from the Clearinghouse for Federal Scientific and Technical Information, National Bureau of Standards, U. S. Department of Commerce, Springfield, Virginia 22151.

USAEC Division of Technical Information Extension, Oak Ridge, Tennessee

PNE-522
NUCLEAR EXPLOSIONS — PEACEFUL APPLICATIONS (TID-4500)

SCHOONER EVENT

A CONTRIBUTION TO THE ANALYSIS OF SEISMIC DATA FROM CRATERING AND CONTAINED EVENTS

July 18, 1969

W.W. Hays, R.A. Mueller, C.T. Spiker, Jr.

Environmental Research Corporation
813 N. Royal Street
Alexandria, Virginia

Prepared under
Contract AT(29-2)-1163
for the
Nevada Operations Office
U. S. Atomic Energy Commission

TABLE OF CONTENTS

LIST OF ILLUSTRATIONS

LIST OF ILLUSTRATIONS
(Continued)

LIST OF ILLUSTRATIONS
(Continued)

LIST OF ILLUSTRATIONS
(Continued)

LIST OF TABLES

LIST OF TABLES
(Continued)

ABSTRACT

Schooner, a nuclear cratering detonation, provides experimental verification of scaling theory which shows that so far as generation of seismic motions is concerned, a cratering detonation can be considered as a contained detonation buried at a relatively shallow depth.

Comparison of the seismic data observed from Schooner and other cratering and contained detonations at Nevada Test Site shows several basic differences in the characteristics of the ground motion. The shallow depth of burial of the cratering detonation causes the seismic energy efficiency to be significantly diminished relative to that of an equivalent yield contained detonation. The spectral composition of the ground motion generated by a cratering detonation is characterized by a lower amplitude level and a shift to the low frequency end of the spectrum. The general deficiency of high frequencies causes the peak vector particle velocities and accelerations to be lower than mean values predicted on the basis of experience with equivalent yield contained detonations. The peak vector particle velocity correlates almost exclusively with the surface wave mode time window for cratering detonations. The level of peak vector particle acceleration and velocity recorded from a cratering detonation at instrument

sites located on alluvium is significantly reduced, relative to that of equivalent yield contained detonations, as a consequence of the lower seismic energy efficiency and the reduced high frequency spectral composition.

The Schooner detonation provides data which will be useful in the prediction and analysis of future nuclear cratering detonations.

CHAPTER 1

INTRODUCTION

1.1 GENERAL BACKGROUND

As part of the continuing Plowshare Program, Project Schooner was a nuclear cratering experiment conducted by the Atomic Energy Commission to develop excavation technology through peaceful uses of nuclear explosives. Extension of this technology is essential to the planning of such proposed nuclear excavation as a sea level canal across the American Isthmus. Five previous cratering events at the Nevada Test Site (see Figure 1-1) are listed in chronological order below, along with a brief description of their respective environments.

- Danny Boy took place in the basalt caprock forming Buckboard Mesa, Area 18, NTS
- Sedan was a relatively large-yield event in the thick alluvium of Yucca Flat, Area 10, NTS
- Palanquin was detonated in a rhyolitic flow on Pahute Mesa, Area 20, NTS
- Cabriolet was about 3,000 feet from Palanquin and shared the same environment
- Buggy I was a row-charge event featuring 5 simultaneous and equally spaced detonations in the basalt caprock of Chukar Mesa, Area 30, NTS

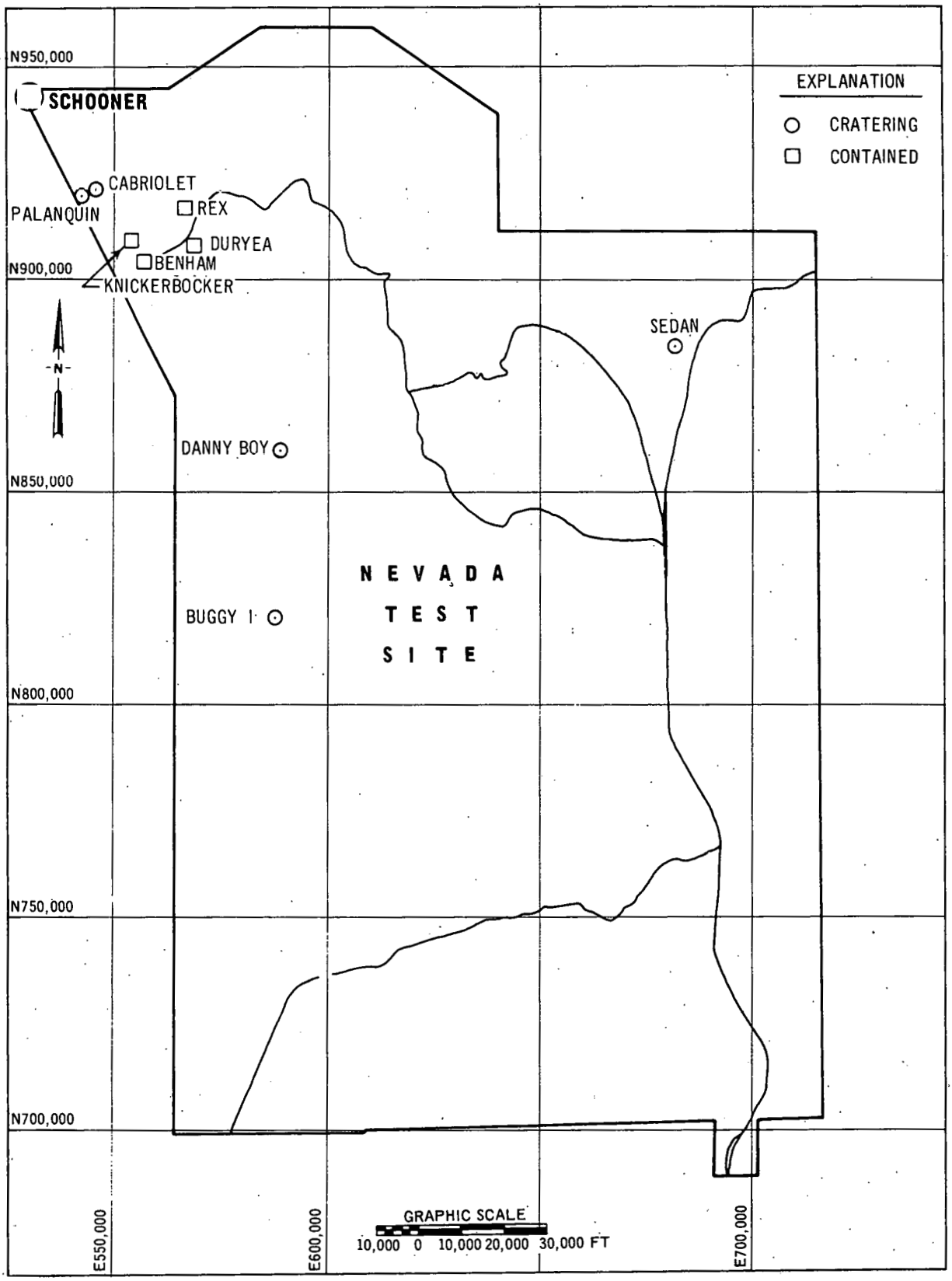

Figure 1-1. Area Map of Nevada Test Site Showing the Location of Schooner Relative to Five Other Nuclear Cratering Detonations and Four Nuclear Contained Detonations

Other nuclear and high explosive cratering experiments have been conducted, but because of their specialized nature, they are not incorporated in this study.

1.2 SCHOONER EVENT-ENVIRONMENT AND TECHNICAL DATA

The Schooner experiment consisted of the detonation of a minimum-fission nuclear device with a yield of 31±4 kilotons. The explosion took place at a depth of 355 feet in a layered tuffaceous medium of Area 20, Nevada Test Site, on December 8, 1968, at 0800:00.149.6 (PST), 1600:00.149.6 (GMT). The emplacement hole was U20u at geodetic coordinates:

Longitude W 116°33' 57.1419"
Latitude N 37°20' 36.3187"

and Nevada State Coordinates (Central Zone):

N 944,010.09
E 529,300.50

In this area of Pahute Mesa, relatively flat-lying ash-flow tuffs of Tertiary age crop out at the surface and display a thickness greater than 450 feet at the Schooner site. The surface topography is relatively flat with surface ground zero at an elevation of 5562.4 feet MSL. The nearest fault occurs about 2,000 feet from the crater. The water table is at a depth of approximately 1,300 feet in Pahute Mesa drill hole No. 2 (Figure 1-2) which is located some 860 feet northwest of the Schooner site.

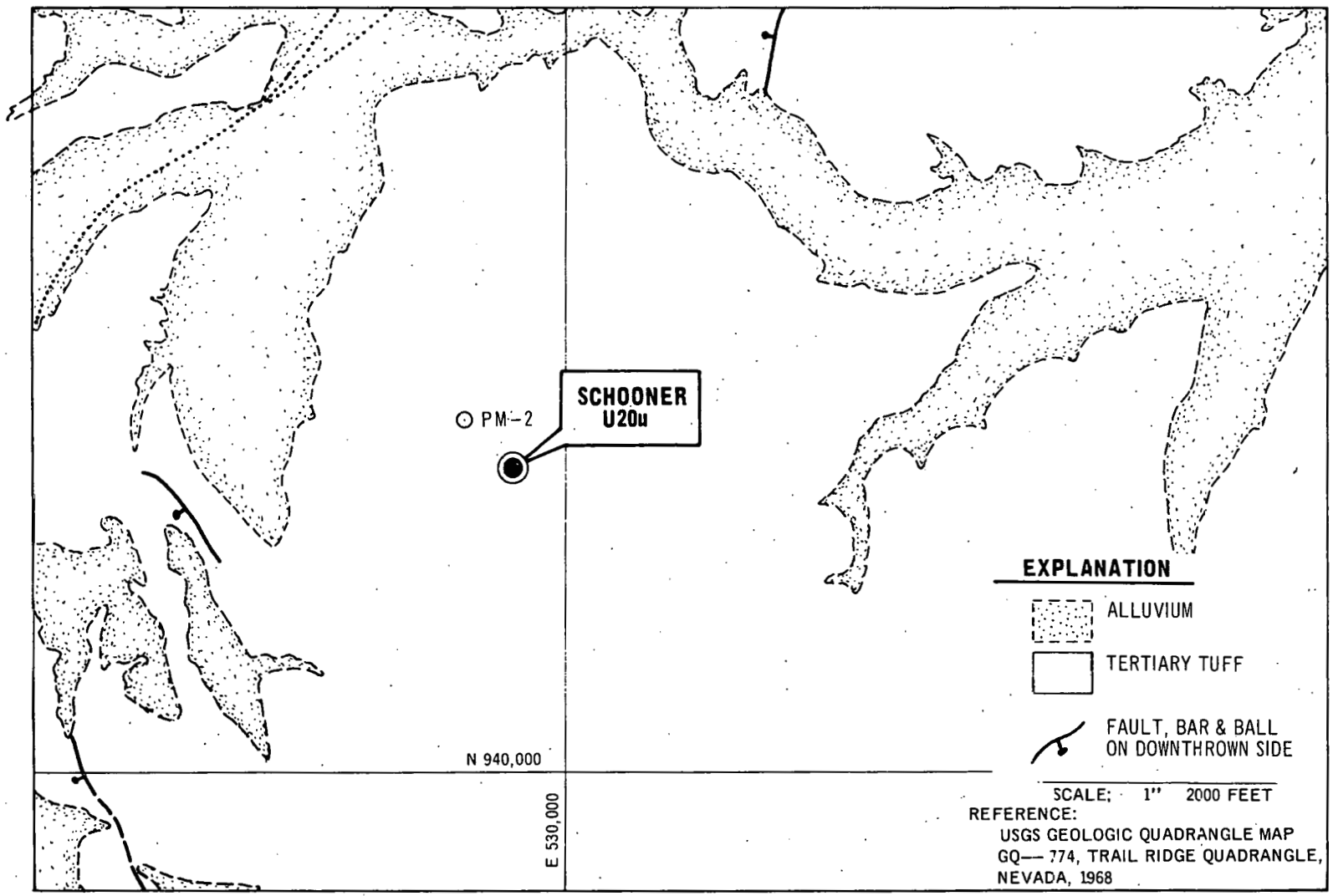

Figure 1-2. Generalized Geologic Map of the Schooner Crater Site, Pahute Mesa, Nevada

The crater resulting from the Schooner experiment was characterized by the following dimensions and volumes (Tewes, 1969):

1) Radius of apparent crater (R_a)... 129.8 meters 426 ft.

2) Maximum depth of apparent crater (D_a)..... 63.4 meters 208 ft.

3) Average apparent crater lip crest height (H_{al})..... 13.4 meters 44 ft.

4) Radius of apparent lip crest (R_{al})..... 147.2 meters 483 ft.

5) Radius of outer boundary of continuous ejecta (R_{eb})..... 539 meters 1768 ft.

6) Lip volume, apparent (V_{al})..... 2,099,000 cubic meters

..... 2,745,330 cubic yards

7) Crater volume, apparent (V_a)..... 1,745,000 cubic meters

..... 2,282,870 cubic yards

1.3 RESPONSIBILITY OF ERC IN PROJECT SCHOONER

Environmental Research Corporation, under contract to the Nevada Operations Office of the U. S. Atomic Energy Commission, is responsible to the Office of Effects Evaluation for providing ground motion evaluations of selected nuclear events. Our responsibility in Project Schooner was to provide the Office of Effects Evaluation with the following:

1. An instrumentation plan designed to document ground motions, utilizing available instruments.

2. Predictions of ground motion at each proposed instrument station for instrument calibration.

3. Processed seismic data (corrected seismograms, Band-Pass Filter (BPF) spectra, etc.).

4. Post-shot analysis of Schooner seismic data to determine relationship to predictions and data from other cratering experiments.

1.4 OBJECTIVES OF THIS REPORT

The objectives of this report are summarized as follows:

- To determine the amplitude and frequency characteristics of ground motion from the cratering event Schooner.
- To relate these results to the development of reliable techniques for predicting the ground motions from cratering events, utilizing theoretical and empirical scaling concepts.

Analyses related to these objectives are presented in detail in the chapters which follow. Chapter 2 contains descriptions of the instrumentation employed for the Schooner experiment and a discussion of the processed data utilized in the analysis. Peak ground motions are discussed in Chapter 3, and are compared with predicted values and data from past cratering events. The frequency content of seismic waves from Schooner is investigated and compared with seismic data from the Cabriolet cratering event at common stations. Theoretical scaling of amplitude spectra to simulate the effect of depth of burial for cratering and contained nuclear detonations is applied and analyzed.

In Chapter 4 the amplitude and frequency characteristics of elastic wave types generated by Schooner are determined and compared with similar data from other events.

Reasonable estimates of the radiated seismic energies from cratering and contained events are determined by procedures set forth in Chapter 5. Also the seismic efficiency of the Schooner event is analyzed and compared with the efficiency determined from contained events.

The basic conclusions of the various analyses are summarized in Chapter 6.

CHAPTER 2

DATA ACQUISITION AND PROCESSING

2.1 INSTRUMENTATION

The instrumentation plan for Schooner was designed with the following objectives in mind:

1. To obtain seismic data at points of interest to document the ground motion characteristics of Schooner.

2. To provide data for direct comparison of Schooner ground motions with ground motions from other cratering and contained events.

3. To generate a representative seismic data sample to use for predicting the ground motion characteristics of future cratering events.

The U.S. Coast and Geodetic Special Projects Party (USC&GS) deployed the 17 velocity instruments which recorded the Schooner event (see Figure 2-1). Of these 17 velocity meters, 14 were L-7's and 3 were NC-21's (King, 1969). These instruments recorded three orthogonal components of particle velocity on magnetic tape.

Seismic data recorded with the NC-21 velocity meters were processed and corrected for frequency response by ERC. Only the data recorded with the NC-21 velocity meters required a correction for frequency response (Table 2-1 shows the frequency range of

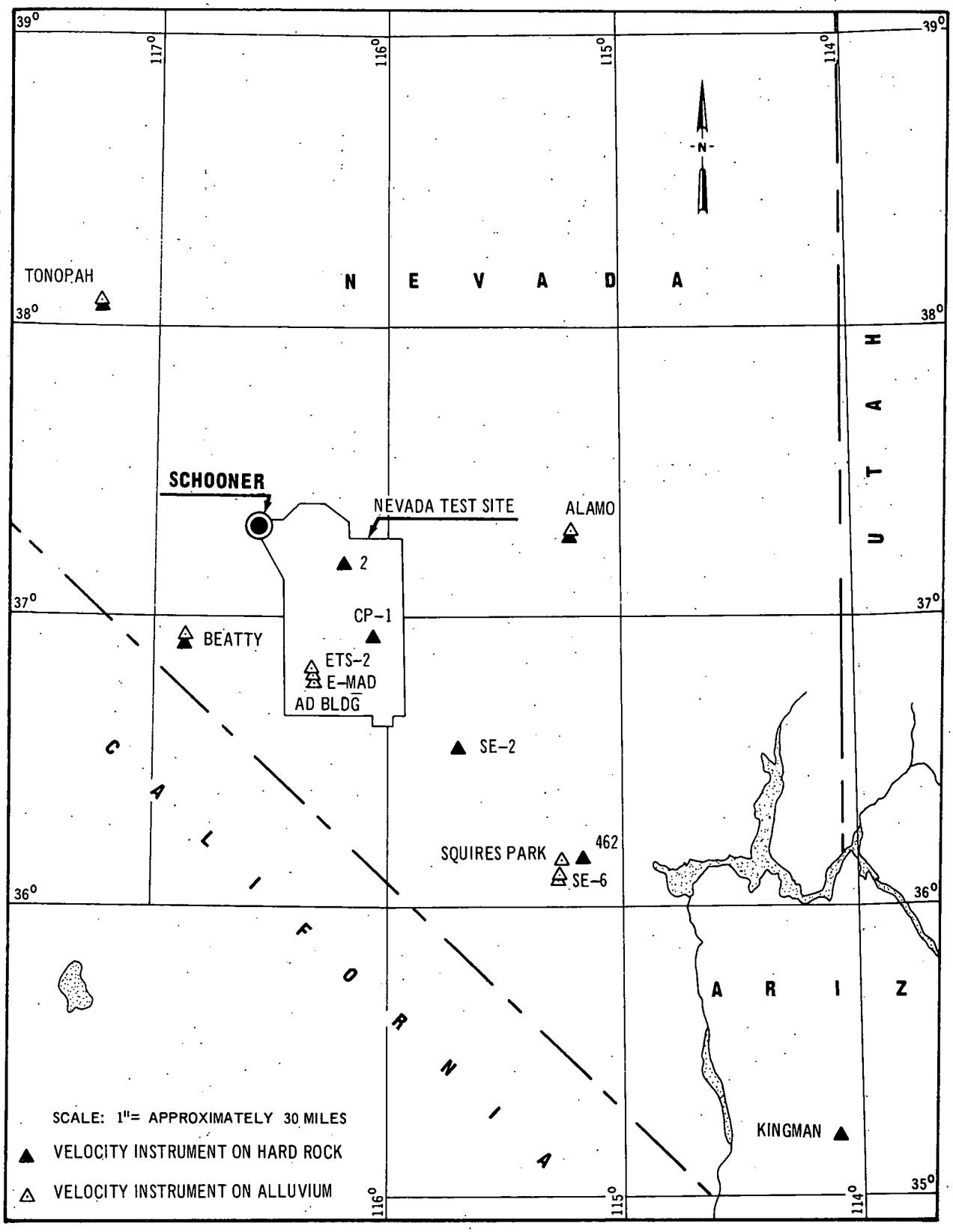

Figure 2-1. Map of Southeastern Nevada Showing Nevada Test Site and Schooner Instrument Stations

Table 2-1. FREQUENCY RANGE OF RECORDED GROUND MOTION DATA

Instrument Type	Frequency Range (Hz) of Instrument Response		Frequency Range (Hz) of Ground Motion after Instrument Correction	
	Low	High	Low	High
NC-21	1.0	45*	0.4	45*
L-7**	0.1	34***	0.1	34***

*Varies with filter setting

**No instrumentation correction applied; filtering applied to eliminate noise outside frequency range of interest

***Limited to 34 Hertz by tape speed

ground motion data recorded by each instrument). Also, particle acceleration and displacement seismograms were derived from the velocity data by differentiation and integration with respect to time.

Locations of the Schooner instrument stations are shown on Figure 2-1 and a summary of station environments, instrument type, and distances is listed in Table 2-2.

2.2 PEAK VECTOR GROUND MOTIONS

Peak values of particle acceleration, velocity and displacement were determined for each component. In addition, the peak value of the resultant vector was obtained to determine the absolute value of particle motion recorded at each station. The resultant vector magnitude is calculated by analyzing simultaneously the three components of motion as a function of time. The peak resultant vector is the largest instantaneous value of the square root of the sum of the squares of the amplitudes of the three components.

$$PM(t) = \sqrt{Z_p(t)^2 + R_p(t)^2 + T_p(t)^2}$$

where

PM = peak resultant vector

$Z_p(t)$ = value of vertical component

$R_p(t)$ = value of radial component

$T_p(t)$ = value of transverse component

TABLE 2-2. SUMMARY OF SCHOONER INSTRUMENT STATIONS YIELDING RECORDS PROCESSED BY ERC

Station	Station Abbreviation	Station Environment	Instrument Type	Slant Distance (km)
Area 12 Camp	2	Hard Rock	L-7	39.3
Beatty	BHR	Hard Rock	L-7	51.2
Beatty #2	BAL	Alluvium	L-7	51.7
ETS-2	ET2	Alluvium	L-7	61.1
E-MAD	E-MAD	Alluvium	L-7	63.9
CP-1	CP-1	Hard Rock	L-7	64.4
NRDS Admin. Bldg.	NRD	Alluvium	L-7	67.6
Tonopah Church	TCH	Hard Rock	NC-21	99.4
Tonopah Motel	TMT	Alluvium	NC-21	99.2
Indian Springs	SE-2	Thin Alluvium	L-7	119.3
Alamo	ALA	Alluvium	L-7	124.0
Alamo	AHR	Hard Rock	L-7	124.0
Squires Park	SQP	Alluvium	L-7	181.8
SE-6	SE-6	Alluvium	L-7, NC-21	187.3
Frenchman Mountain	462	Hard Rock	L-7	189.7
Kingman, Arizona	KAR	Hard Rock	L-7	340.0

The recorded peak values of each of the three components of velocity and the peak particle velocity vector are tabulated in Tables 2-3 and 2-4 for alluvium and hard rock stations respectively. Arrival times and the period of the peak particle velocity are also given in these tables. Values of the derived peak vector particle accelerations and displacements are given in Tables 2-5 and 2-6. The symbol notation used in the tables is as follows:

Instruments

L-7 = Mark Products Velocity Meter

NC-21 = National Geophysical Company Velocity Meter

Components

Z = vertical

R = radial

T = transverse

V = resultant vector

Peak Arrival Times

Arrival times are from shot time except when given in parentheses which indicates time after first motion.

TABLE 2-3. PEAK SURFACE VELOCITY RECORDED AT STATIONS ON ALLUVIUM

STATION/ INSTRUMENT	COMPONENT	DISTANCE (km)	FIRST ARRIVAL TIME (sec)	PEAK VELOCITY (cm/sec)	TIME OF PEAK (sec)	PERIOD (sec)
Beatty (L-7)	Z	51.7	9.95	4.06×10^{-2}	33.95	1.10
	R		9.95	6.03×10^{-2}	48.27	1.56
	T		9.95	3.58×10^{-2}	29.98	1.45
	V			6.84×10^{-2}	48.33	--
ETS-2 (L-7)	Z	61.1	11.55	4.96×10^{-2}	26.23	1.55
	R		11.55	5.32×10^{-2}	25.08	0.66
	T		11.55	7.61×10^{-2}	42.12	1.70
	V			8.14×10^{-2}	42.13	--
E-MAD (L-7)	Z	63.9	12.65	4.55×10^{-2}	49.48	1.45
	R		12.65	4.76×10^{-2}	29.20	1.28
	T		12.65	6.97×10^{-2}	50.17	1.92
	V			8.37×10^{-2}	45.35	--
NRDS Adm. Bldg. (L-7)	Z	67.5	13.35	5.88×10^{-2}	53.88	1.45
	R		13.35	1.01×10^{-1}	29.23	0.82
	T		13.35	6.85×10^{-2}	29.00	0.73
	V			1.05×10^{-1}	29.28	--
Tonopah Motel (NC-21)	Z	99.2	--	9.68×10^{-3}	(47.22)	1.77
	R		--	1.47×10^{-2}	(15.24)	0.53
	T		--	2.14×10^{-2}	(19.79)	0.53
	V			2.30×10^{-2}	(19.86)	--
Alamo (L-7)	Z	124.0	22.65	1.22×10^{-2}	23.85	0.70
	R		22.65	2.26×10^{-2}	58.13	0.82
	T		22.65	2.57×10^{-2}	43.43	0.65
	V			3.28×10^{-2}	41.20	--
Squires Park (L-7)	Z	181.8	33.05	1.64×10^{-2}	77.25	1.12
	R		33.05	3.00×10^{-2}	63.95	2.42
	T		33.05	4.32×10^{-2}	64.99	1.74
	V			4.34×10^{-2}	65.07	--
SE-6 (L-7)	Z	187.3	--	2.64×10^{-2}	(92.58)	1.42
	N/S		--	5.59×10^{-2}	(64.08)	2.15
	E/W		--	5.10×10^{-2}	(34.08)	1.15
	V			7.02×10^{-2}	(40.90)	--
SE-6 (NC-21)	Z	187.3	--	1.16×10^{-2}	(39.12)	1.73
	N/S		--	--	--	--
	E/W		--	2.05×10^{-2}	(33.90)	1.33
	V			2.16×10^{-2}	(33.95)	--

TABLE 2-4. PEAK SURFACE VELOCITY RECORDED AT STATIONS ON HARD ROCK

STATION/ INSTRUMENT	COMPONENT	DISTANCE (km)	FIRST ARRIVAL TIME (sec)	PEAK VELOCITY (cm/sec)	TIME OF PEAK (sec)	PERIOD (sec)
2 (L-7)	Z	39.3	10.35	3.33×10^{-2}	51.12	1.48
	R		10.35	4.54×10^{-2}	33.81	1.75
	T		10.35	3.80×10^{-2}	26.02	1.48
	V			5.06×10^{-2}	32.80	--
Beatty (L-7)	Z	51.2	--	3.19×10^{-2}	(38.02)	1.63
	R		--	4.30×10^{-2}	(37.48)	1.60
	T		--	2.95×10^{-2}	(34.57)	1.43
	V			4.72×10^{-2}	(37.47)	--
CP-1 (L-7)	Z	64.4	14.31	2.57×10^{-2}	36.94	1.30
	R		14.31	3.61×10^{-2}	43.96	1.53
	T		14.31	3.81×10^{-2}	46.05	2.47
	V			4.51×10^{-2}	46.06	--
Tonopah Church (NC-21)	Z	99.4	--	1.10×10^{-2}	(48.15)	2.15
	R		--	1.38×10^{-2}	(15.23)	0.75
	T		--	2.04×10^{-2}	(19.80)	0.58
	V			2.13×10^{-2}	(19.83)	--
SE-2 (L-7)	Z	119.3	20.75	8.17×10^{-3}	22.29	0.56
	R		20.75	1.07×10^{-2}	75.27	1.70
	T		20.75	9.03×10^{-3}	46.02	0.87
	V			1.14×10^{-2}	75.29	--
Alamo (L-7)	Z	124.0	22.95	1.50×10^{-2}	23.78	0.76
	R		22.95	2.03×10^{-2}	41.20	1.22
	T		22.95	2.35×10^{-2}	56.35	1.18
	V			2.49×10^{-2}	55.66	--
462 (L-7)	Z	189.7	31.85	5.25×10^{-3}	66.26	1.44
	R		31.85	3.50×10^{-3}	66.46	1.33
	T		31.85	6.00×10^{-3}	63.46	1.08
	V			6.88×10^{-3}	63.55	--
Kingman (Arizona) (L-7)	Z	340.0	57.65	1.93×10^{-3}	137.52	3.07
	R		57.65	1.39×10^{-3}	128.88	1.95
	T		57.65	1.26×10^{-3}	110.72	1.27
	V			2.02×10^{-3}	137.53	--

TABLE 2-5. DERIVED PEAK ACCELERATION AND DISPLACEMENT AT STATIONS ON HARD ROCK

STATION/ INSTRUMENT	COMPONENT	DISTANCE (km)	PEAK ACCELERATION (g)	PEAK DISPLACEMENT (cm)
2 (L-7)	Z	39.3	--	8.88×10^{-3}
	R		--	1.48×10^{-2}
	T		--	7.92×10^{-3}
	V			1.83×10^{-2}
Beatty (L-7)	Z	51.2	--	8.21×10^{-3}
	R		--	1.11×10^{-2}
	T		--	7.24×10^{-3}
	V		--	1.21×10^{-2}
CP-1 (L-7)	Z	64.4	1.05×10^{-4}	6.86×10^{-3}
	R		1.30×10^{-4}	9.62×10^{-3}
	T		1.27×10^{-4}	1.40×10^{-2}
	V		1.47×10^{-4}	1.56×10^{-2}
Tonopah Church (NC-21)	Z	99.4	9.69×10^{-5}	3.36×10^{-3}
	R		1.42×10^{-4}	2.85×10^{-3}
	T		1.78×10^{-4}	3.36×10^{-3}
	V		1.87×10^{-4}	4.14×10^{-3}
SE-2 (L-7)	Z	119.3	1.07×10^{-4}	2.15×10^{-3}
	R		1.10×10^{-4}	3.36×10^{-3}
	T		9.31×10^{-5}	3.06×10^{-3}
	V		1.19×10^{-4}	3.61×10^{-3}
Alamo (L-7)	Z	124.0	1.27×10^{-4}	2.20×10^{-3}
	R		1.56×10^{-4}	3.96×10^{-3}
	T		1.81×10^{-4}	5.00×10^{-3}
	V		2.19×10^{-4}	5.97×10^{-3}
462 (L-7)	Z	189.7	2.96×10^{-5}	1.44×10^{-3}
	R		2.56×10^{-5}	1.06×10^{-3}
	T		3.28×10^{-5}	1.50×10^{-3}
	V		3.92×10^{-5}	1.62×10^{-3}
Kingman, Arizona (L-7)	Z	340.0	1.24×10^{-5}	4.95×10^{-4}
	R		9.15×10^{-6}	4.20×10^{-4}
	T		9.42×10^{-6}	3.75×10^{-4}
	V		1.51×10^{-5}	7.80×10^{-4}

TABLE 2-6. DERIVED PEAK ACCELERATION AND DISPLACEMENT AT STATIONS ON ALLUVIUM

STATION/ INSTRUMENT	COMPONENT	DISTANCE (km)	PEAK ACCELERATION (g)	PEAK DISPLACEMENT (cm)
Beatty	Z	51.7	--	9.05×10^{-3}
(L-7)	R		--	1.56×10^{-2}
	T		--	8.52×10^{-3}
	V		--	1.72×10^{-2}
ETS-2	Z	61.1	5.30×10^{-4}	1.25×10^{-2}
(L-7)	R		6.91×10^{-4}	1.23×10^{-2}
	T		5.41×10^{-4}	1.93×10^{-2}
	V		7.61×10^{-4}	2.16×10^{-2}
E-MAD	Z	63.9	--	1.08×10^{-2}
(L-7)	R		--	1.13×10^{-2}
	T		--	1.93×10^{-2}
	V		--	2.18×10^{-2}
NRDS	Z	67.5	4.69×10^{-4}	1.47×10^{-2}
Adm. Bldg.	R		6.83×10^{-4}	2.02×10^{-2}
(L-7)	T		4.79×10^{-4}	1.33×10^{-2}
	V		7.21×10^{-4}	2.26×10^{-2}
Tonopah	Z	99.2	1.41×10^{-4}	3.55×10^{-3}
Motel	R		2.60×10^{-4}	2.66×10^{-3}
(NC-21)	T		2.69×10^{-4}	3.60×10^{-3}
	V		2.83×10^{-4}	4.22×10^{-3}
Alamo	Z	124.0	1.18×10^{-4}	2.40×10^{-3}
(L-7)	R		2.33×10^{-4}	5.16×10^{-3}
	T		3.20×10^{-4}	4.80×10^{-3}
	V		3.52×10^{-4}	5.64×10^{-3}
Squires	Z	181.8	1.04×10^{-4}	3.83×10^{-3}
Park	R		1.80×10^{-4}	9.34×10^{-3}
(L-7)	T		2.13×10^{-4}	1.18×10^{-2}
	V		2.20×10^{-4}	1.19×10^{-2}

(Continued on following page)

TABLE 2-6. DERIVED PEAK ACCELERATION AND DISPLACEMENT AT STATIONS ON ALLUVIUM (Continued)

STATION/ INSTRUMENT	COMPONENT	DISTANCE (km)	PEAK ACCELERATION (g)	PEAK DISPLACEMENT (cm)
SE-6 (L-7)	Z	187.3	1.62×10^{-4}	6.67×10^{-3}
	N/S		3.90×10^{-4}	1.69×10^{-2}
	E/W		2.89×10^{-4}	1.28×10^{-2}
	V		4.11×10^{-4}	1.72×10^{-2}
SE-6 (NC-21)	Z	187.3	5.70×10^{-5}	2.44×10^{-3}
	N/S		--	--
	E/W		1.12×10^{-4}	5.20×10^{-3}
	V		--	--

2.3 BAND-PASS FILTER SPECTRA

Band-pass filtering of a seismogram is a technique developed to analyze the peak particle velocity recorded from nuclear events as a function of frequency. The three components of particle velocity of a seismogram are individually passed through twelve narrow band-pass filters to obtain information relating to the frequency content of the seismic signal. The peak amplitude of the output from each filter is plotted as a function of the center frequency of the filter and the points are connected, giving a continuous curve called the BPF spectrum.

Band-pass filter spectra from the Schooner event are shown on Figures 2-2 through 2-5. Superposed on each graph is the mean BPF spectrum typically measured at that distance from a contained NTS event of the yield of Schooner. The mean BPF spectrum shown is based on frequency, yield and distance dependent regression equations derived from band-pass filter data observed from 20 underground nuclear detonations at Nevada Test Site. The data sample contains approximately 2,400 spectral amplitudes over the frequency range 0.4 - 11.3 Hz. The distance and yield ranges of the data are 40 - 200 km and 16 kt (yield of Rex) - 825 kt (yield of Greeley), respectively. Thus, the BPF spectrum defined by these equations represents a good approximation of the average spectral composition observed from contained Nevada Test Site detonations.

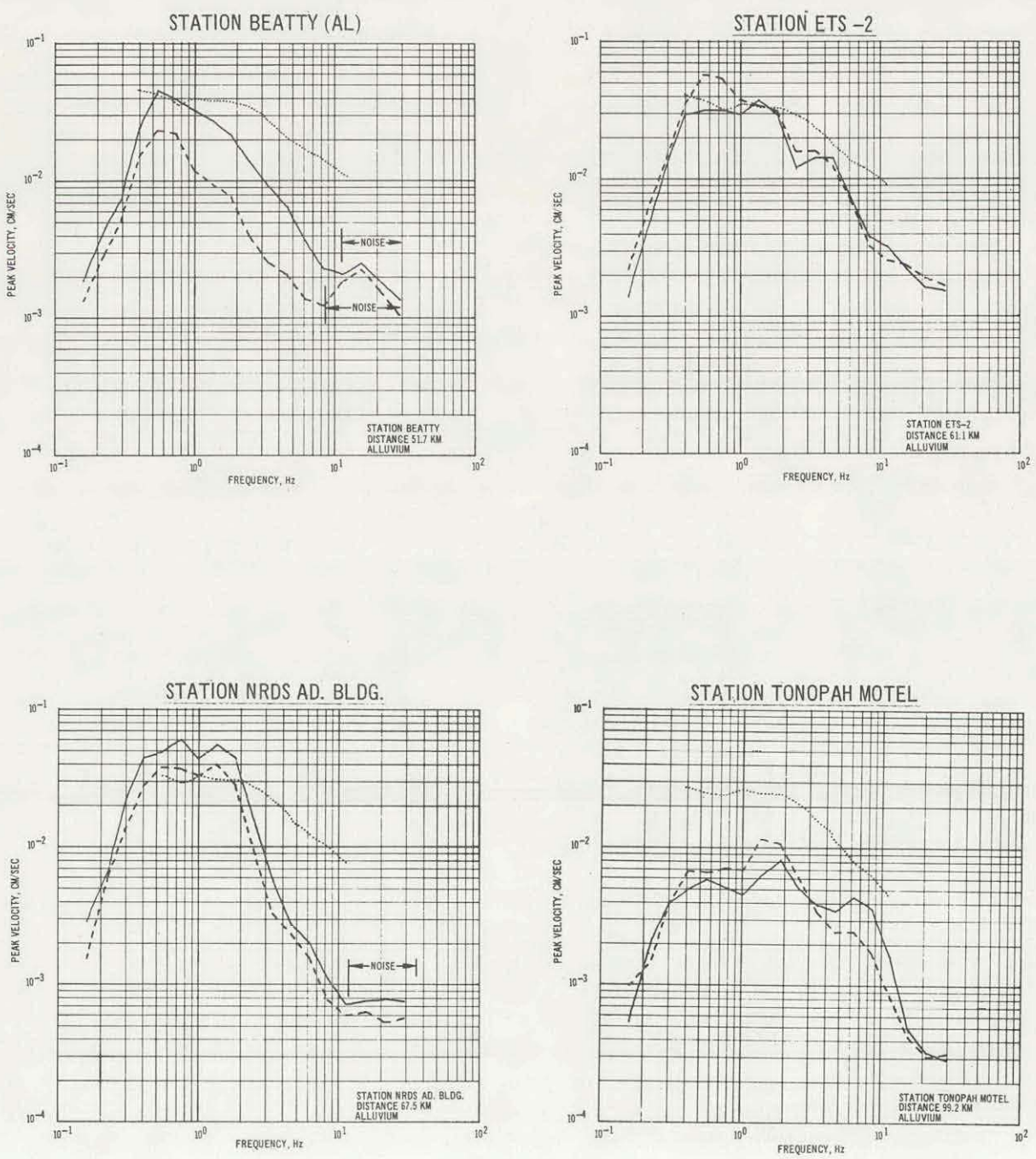

Figure 2-2. Comparison of Observed (Schooner Detonation) and Predicted (equivalent yield contained detonation) BPF Spectra

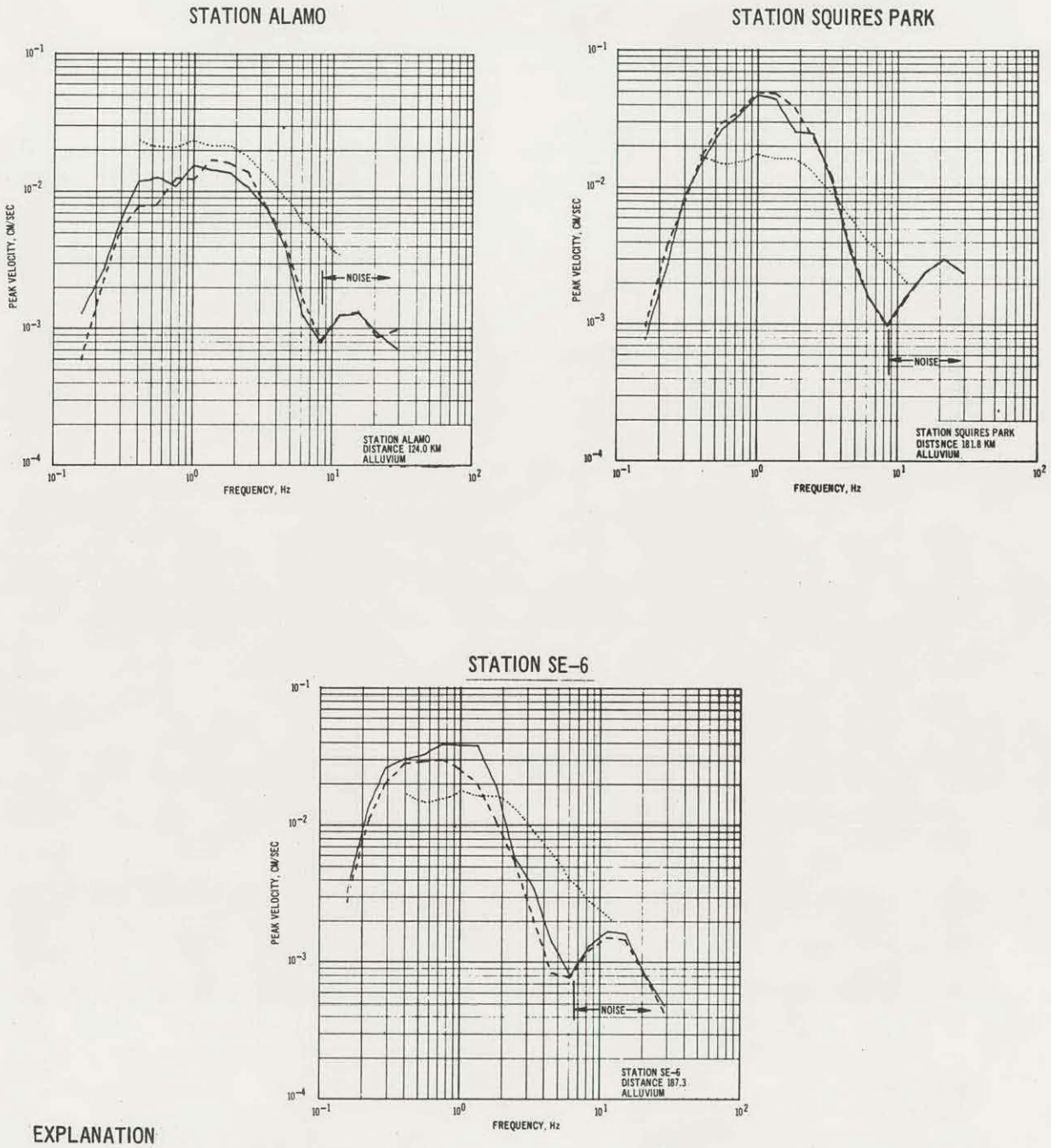

Figure 2-3. Comparison of Observed (Schooner Detonation) and Predicted (equivalent yield contained detonation) BPF Spectra

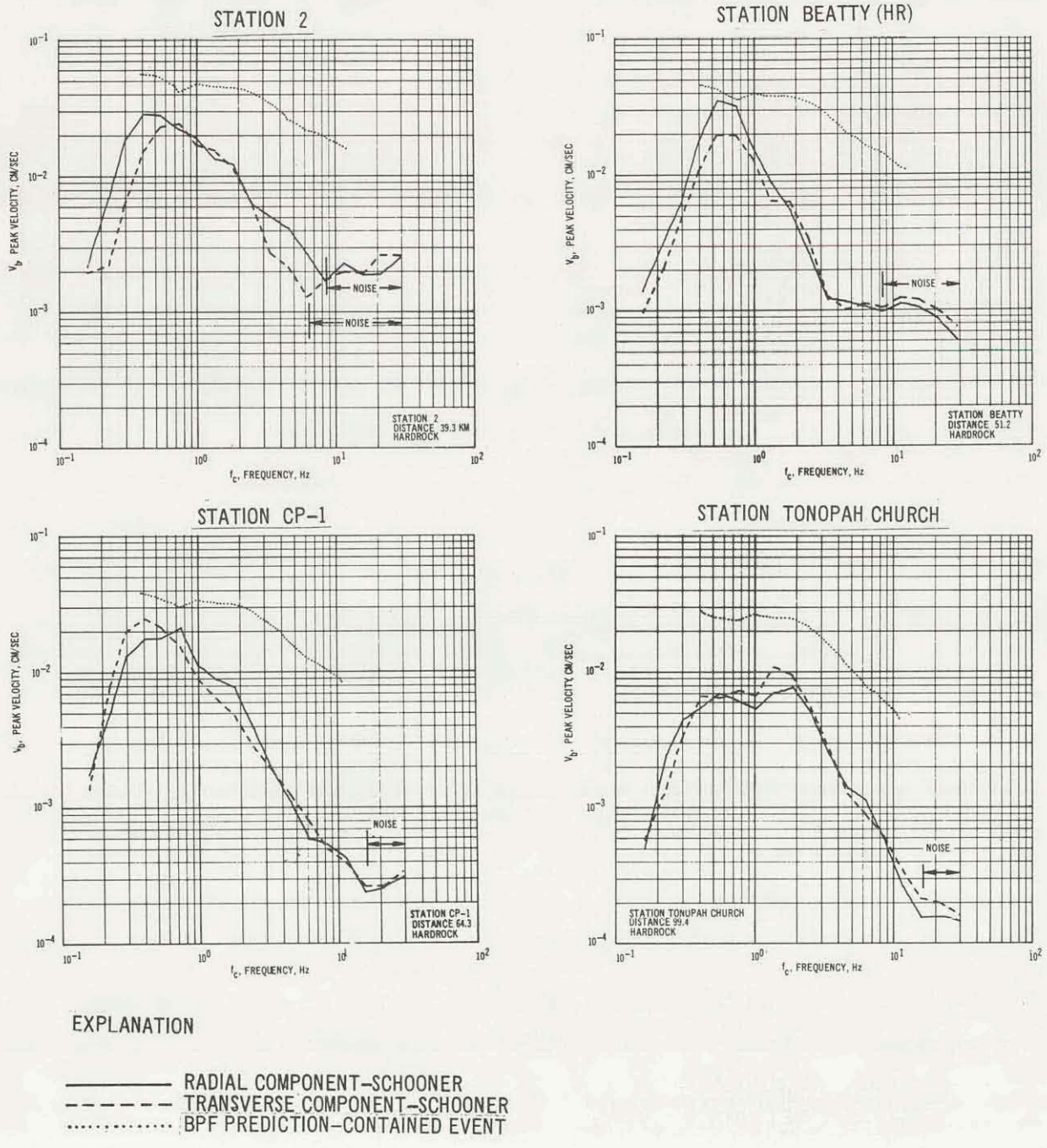

Figure 2-4. Comparison of Observed (Schooner Detonation) and Predicted (equivalent yield contained detonation) BPF Spectra

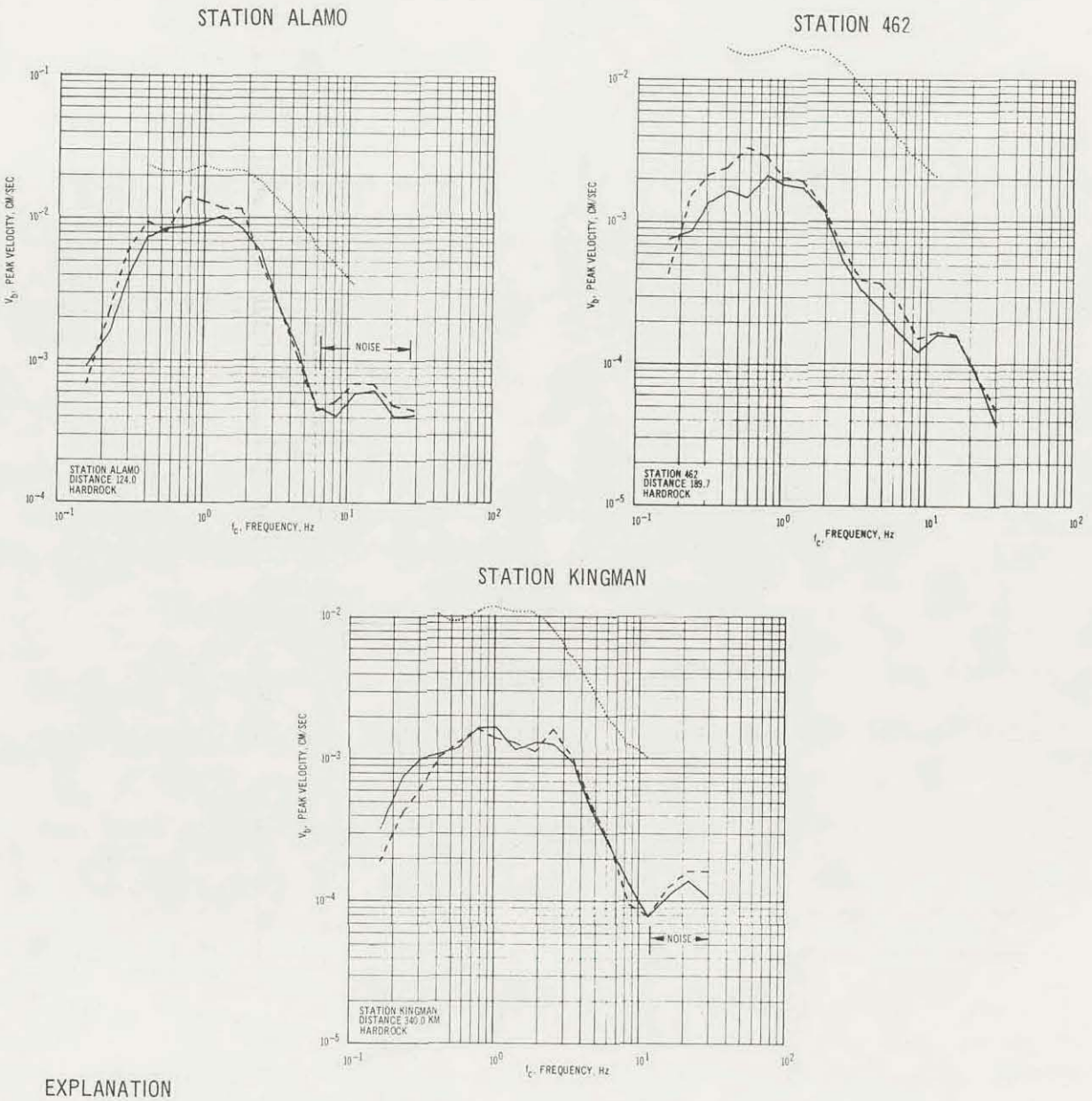

Figure 2-5. Comparison of Observed (Schooner Detonation) and Predicted (equivalent yield contained detonation) BPF Spectra

CHAPTER 3

ANALYSIS OF SCHOONER DATA

3.1 PEAK AMPLITUDE DATA

Multiple regression analyses, utilizing a large quantity of peak amplitude data recorded from 99 contained nuclear events detonated on the Nevada Test Site, have resulted in statistically based regression equations (Murphy and Lahoud, 1969). These equations are currently being used to predict the mean peak resultant vector ground motions expected from nuclear tests. A corresponding data sample is not yet available for cratering events. Although only limited cratering data are available, it is now established (Klepinger and Mueller, 1969 and Chapters 4 and 5 of this report) that the amplitude and spectral characteristics of ground motions from cratering events, as well as seismic efficiency, are quite different from that of contained events.

In an effort to define these differences, Klepinger and Mueller (1969) performed a regression analysis on the peak amplitude data sample from the Cabriolet, Palanquin, Sedan, and Danny Boy cratering events. The results of this analysis, and the analysis for contained events discussed above, are compared with Schooner results on Figures 3-1 through 3-6. These figures show

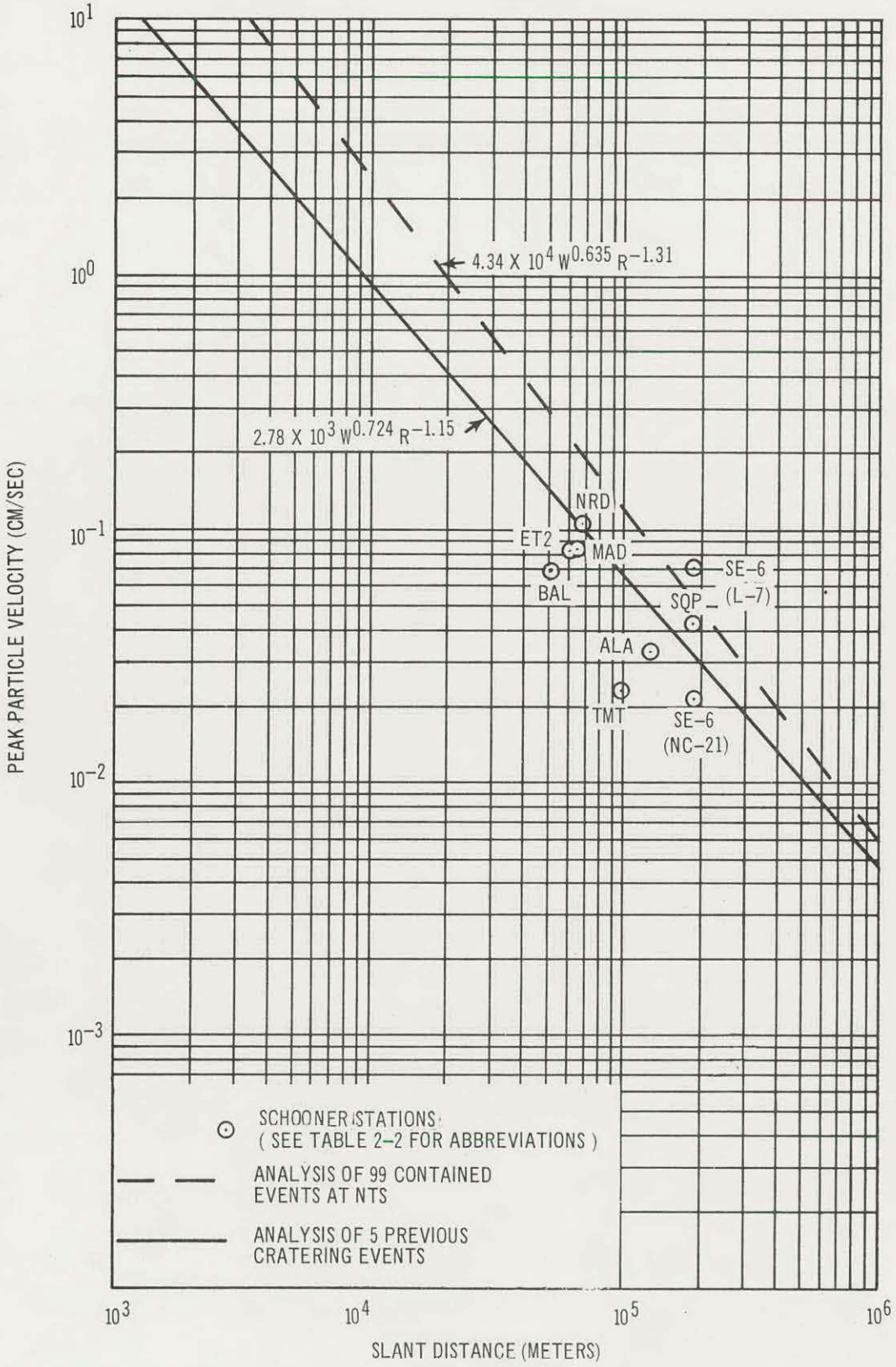

Figure 3-1. Peak Particle Resultant Vector Velocities Recorded for Schooner Compared to Multiple Regression Analyses of Contained and Cratering Event Velocities - Alluvium Sites

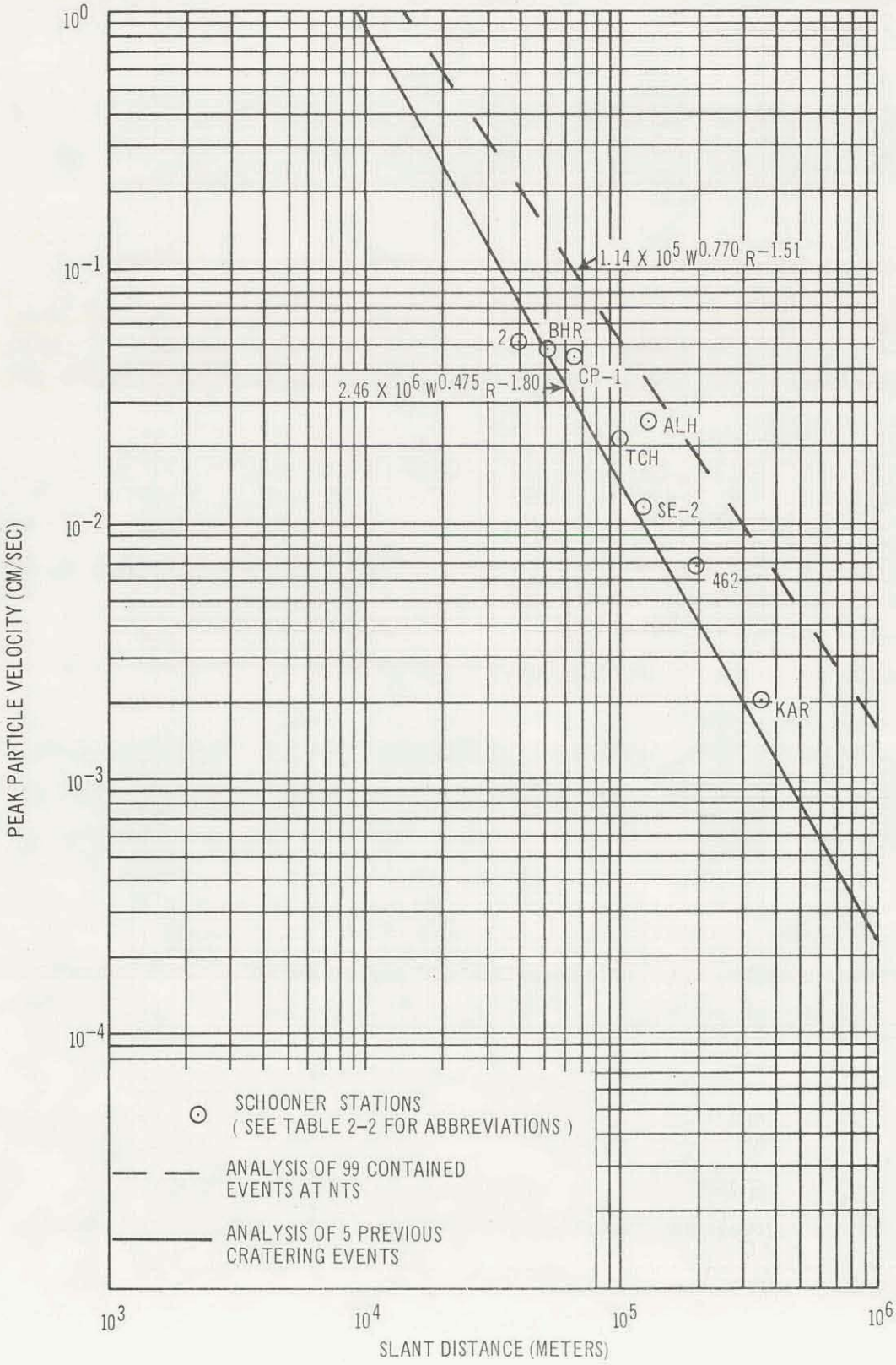

Figure 3-2. Peak Particle Resultant Vector Velocities Recorded for Schooner Compared to Multiple Regression Analyses of Contained and Cratering Event Velocities - Hard Rock Sites

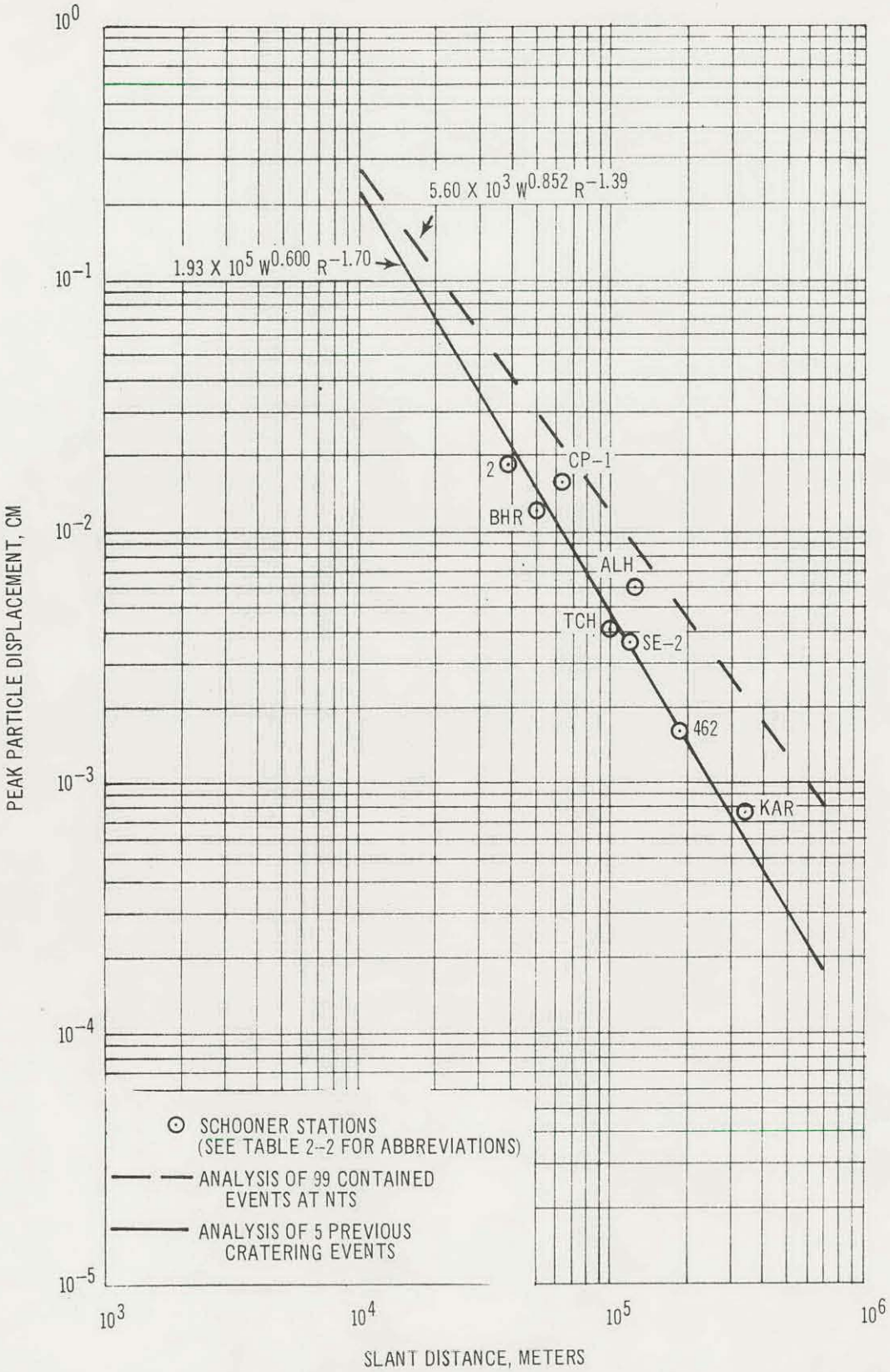

Figure 3-3. Peak Particle Resultant Vector Displacements Derived from Schooner Particle Velocity Seismograms Compared to Multiple Regression Analyses of Contained and Cratering Event Displacements - Hard Rock Sites

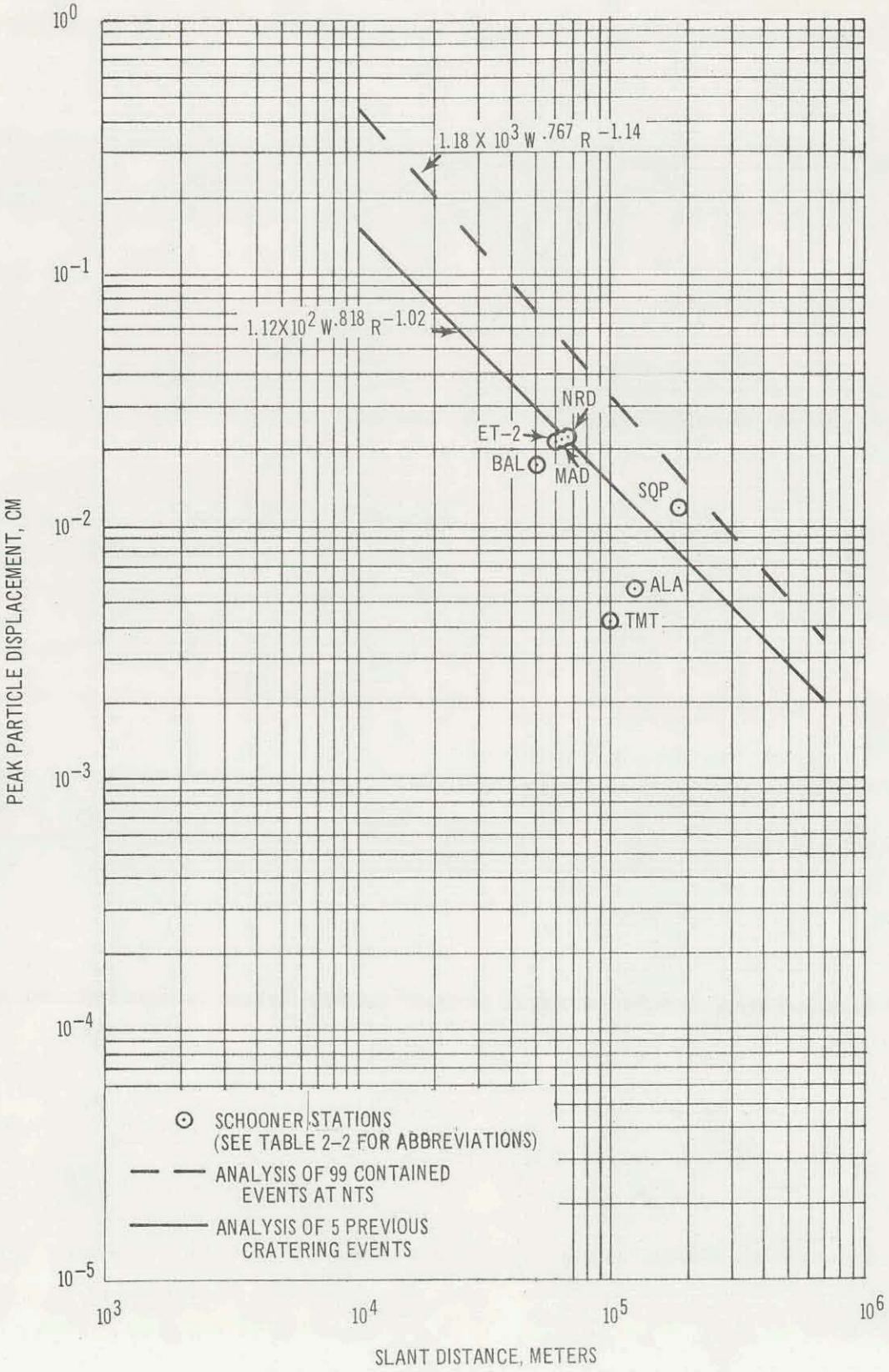

Figure 3-4. Peak Particle Resultant Vector Displacements Derived from Schooner Particle Velocity Seismograms Compared to Multiple Regression Analyses of Contained and Cratering Event Displacements - Alluvium Sites

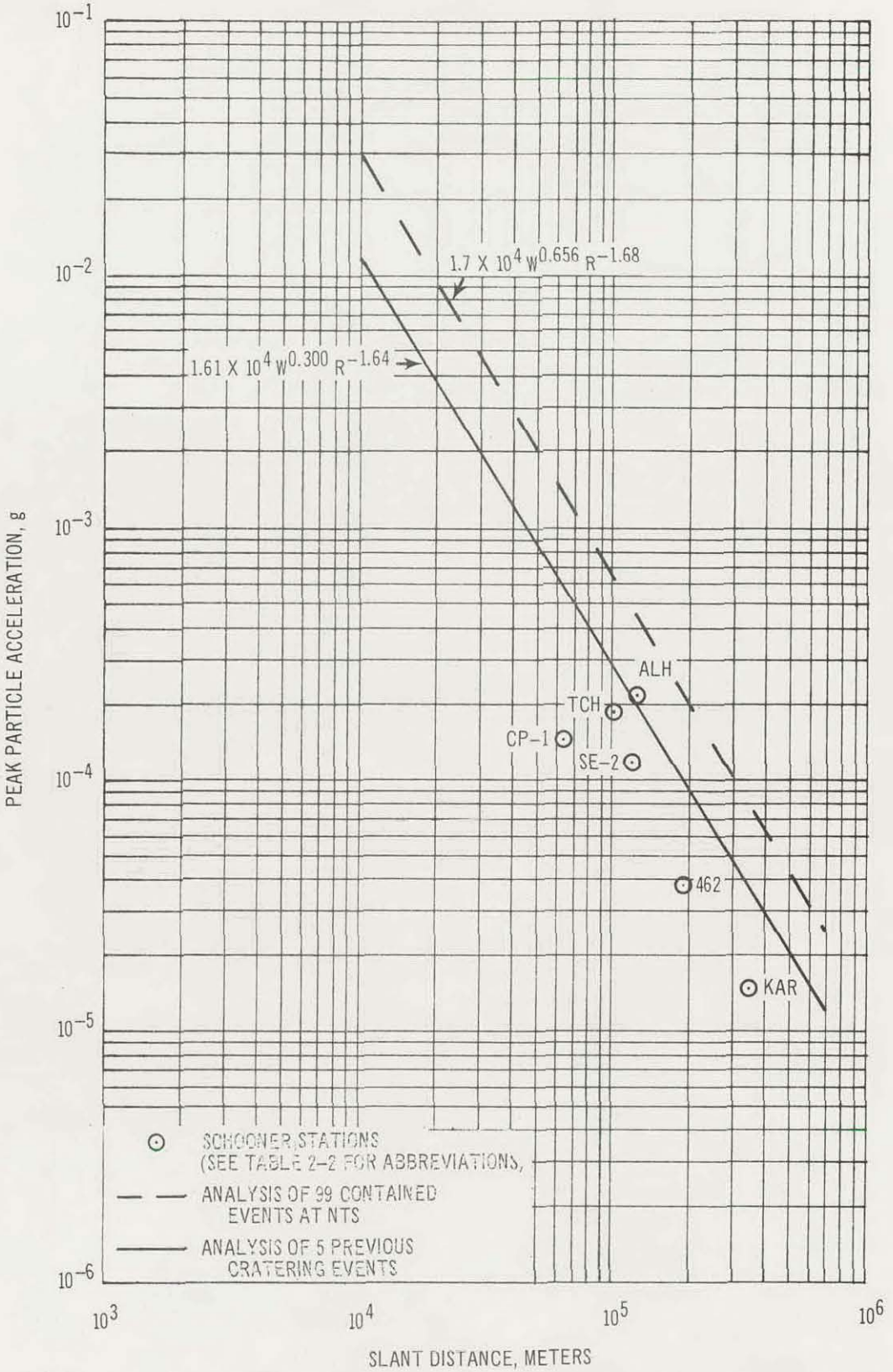

Figure 3-5. Peak Particle Resultant Vector Accelerations Derived from Schooner Particle Velocity Seismograms Compared to Multiple Regression Analyses of Contained and Cratering Event Accelerations - Hard Rock Sites

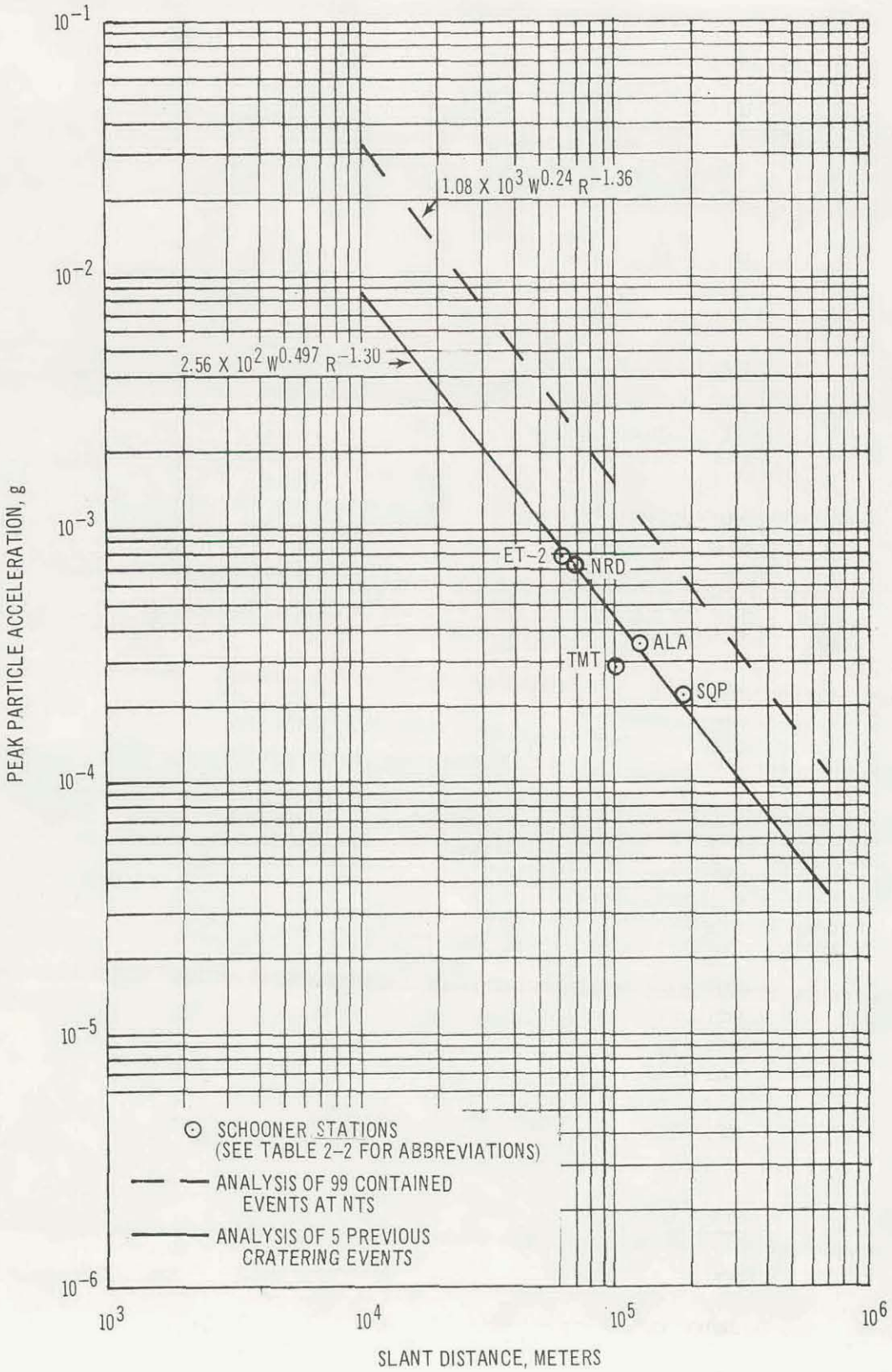

Figure 3-6. Peak Particle Resultant Vector Accelerations Derived from Schooner Particle Velocity Seismograms Compared to Multiple Regression Analyses of Contained and Cratering Event Accelerations - Alluvium Sites

Schooner peak resultant vector particle motions recorded at alluvium and hard rock sites as a function of station distance.

Superposed on these data points are the predicted values of peak particle motions made on the basis of the 99 event data sample and the cratering event data sample. The following observations are made on the basis of these data:

1. Schooner peak vector particle motions recorded at both hard rock and alluvium sites exhibit lower amplitudes than the particle motions predicted on the basis of contained events (with the exception of SE-6). This is consistent with previous experience (Klepinger and Mueller, 1969).

2. Previous experience (Klepinger and Mueller, 1969) indicates a tendency for ground motions generated by cratering events to attenuate faster at hard rock stations than corresponding ground motions from contained events. However, peak vector particle velocities from Schooner (Figure 3-2) appear to decay at about the same rate predicted on the basis of an equivalent yield contained event.

3. Predictions of peak motion based on equivalent yield contained events appear to be conservative estimates of the ground motion levels expected for cratering events. Additional cratering event data are required, however, to establish a sound statistical and physical basis for predicting cratering event peak particle ground motions.

3.2 AMPLITUDE-FREQUENCY DATA

The objectives of this section are twofold: 1) to examine the frequency content of the ground motion resulting from cratering and contained nuclear detonations in order to determine any significant and consistent patterns existing between the two types of

explosions, and 2) to evaluate the observations within a self-consistent theory on the scaling of the amplitude spectra of underground explosions. To accomplish these objectives, parameters influencing the seismic signals must be minimized such that comparisons of the amplitude spectra are effectively comparisons of the sources. Therefore, it is necessary to eliminate, as far as possible, transmission path variables, station site variables, and source media effects.

The contained nuclear detonations Knickerbocker, Duryea and Rex, were detonated within the immediate locality (10 km) of Schooner (Figure 1-1). These contained detonations were executed in rhyolite. Common stations instrumented for these detonations are given in Table 3-1. Comparisons of BPF at these common stations for the various events, scaled to the Cabriolet yield of 2.3 kt, should therefore, indicate any general pattern existing between cratering and contained shots.

Scaling of the Band-Pass Filter (BPF) spectrum, which is an approximation of the Fourier amplitude spectrum, is normally accomplished by applying frequency-dependent yield scaling exponents. These exponents are statistically derived from a large number of underground explosions, the major portion of which are buried at a set scaled depth of 350 to 450 (scaled depth is the ratio, depth

TABLE 3-1. SLANT DISTANCES OF COMMON STATIONS

STATION	EVENT				
	Schooner	Cabriolet	Knickerbocker	Duryea	Rex
SE-6	187.3 km	182.0 km	175.0 km	170.0 km	173.0 km
Alamo	124.0 km	123.0 km	120.0 km		
Tonopah Church	99.4 km	111.0 km	112.0 km	116.0 km	112.0 km
Tonopah Motel	99.2 km	111.0 km	112.0 km	116.0 km	112.0 km
CP-1	64.4 km	57.0 km		48.0 km	

of burial/cube root of yield). Therefore, the empirical scaling may be considered, as a fair approximation, to be scaling at a set scaled depth; although, it has been found theoretically that the yield exponents are also yield and depth dependent (Mueller, 1969) Schooner, Knickerbocker, Duryea and Rex BPF spectra were scaled to 2.3 kt (Cabriolet yield) by use of the statistical exponents described above. Each spectrum is then appropriately scaled to the Cabriolet depth of burial. Knickerbocker and Duryea are buried at a normal scaled depth while Rex is slightly overburied. The depth of burial for Cabriolet is 171 feet.

Comparisons of the BPF spectra from cratering and contained explosions (Klepinger and Mueller, 1969 and Figures 2-2 through 2-5) indicate that the level and frequency content are different. The spectra from the cratering events are generally somewhat lower in magnitude and the dominant energy content is shifted to lower frequencies. The observation that the spectra are different is not an unexpected result, since cratering and contained events are explicitly different. The fundamental questions are in what respects are they different and how can this be formulated into a quantitative theory. The answers require a consideration of the elastic wave production mechanism and the parameters influencing this mechanism.

A theory using the solution of a spherically symmetric forcing function acting in an infinite homogeneous medium has been developed into a general scaling law of the amplitude spectrum for underground explosions (Mueller, 1969). The analytic development takes into account source parameters such as medium type and device depth of burial. For a particular medium, the elastic radii of two events of arbitrary yield and depth of burial vary as

$$\left(\frac{a_1}{a_2}\right) = \left(\frac{h_2}{h_1}\right)^{1/n} \left(\frac{W_1}{W_2}\right)^{1/3} \qquad (3\text{-}1)$$

where a_1 and a_2 are the elastic radii; i.e., the radii where the material behaves elastically, h_1 and h_2 are the depths of burial, and W_1 and W_2 are the yields of events 1 and 2, respectively. The parameter n is the distance exponent of the shock pressure (or velocity) in the inelastic region. Also, the seismic efficiency defined as the proportion of initial energy (E) reaching the radiation zone of the elastic region ($b = E/W$), for a particular medium, scales as

$$\frac{b_1}{b_2} = \left(\frac{h_1}{h_2}\right)^{2-3/n} \qquad (3\text{-}2)$$

for arbitrary yields and depths of burial. The scaling of the elastic radii, alone, determines the relative shape of the amplitude spectra, whereas the elastic radii in conjunction with the depths of burial determine the level of the spectra. For the rhyolite and tuff (Schooner) media in which these events were detonated, n was taken to be 2.4, the value observed for granite (Perret, 1963).

The BPF amplitude spectra of Schooner, Cabriolet, and the average spectra of the contained detonations, Knickerbocker, Duryea and Rex, (scaled to the Cabriolet yield and depth of burial by the theoretical scaling law) at the distant stations SE-6, Tonopah Church, Tonopah Motel and Alamo are shown in Figures 3-7 to 3-10. Also shown is the average of the empirically scaled spectra for the contained detonations. This average spectrum corresponds to the spectrum of a normal 2.3 kt contained detonation. In all cases the theoretically scaled spectra from the three contained events lie closer to the Schooner and Cabriolet spectra than the empirical curves; in some cases the agreement is excellent.

Two basic conclusions follow. First, as far as the seismic motion is concerned, the nuclear cratering detonations Schooner and Cabriolet may be considered as contained explosions buried

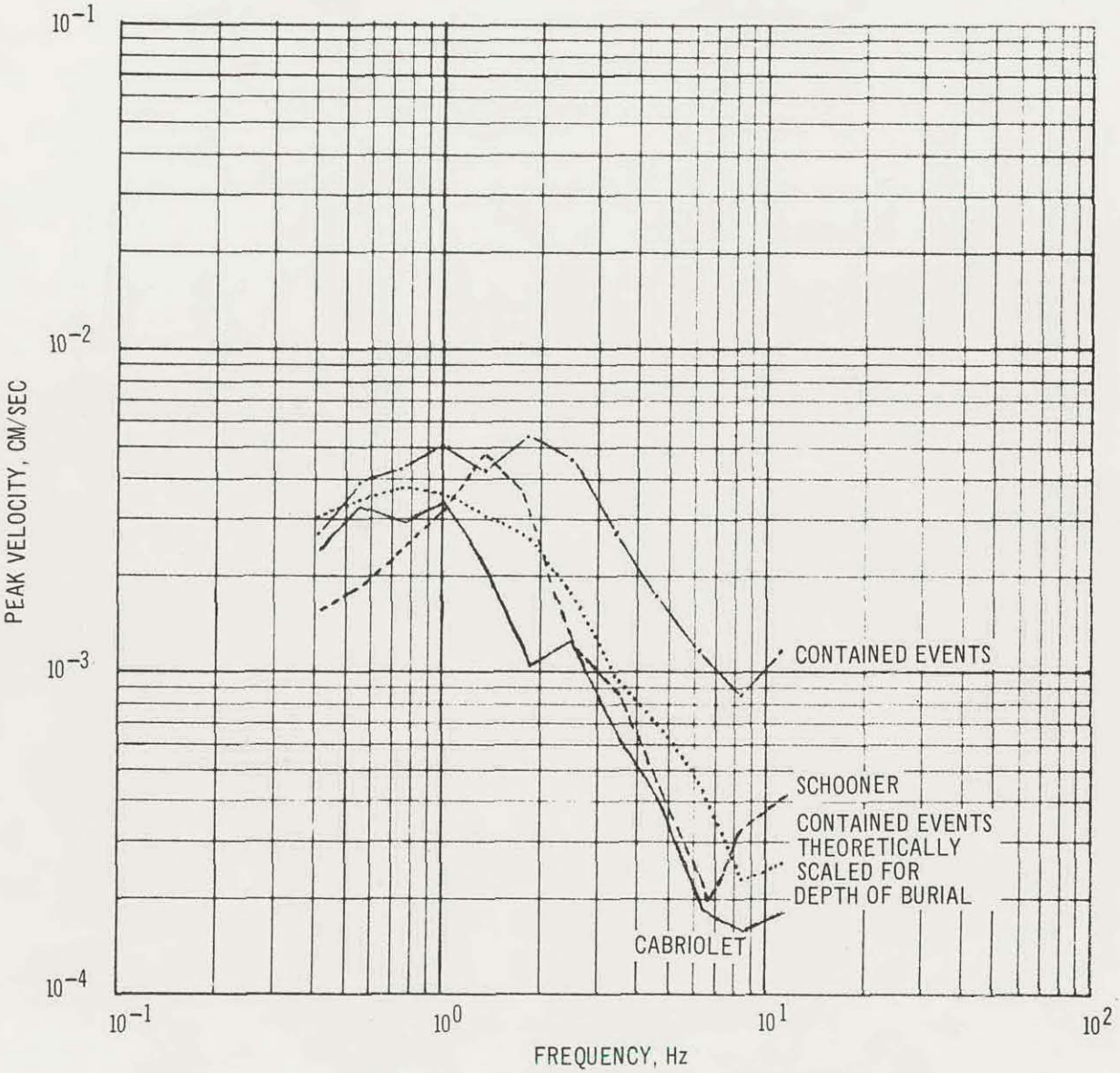

Figure 3-7. Comparison of BPF Data From Schooner, Cabriolet, and Contained Events (Knickerbocker, Duryea and Rex) at 2.3 kt, Radial Component, SE-6

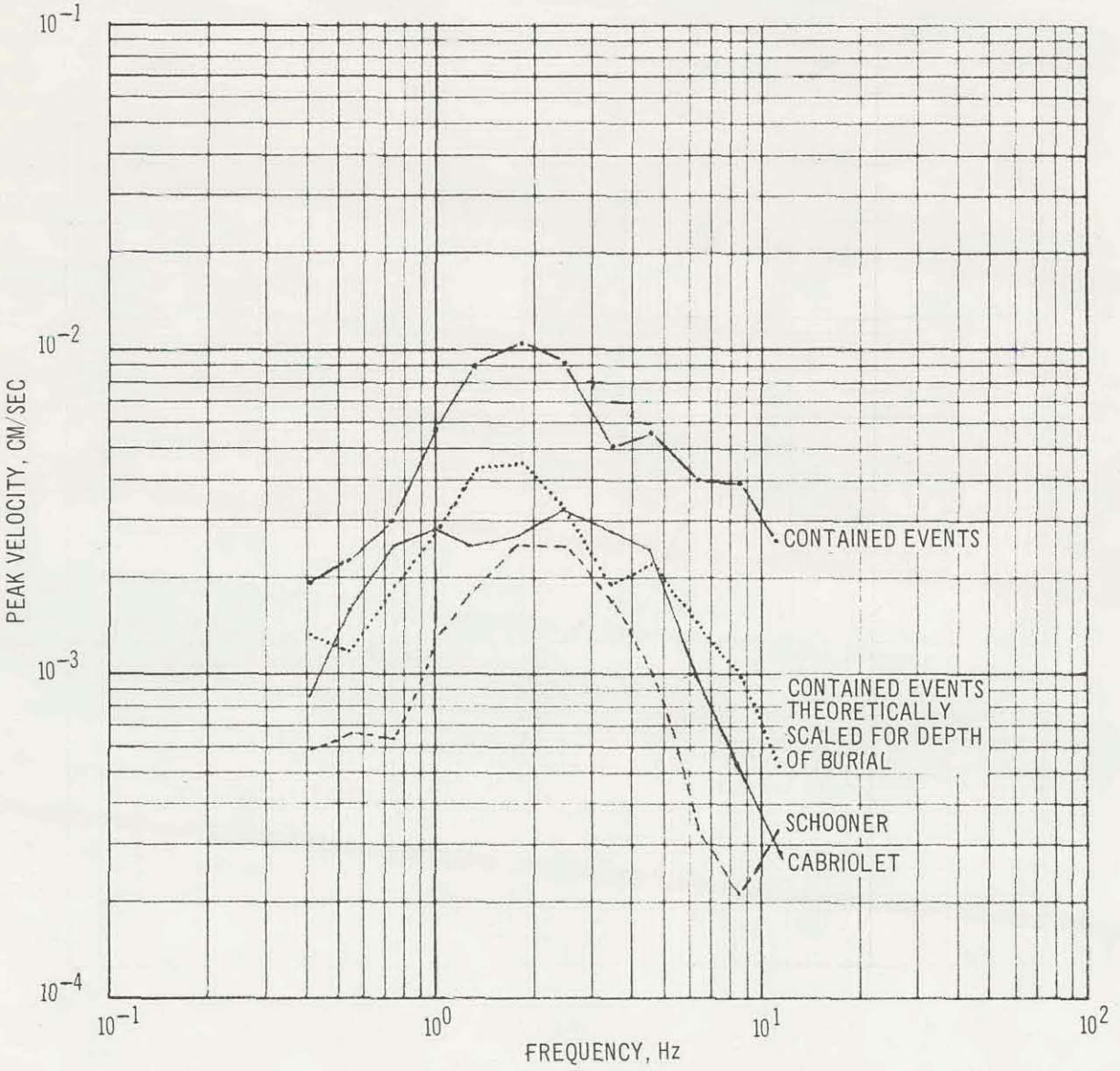

Figure 3-8. Comparison of BPF Data From Schooner, Cabriolet, and Contained Event (Knickerbocker) at 2.3 kt, Radial Component, Alamo

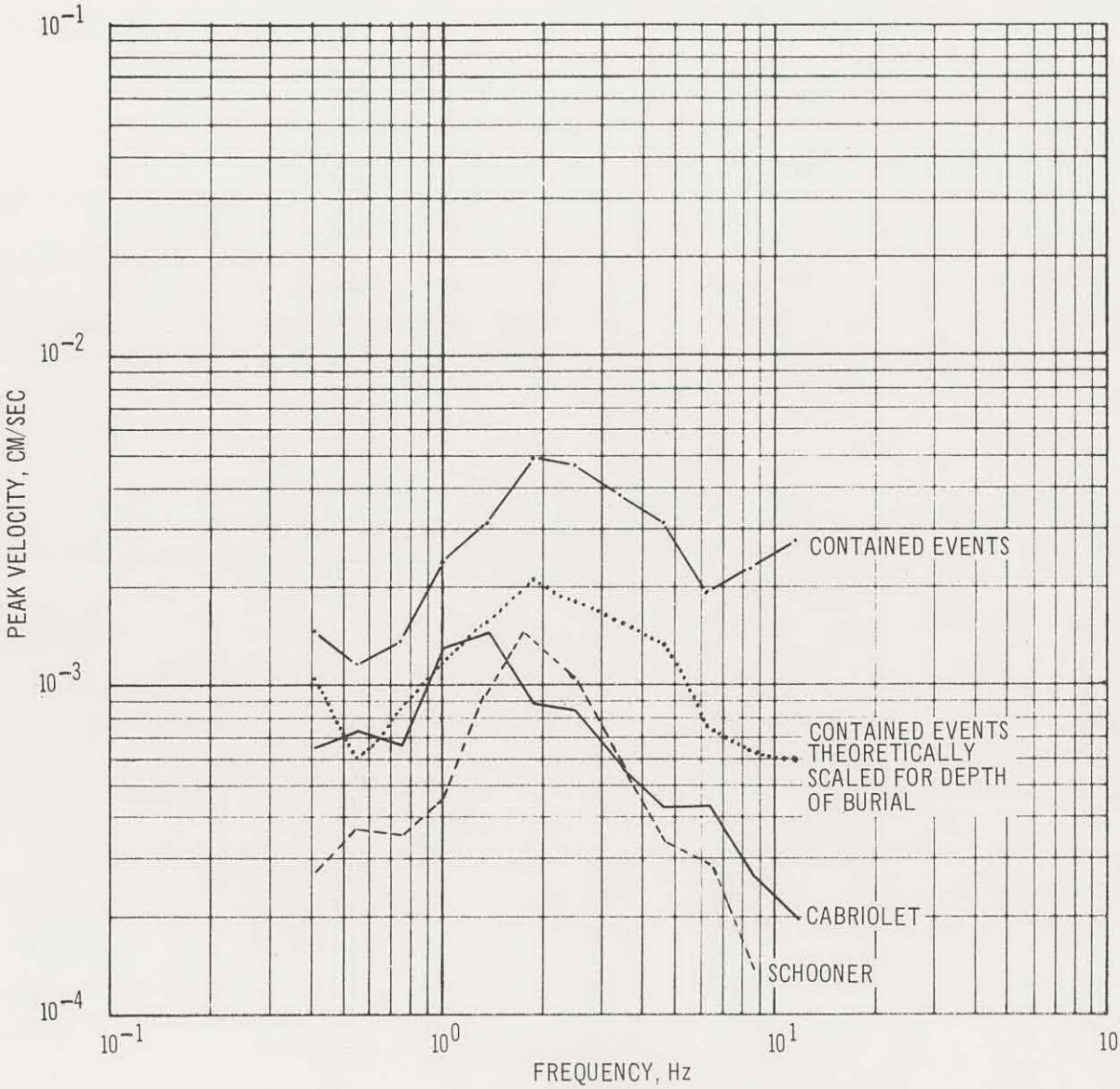

Figure 3-9. Comparison of BPF Data From Schooner, Cabriolet, and Contained Events (Knickerbocker and Duryea) at 2.3 kt, Radial Component, Tonopah Church

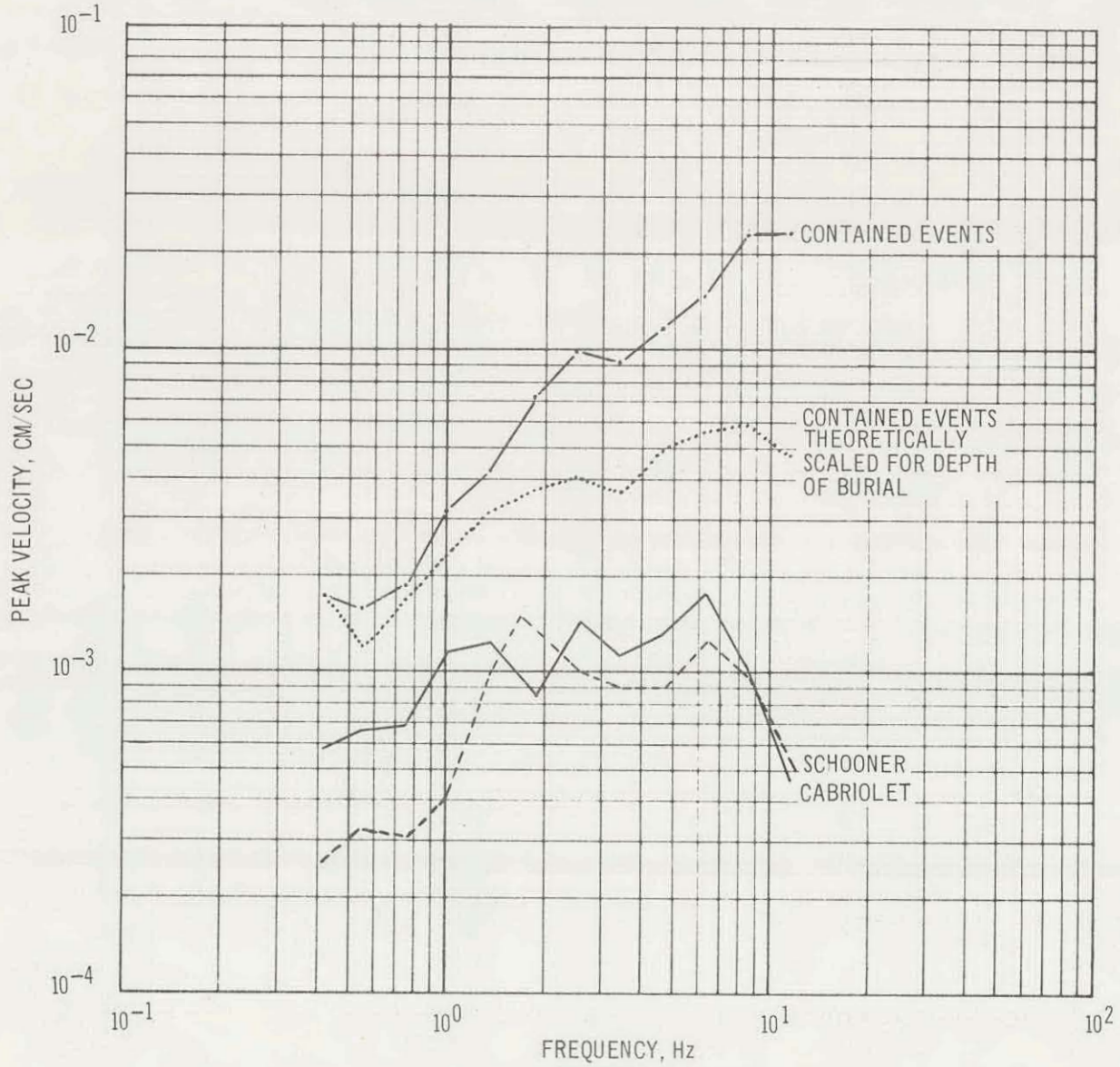

Figure 3-10. Comparison of BPF Data From Schooner, Cabriolet, and Contained Events (Knickerbocker, Duryea, and Rex) at 2.3 kt, Radial Component, Tonopah Motel

at relatively shallow depths of burial using presently available theoretical techniques. The relationships between seismic efficiency, elastic radii and depths of burial (Equations 3-1 and 3-2) adequately account for the differences in amplitude spectra between the contained events and the cratering events. Physically, this suggests that most of the energy that goes into the formation of elastic waves is coupled into the ground before the fireball breaks the surface with a subsequent sudden release of energy to the atmosphere. This description is physically sound, for the shock wave which is the precursor to the elastic waves is liberated into the ground at the end of the vaporization phase. (The vaporization cavity is of the order of a few meters for a one kiloton shot.) Thus, most of the energy going into the elastic region is independent of the cavity expansion after the vaporization phase. Thus, as far as the elastic region is concerned, a cratering event may be considered to be a contained event buried at a relatively shallow depth, with depth of burial controlling the seismic efficiency.

The second conclusion is that for two events of the same yield in the same medium, the dominant spectral amplitude of the event with the shallower depth of burial occurs at lower frequencies. This is evident from Equation (3-1) where the elastic radii scale

inversely to the ratio of depths of burial for equivalent yield and

$$\frac{a_1}{a_2} = \left(\frac{h_2}{h_1}\right)^{1/n} \qquad (3\text{-}3)$$

and the frequency of the dominant energy portion of the amplitude spectrum varies inversly with a. Thus at smaller depths of burial, the amplitude spectrum is shifted to lower frequencies. This characteristic may be noted in the spectra for Schooner and Cabriolet, the two detonations with the shallow depth of burial. The main observation is that the high frequency content of cratering events is considerably reduced relative to that of contained events while the low frequency content is only slightly reduced. This physical result probably has an influence on the characteristics of the peak ground motions observed from cratering detonations. In particular, it appears that the correlation of peak ground motions and elastic wave types might be affected differently for cratering and contained detonations due to the differences in the amplitude spectrum. Also, the resultant amplification of high frequency body waves (Davis and Murphy, 1967) by low velocity surface layers should be affected; although, the basic physical effect of the layered system should be independent of a change from a nuclear cratering detonation input energy source to a nuclear contained detonation input energy source.

Chapter 4 will describe some of the characteristics of the correlation of the peak ground motion and elastic wave types generated by the Schooner detonation.

CHAPTER 4

AMPLITUDE AND FREQUENCY CHARACTERISTICS OF ELASTIC WAVE TYPES

The primary objective of this chapter is to determine the correlation of the amplitude and frequency characteristics of the ground motion generated by Schooner with elastic wave mode windows (P, S, and surface) and to compare the correlation with results obtained from similar analysis of other cratering and contained events.

4.1 IDENTIFICATION OF ELASTIC WAVE TYPE WINDOWS

Figures 4-1 and 4-2 illustrate typical particle velocity seismograms recorded at Beatty (HR), Nevada and Frenchman Mountain, Nevada from the Schooner detonation. The radial-vertical component product waveform is displayed as the bottom trace on each seismogram. Inspection of the seismogram and the component product waveform permits the P, SV, and Rayleigh waves to be identified (Sutton et al., 1967).

Figure 4-3 illustrates the first arrival time as a function of distance from the energy source for three nuclear detonations - Schooner, Cabriolet (cratering detonations), and Benham (contained detonation). These are located on Figure 1-1. Cabriolet and Benham travel time data were added because the three detonation

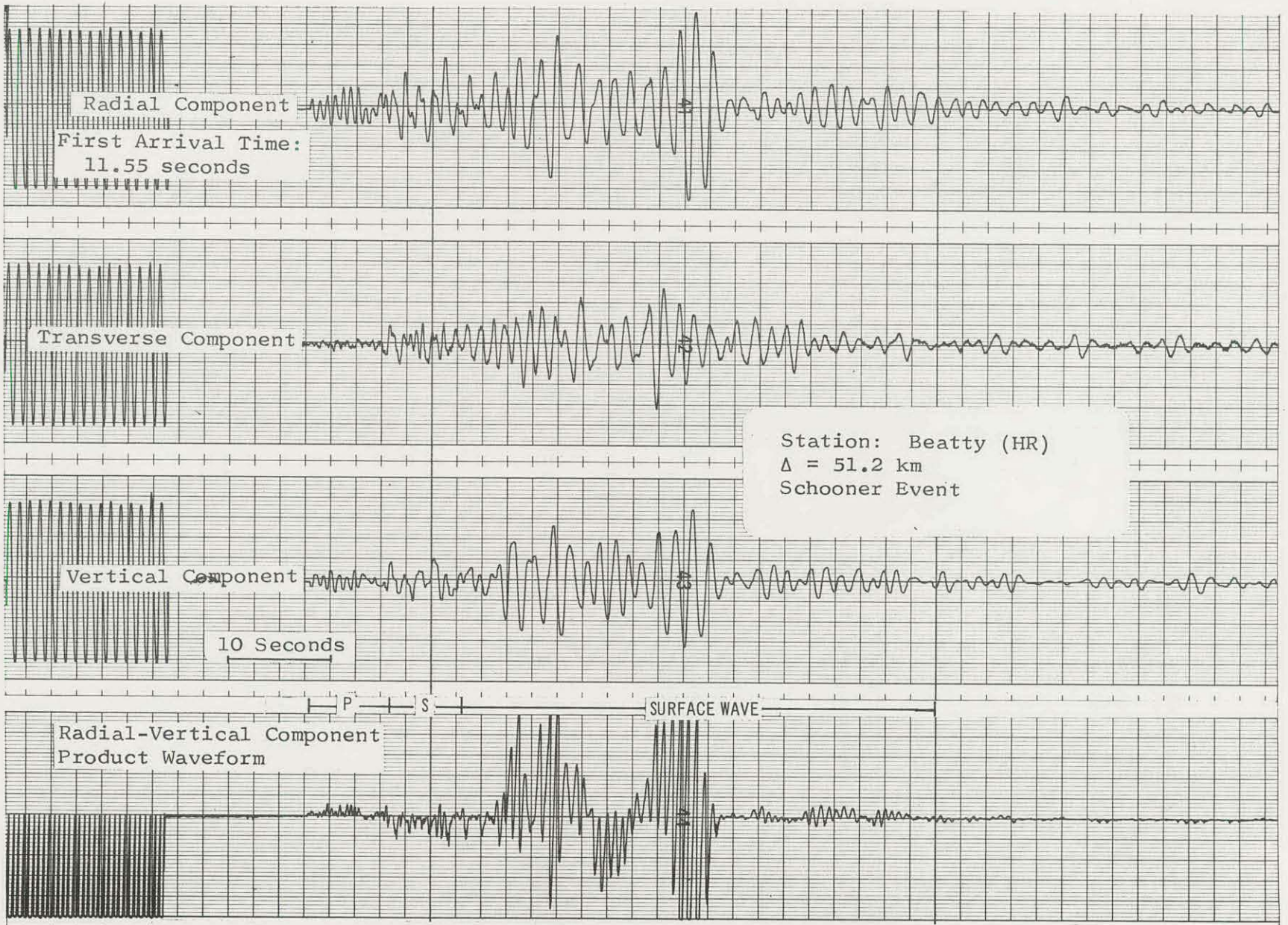

Figure 4-1. Particle Velocity Seismogram Recorded at Beatty (Hard Rock), Nevada - Schooner Event

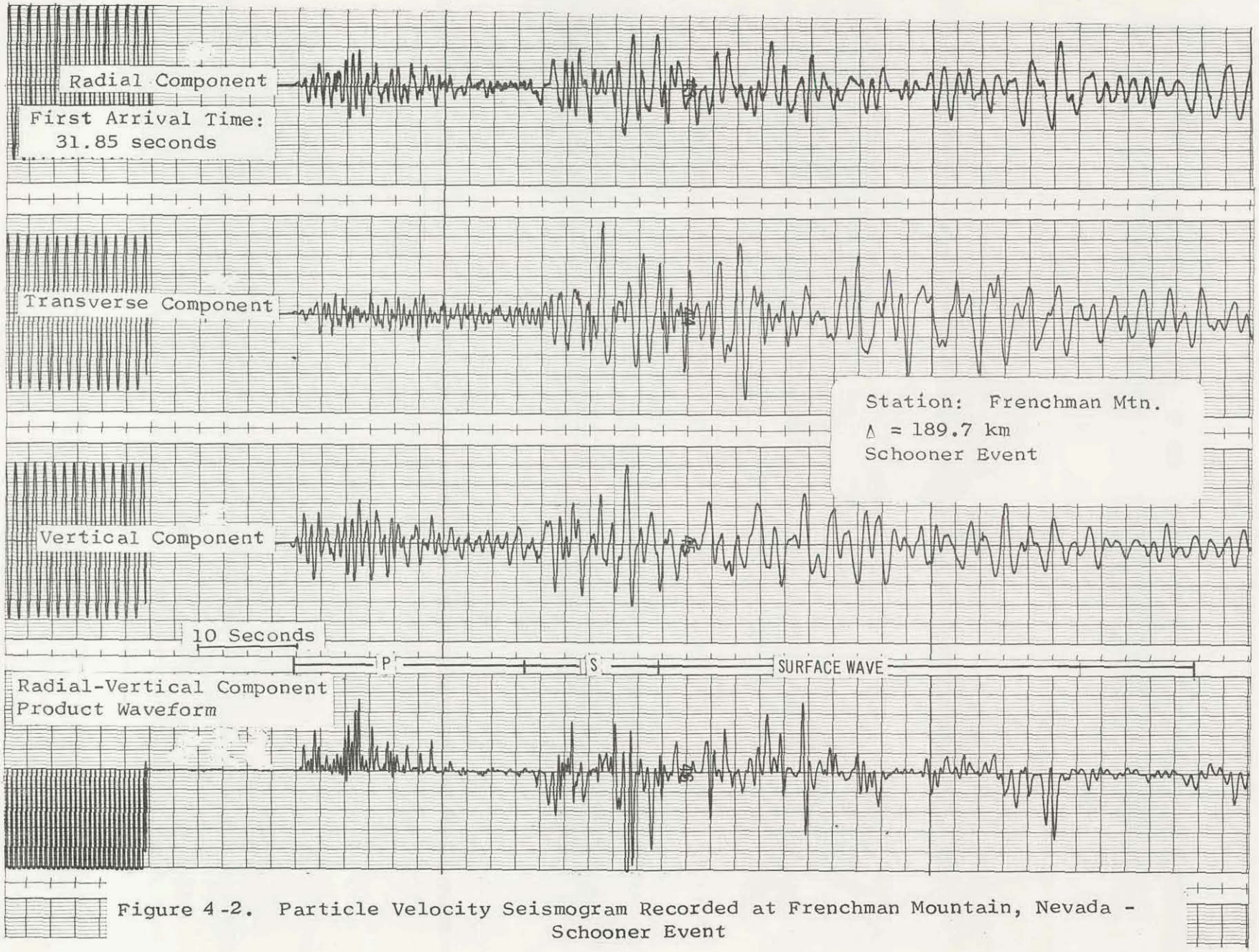

Figure 4-2. Particle Velocity Seismogram Recorded at Frenchman Mountain, Nevada - Schooner Event

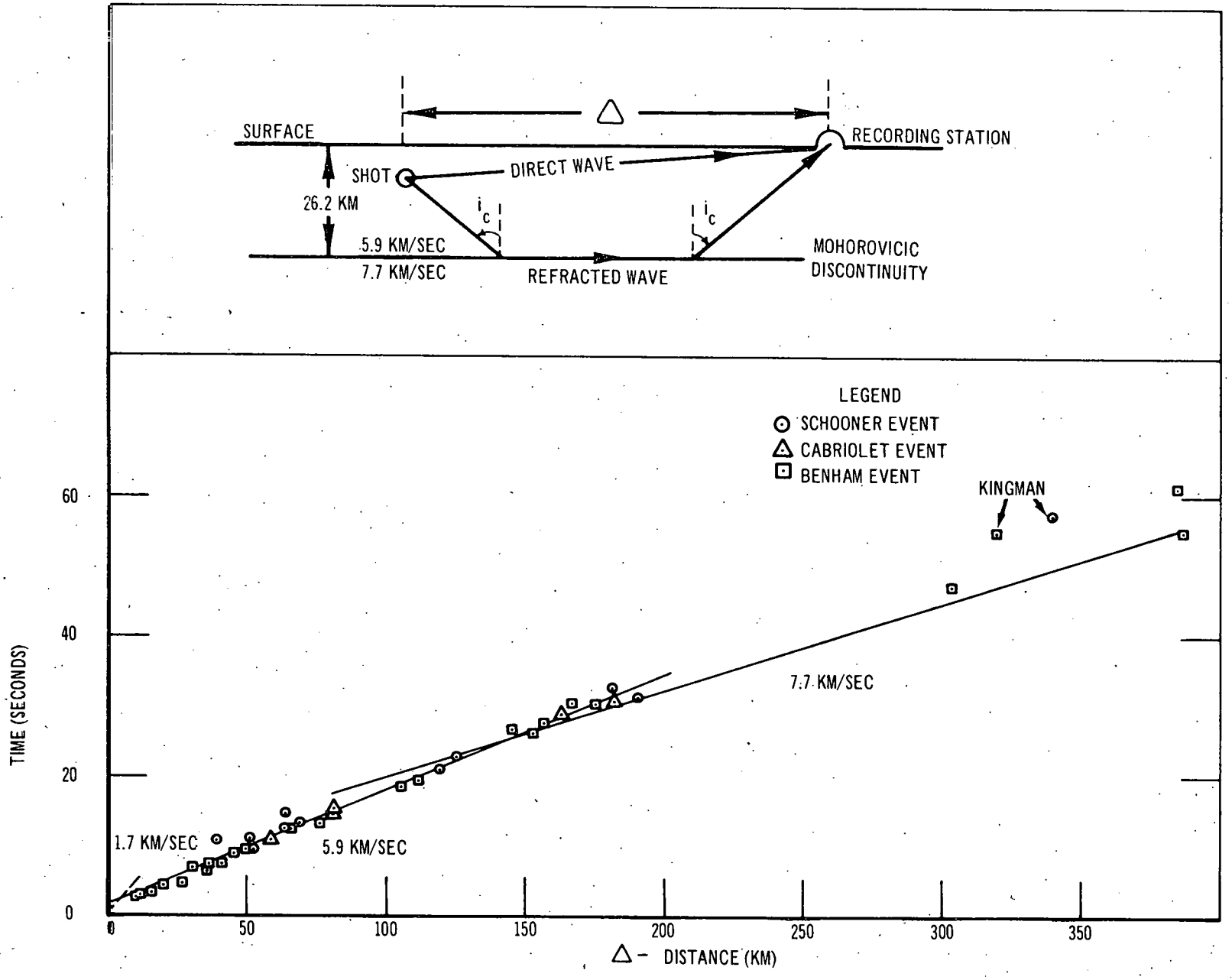

Figure 4-3. First Arrival Time as a Function of Station Distance

points are fairly close together and the Schooner data sample alone is inadequate for analysis.

The first arrival times can be approximated fairly closely by two straight line segments. The first, in the distance interval 0-144 km, indicates a propagation velocity for Pg, the direct wave, of 5.9 km/sec. The second, in the distance interval 144-400 km is based on limited data but suggests a propagation velocity of about 7.7 km/sec for Pn, the P wave critically refracted from the Mohorovicic discontinuity. Data such as this and the two velocity values are typical of the results of other investigators such as Diment, et al. (1961), Stuart, et al. (1964), and Hill, et al. (1967) obtained at the Nevada Test Site (NTS). These values of velocity and the value of 144 km for the critical distance indicate a NTS crustal model with a thickness of 26.2 km.

On the basis of travel time data and the radial-vertical component product waveforms, the time history of a typical seismogram can be divided into three time windows:

1. A P wave window (beginning with the first arrival and extending to the first S wave arrival).
2. A S wave window (beginning at the first S wave arrival; i.e., at a time about 1.7 times the first arrival time, and extending to the onset of the surface wave train).
3. A surface wave window (beginning with the onset of the long period surface wave to the end of significant motion on the seismogram).

These wave mode time windows are necessarily generalized and vary in length and complexity according to factors such as: 1) the distance of the station from the source, 2) the geologic layering at the recording site, and 3) the many complex geological and geophysical parameters of the earth's crust which impress their signature upon the propagating waves. The P wave time window, for example, contains at least the direct wave, the wave critically refracted from the Mohorovicic (M) discontinuity and the reflection from the M discontinuity in an order which depends upon the source-to-station distance relative to the M discontinuity.

4.2 CORRELATION OF PEAK PARTICLE VELOCITY AND ELASTIC WAVE MODE TIME WINDOWS

Each of the particle velocity seismograms recorded from Schooner was analyzed to determine the correlation between the peak vector and the peak horizontal particle velocity with wave mode time window. Table 4-1 lists the results of this analysis. Both the peak vector and the peak horizontal particle velocity correlate with the surface wave mode time window at all Schooner stations except Frenchman Mountain and Alamo. The peak horizontal velocity values occur most often on the transverse component of the seismogram.

The peak vector and the peak horizontal particle velocity observed at seismograph stations which recorded the Cabriolet

RECORDING STATION	DISTANCE (km)	STATION GEOLOGY	WAVE MODE WINDOW WHERE PEAK VECTOR PARTICLE VELOCITY OCCURS			WAVE MODE WINDOW AND COMPONENT WHERE PEAK HORIZONTAL PARTICLE VELOCITY OCCURS		
			P Wave	S Wave	Surface Wave	P Wave	S Wave	Surface Wave
2	39.3	Rock			X			X(R)
Beatty	51.2	Rock			X			X(R)
CP-1	64.4	Rock			X			X(T)
Tonopah Church	99.4	Rock			X			X(T)
SE-2	119.3	Rock			X			X(R)
Frenchman Mountain	189.7	Rock		X			X(T)	
Kingman (Arizona)	340.0	Rock			X			X(R)
Beatty	51.7	Alluvium			X			X(T)
ETS-2	61.1	Alluvium			X			X(T)
E-MAD	63.9	Alluvium			X			X(T)
NRDS (Admin. Bldg.)	67.6	Alluvium			X			X(R)
Tonopah Motel	99.2	Alluvium			X			X(T)
Alamo	124.0	Alluvium		X				X(T)
Squires Park	181.8	Alluvium			X			X(T)
SE-6	187.3	Alluvium			X			X(N/S)

TABLE 4-1. CORRELATION OF PEAK HORIZONTAL AND PEAK VECTOR PARTICLE VELOCITY WITH WAVE MODE TIME WINDOW -- SCHOONER EVENT

detonation, a 2.3 kt nuclear cratering experiment, were identified and correlated with the three wave mode time windows. The results are given in Table 4-2. As observed for Schooner, both the peak vector and the peak horizontal particle velocities correlate primarily with the surface wave mode time window.

Peak vector and horizontal particle velocity values were determined on seismograms recorded from Benham, a 1,100 kt contained nuclear detonation, in order to correlate the peak particle velocity and wave mode time windows for a contained event. The results are shown in Table 4-3. In this case, the peak particle velocities recorded at several stations (Beatty, Tonopah, and NRDS stations) correlate with the P wave time window instead of the surface wave time window. At other stations, the peak particle velocities correlate with the surface wave time window, as noted for Schooner and Cabriolet.

Insufficient data are available at this time to establish a physical basis for the correlation between peak particle velocity and the surface wave mode time window for cratering events. Perhaps the basic difference in the amplitude spectrum of cratering and contained events (i.e., the shift of the dominant energy to the low frequency end of the spectrum for cratering events) enhances the surface wave generation mechanism more for cratering detonations

RECORDING STATION	DISTANCE (km)	STATION GEOLOGY	WAVE MODE WINDOW WHERE PEAK VECTOR PARTICLE VELOCITY OCCURS			WAVE MODE WINDOW AND COMPONENT WHERE PEAK HORIZONTAL PARTICLE VELOCITY OCCURS		
			P Wave	S Wave	Surface Wave	P Wave	S Wave	Surface Wave
CP-1	57.0	Rock			X			X(T)
SE-1	81.0	Rock			X			X(R)
Tonopah Church	111.0	Rock			X			X(T)
Q-25	82.5	Alluvium			X			X(R)
Tonopah Motel	111.0	Alluvium			X			X(T)
Alamo	123.0	Alluvium			X			X(T)
SE-5	163.0	Alluvium			X			X(R)
SE-6	182.0	Alluvium			X			X(N/S)

TABLE 4-2. CORRELATION OF PEAK HORIZONTAL AND PEAK VECTOR PARTICLE VELOCITY WITH WAVE MODE TIME WINDOW -- CABRIOLET EVENT

RECORDING STATION	DISTANCE (km)	STATION GEOLOGY	WAVE MODE WINDOW WHERE PEAK VECTOR PARTICLE VELOCITY OCCURS			WAVE MODE WINDOW AND COMPONENT WHERE PEAK HORIZONTAL PARTICLE VELOCITY OCCURS		
			P Wave	S Wave	Surface Wave	P Wave	S Wave	Surface Wave
2	27.9	Rock	X			X(R)		
Beatty	43.9	Rock	X					X(R)
Tonopah Church	114.1	Rock	X			X(R)		
SE-2	105.0	Rock			X			X(R)
Frenchman Mountain	175.0	Rock			X			X(R)
Kingman (Arizona)	320.0	Rock			X			X(T)
Beatty	44.8	Alluvium	X			X(R)		
ETS (Dewar)	46.7	Alluvium	X			X(R)		
E-MAD	49.4	Alluvium	X			X(R)		
NRDS (Admin. Bldg.)	53.1	Alluvium			X			X(R)
Tonopah Motel	114.1	Alluvium	X			X(R)		
Alamo	116.8	Alluvium			X			X(R)
Squires Park	167.0	Alluvium			X			X(T)
SE-6	172.7	Alluvium			X			X(N/S)

TABLE 4-3. CORRELATION OF PEAK HORIZONTAL AND PEAK VECTOR PARTICLE VELOCITY WITH WAVE MODE TIME WINDOW -- BENHAM EVENT

than for contained detonations. Additional study of data from both cratering and contained detonations is required to establish the basic physical relationship. Also, as more ground motion data from nuclear cratering detonations are obtained, the amplitude of particular wave modes (e.g., the direct P and S waves critically refracted and reflected from the M discontinuity) will be determined as a function of yield and source-recording station distance and compared with similar data from contained nuclear detonations (Hays, 1969).

4.3 DETERMINATION OF FREQUENCY CHARACTERISTICS OF ELASTIC WAVE MODE TIME WINDOWS

Two frequency analysis techniques, Band-Pass filter (BPF) and the Fourier transform, were used to determine the frequency characteristics of elastic wave mode time windows of particle velocity seismograms recorded from Schooner.

Figure 4-4 shows the BPF spectrum of the radial particle velocity observed at two seismograph stations, Beatty (hard rock) and ETS-2 (alluvium.) Superposed on each spectrum are spectra of the three wave mode time windows. Inspection of this figure leads to the following conclusions:

1. The peak radial particle velocity recorded at Beatty correlates with the surface wave mode time window. The peak radial particle velocity recorded at ETS-2 correlates with the S wave mode time window, being slightly greater than the response of the surface wave mode time window.

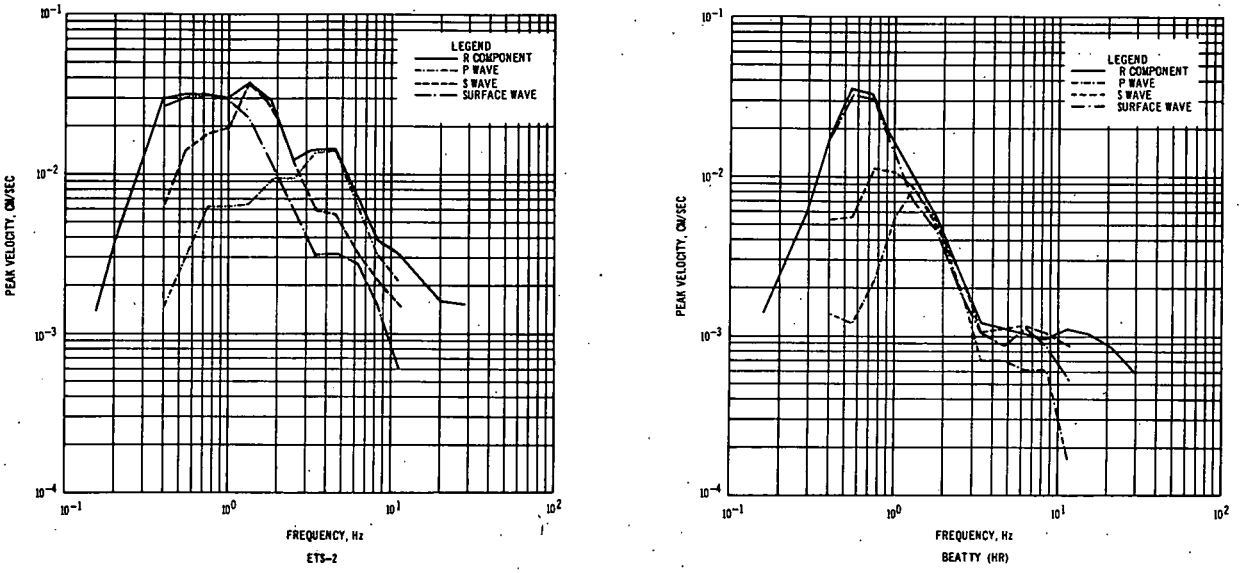

Figure 4-4. Band-Pass Filter Spectra of Wave Mode Windows Measured On the Radial Component of Particle Velocity, Stations Beatty (HR) and ETS-2, Nevada - Schooner Event

2. The individual contribution of the three wave mode windows to the peak radial particle velocity observed on the seismograms is a function of both wave mode window and frequency. That is, the surface wave mode window contribution to the radial particle velocity occurs at a dominant frequency of about 0.8 Hz at Beatty and 1.2 Hz at ETS-2. The P wave mode time window contributes the smallest radial particle velocities at a dominant frequency of about 1.2 Hz and 4.5 Hz respectively for Beatty and ETS-2.

Figure 4-5 illustrates the radial component of particle velocity recorded at five hard rock sites. These stations, with the exception of Beatty, are approximately in-line with the Schooner source, and are distributed over a total distance range of 340 km. The wave mode time windows are identified on each radial component waveform.

The smoothed Fourier amplitude spectra of each of the three wave mode windows illustrated in Figure 4-5 are shown in Figure 4-6. These data support the following conclusions:

1. The surface wave mode time window contributes the peak Fourier amplitude on the five seismograms, as noted earlier.

2. Considering the three amplitude spectra of each individual station, the frequency of the dominant energy varies as a function of the wave mode window. That is, the peak amplitude of the P wave mode window spectrum occurs at a higher relative frequency than the peak amplitude of the other two wave mode spectra. The peak amplitude of the surface wave mode window spectrum occurs at the lowest relative frequency. This phenomenon is related to the well known fact that the three elastic wave types propagate with different wave velocities and, consequently, different characteristic frequencies.

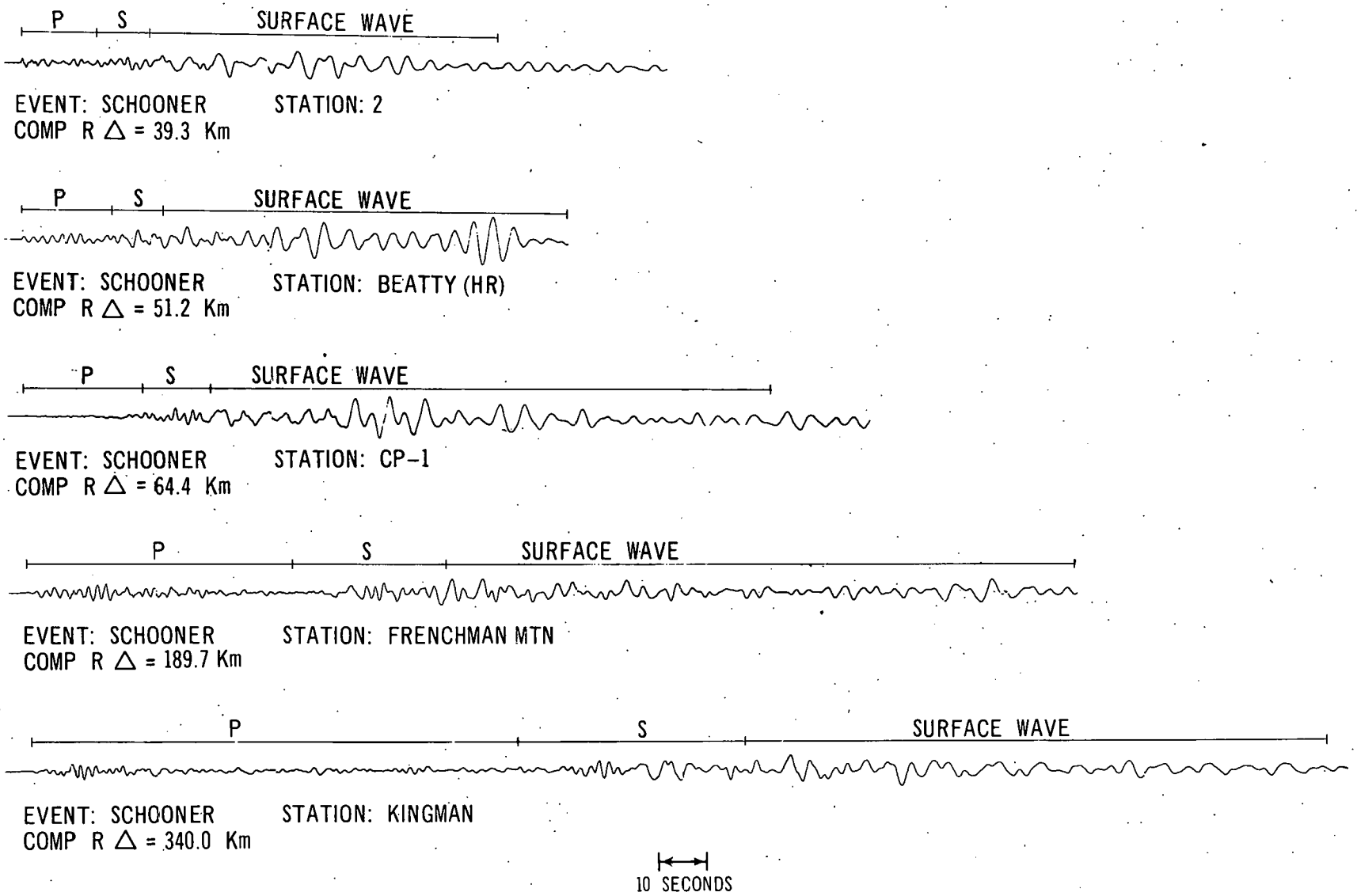

Figure 4-5. Radial Component of Particle Velocity Recorded at Five Stations Located on Hard Rock - Schooner Event

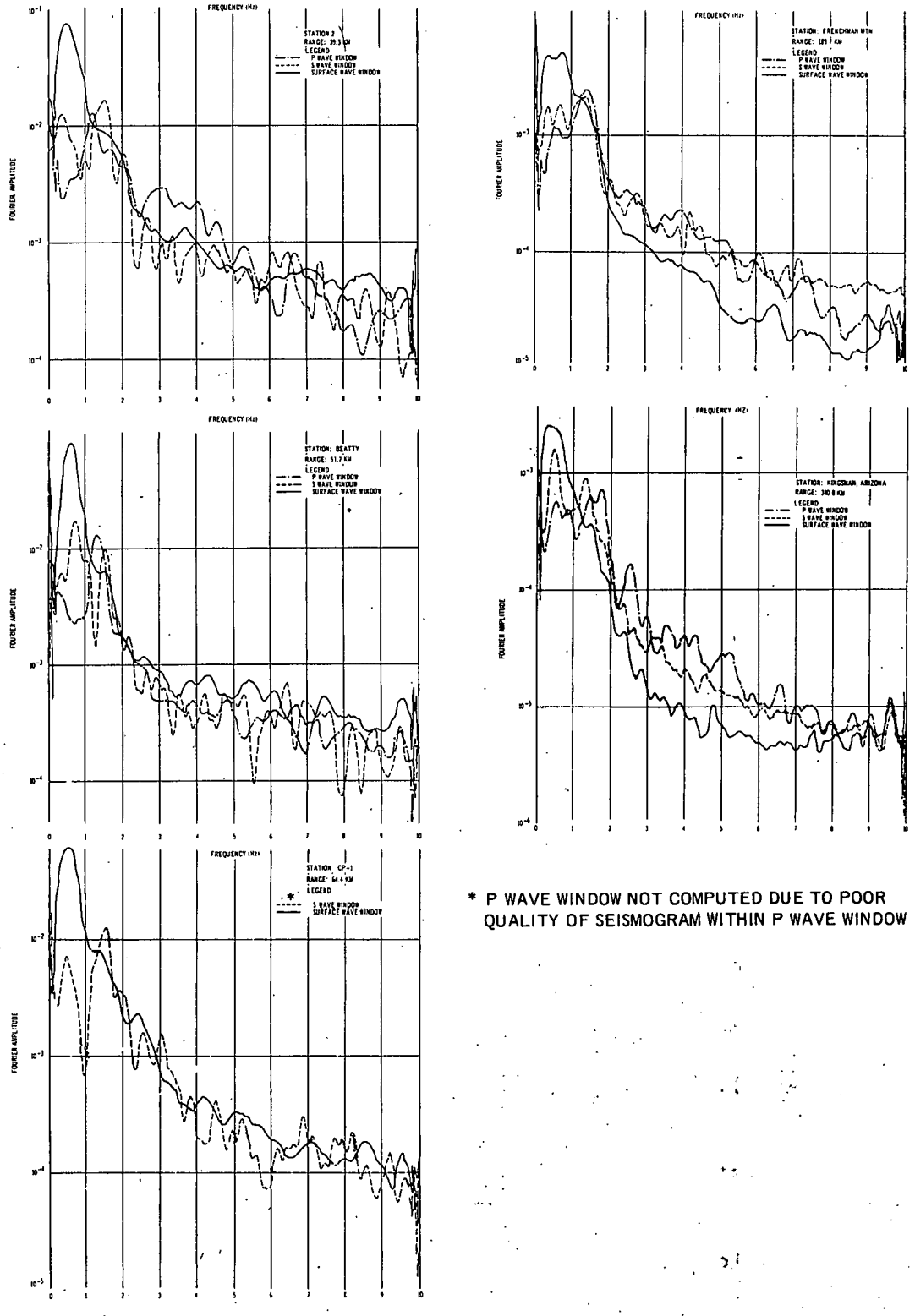

* P WAVE WINDOW NOT COMPUTED DUE TO POOR QUALITY OF SEISMOGRAM WITHIN P WAVE WINDOW

Figure 4-6. Smoothed Fourier Amplitude Spectra of Identified Wave Mode Time Windows - Schooner Event

In summary, the spectral characteristics of the wave mode time windows for Schooner are similar to those observed for contained events (Hays, 1969) with one exception, the apparent dominance of surface wave energy for Schooner. Additional analysis is required to extend this observation to all cratering events.

4.4 FREQUENCY DEPENDENT AMPLIFICATION

Amplification of seismic motion at recording stations located on alluvium has been noted since the early days of seismology. Haskell (1953), Hannon (1964), Davis and Murphy (1967), Murphy and Davis (1969) and a number of others since 1930 have shown that the shallow low velocity layers of the earth's crust act as a filter with respect to the seismic energy arriving at a seismograph station and significantly affect the ground motion.

The transfer function of the layered system is a complex function which has been shown to involve several variables (Davis and Murphy, 1967):

1. The elastic wave type (P, S, Rayleigh, Love)

2. The angle of incidence of the incident wave

3. The physical parameters (thickness, density, rigidity, compressional and shear-wave velocities) of the layered system and the underlying rock.

In actual practice, only the amplitude term of the transfer function is used to calculate a frequency dependent amplification factor for the layered system.

A practical procedure to determine the frequency dependent amplification of a layered system to a seismic input generated by an underground nuclear explosion is to use the seismograms measured at adjacent stations; one located on hard rock and the other on alluvium (or a low velocity surface layer). The basic assumption is made that the input at the base of the alluvium layer is the same as the output measured at the hard rock station; therefore, the amplification factor can be determined by dividing the Fourier amplitude spectrum of the seismic energy measured at the alluvium site by the Fourier amplitude spectrum of the seismic energy measured at the hard rock site. The time history of the seismogram is divided into P, S, and surface wave mode windows, as described in 4.2, and the ratio of the Fourier amplitude spectra of corresponding wave mode windows is taken to determine the amplification factor as a function of a particular incident wave type. Seismic measurements at the pair of stations at Tonopah, Nevada, are well suited for an analysis of this type. The Tonopah Motel station is located on approximately 30 feet of unconsolidated fill overlying dacite. The Tonopah Church station, located about 600 feet away, is on the same material which underlies the Motel station. Thus, it seems reasonable that the output measured at the Church station is identical to the input at the base of the fill at the Motel station.

Figure 4-7 illustrates the radial component of particle velocity recorded at the two Tonopah stations from the Schooner event. The wave mode time windows are identified on the figure.

Fourier amplitude spectra for each of the wave mode windows of Figure 4-7 are shown in Figure 4-8 for the two Tonopah stations. The spectra of both stations exhibit peak amplitudes at approximately 1.3 Hz for the P wave window, 1.4 Hz for the S wave window, and 0.5 Hz for the surface wave window; however, the spectral composition at other frequencies is different. Figure 4-9 shows the amplification factor as a function of frequency for each of the three wave mode windows. The amplification factor is greatest for the P wave window, being a factor of 10 at 7.5 Hz. Amplification factors of 8 at 8.5 Hz and 4 at 6.2 Hz are observed for the S and surface wave windows respectively. The theoretical amplification factor for the P and S wave windows are superposed for reference on the corresponding curves in Figure 4-9. Qualitative agreement between observation and theory is noted showing that the amplification due to the layered system is independent of whether the input energy source is a cratering or a contained nuclear detonation. Lack of agreement between observation and theory is related to the fact that the theoretical model considers a single input pulse at the base of the layered system, whereas the observed P wave (or S wave) window contains several pulses

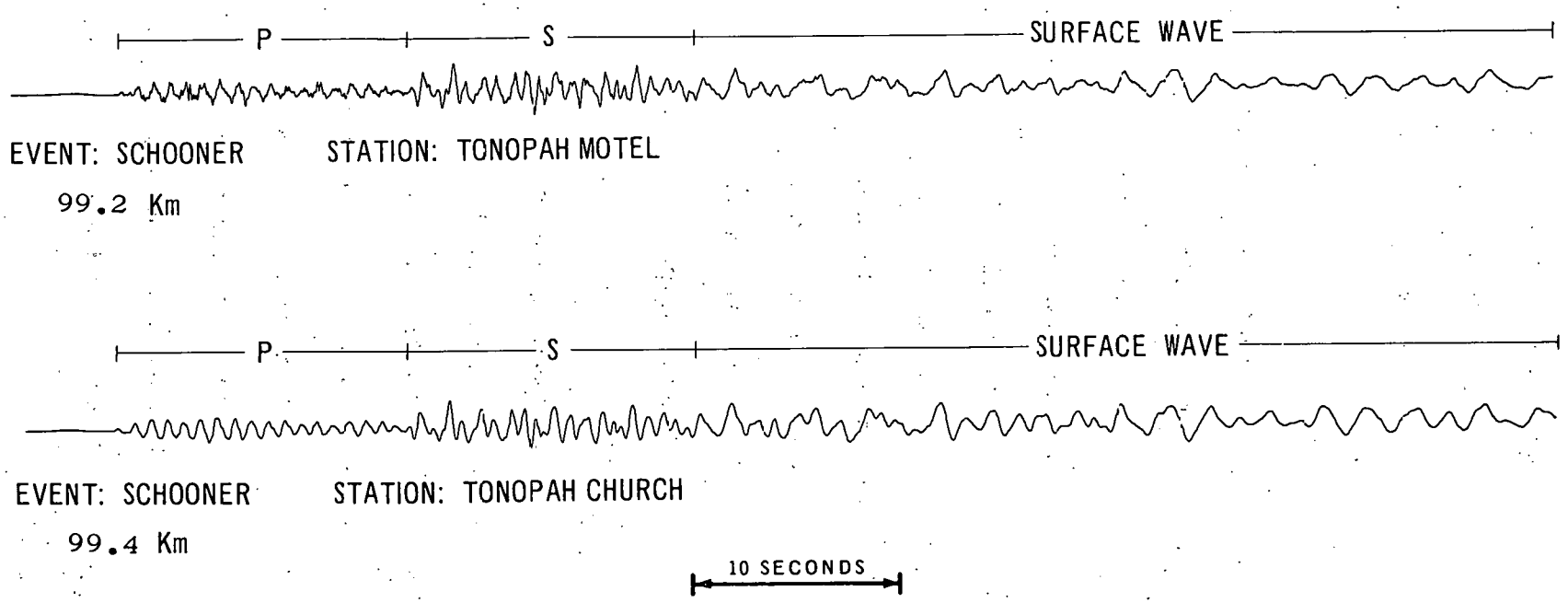

Figure 4-7. Radial Component of Particle Velocity Recorded at Tonopah Church and Tonopah Motel, Schooner Event

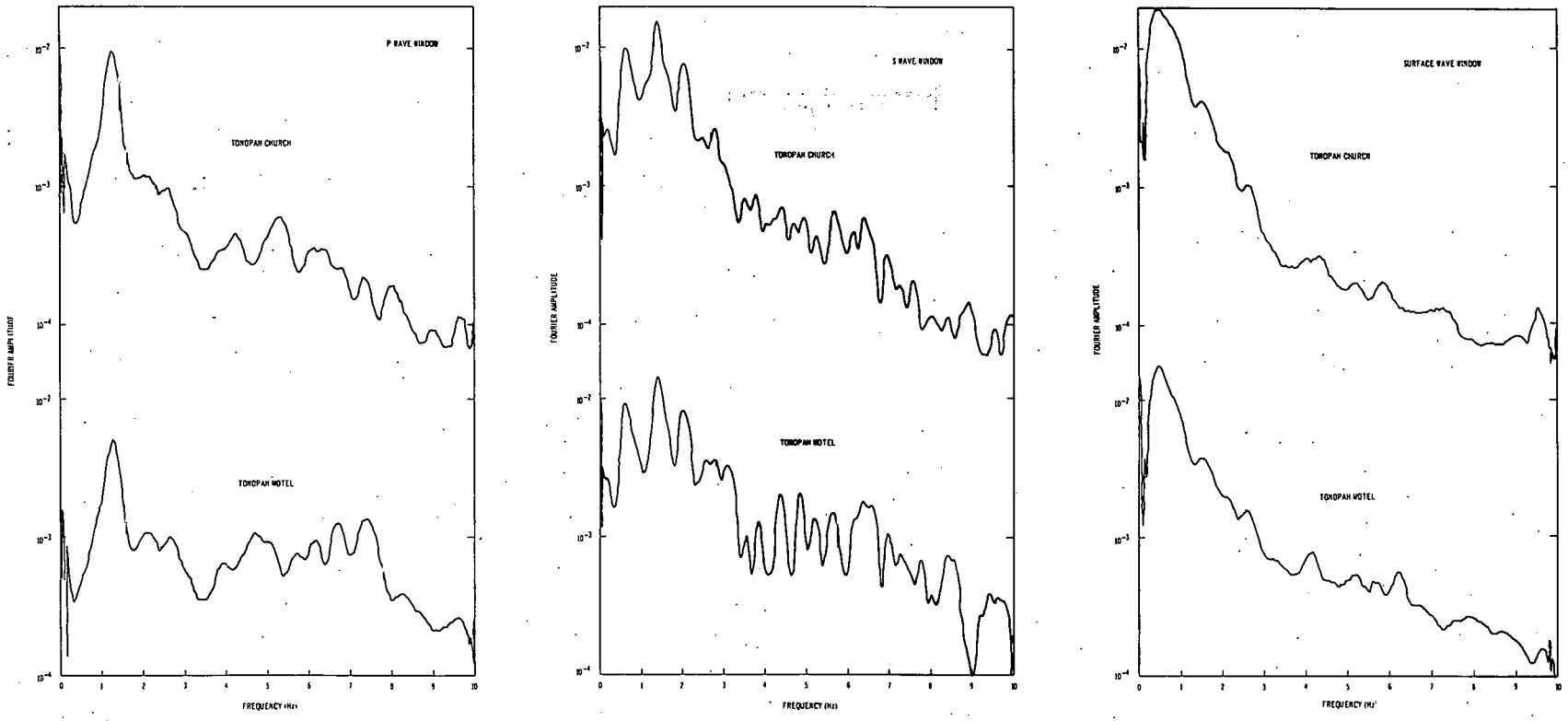

Figure 4-8. Smoothed Fourier Amplitude Spectra of Identified Wave Mode Time Windows, Tonopah Stations - Schooner Event

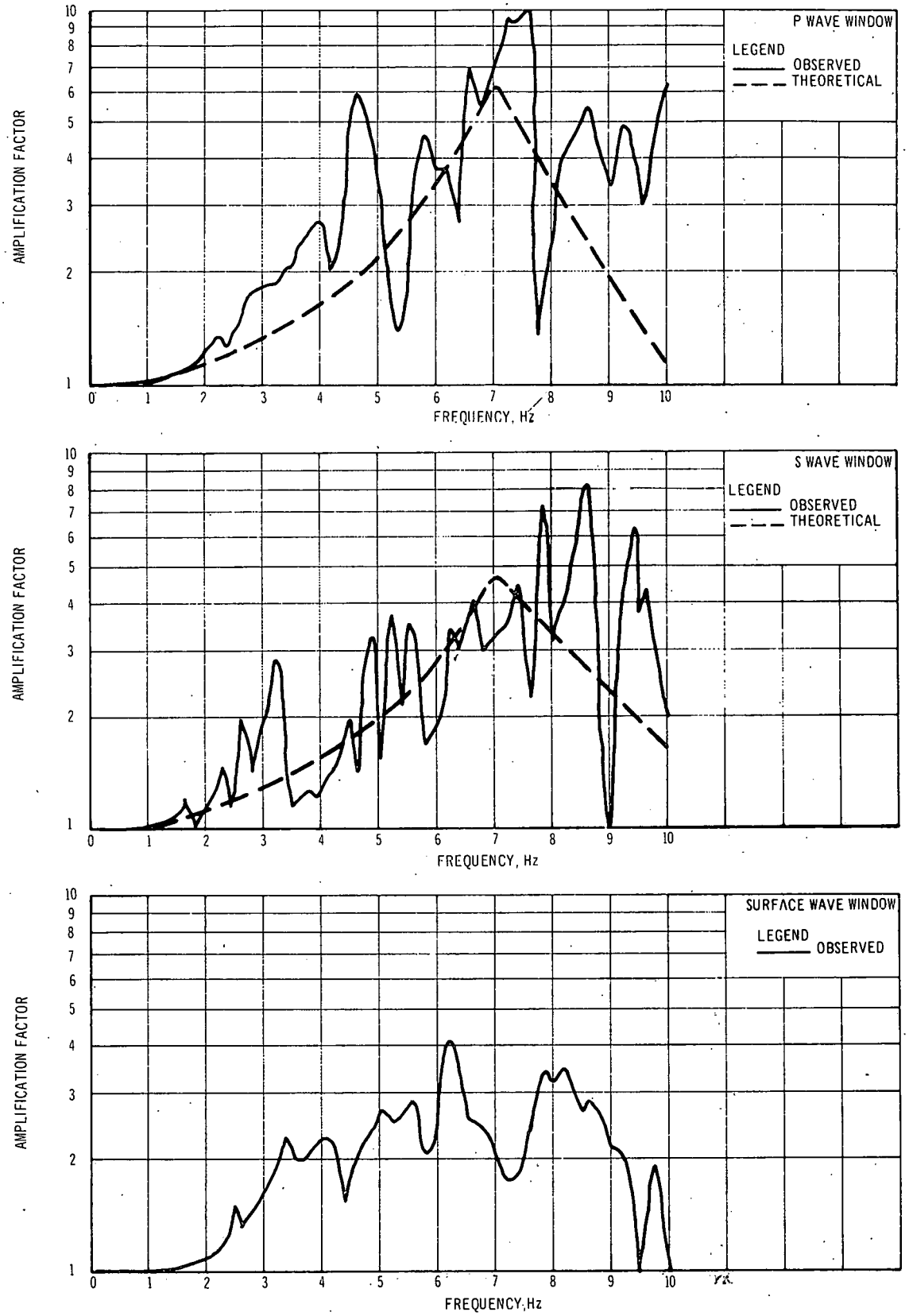

Figure 4-9. Amplification Factor as a Function of Frequency, Tonopah Stations - Schooner Event

(such as the direct wave, the critically refracted wave from the Mohorovicic discontinuity, and the reflected wave from the Mohorovicic discontinuity).

Table 4-4 shows the comparison of the peak vector motions recorded at the Tonopah Church and Tonopah Motel stations from Schooner with the peak motion expected on the basis of the Nevada Test Site prediction equations (Murphy and Lahoud, 1969). Note that the peak particle vector motions recorded at Tonopah from Schooner are lower than the levels of motion expected on the basis of average NTS experience, with the exception of the peak particle velocity recorded at Tonopah Motel which is only slightly higher. This observation is contrary to NTS experience, because the measurements at Tonopah Motel from contained detonations are nearly always higher than the average predicted values.

STATION	MEASURED PEAK VECTOR MOTION			PREDICTED PEAK VECTOR MOTION		
	Acceleration (g)	Velocity (cm/sec)	Displacement (cm)	Acceleration (g)	Velocity (cm/sec)	Displacement (cm)
Tonopah Church	1.87×10^{-4}	2.13×10^{-2}	4.14×10^{-3}	7.0×10^{-4}	5.0×10^{-2}	1.3×10^{-2}
Tonopah Motel	2.83×10^{-4}	2.30×10^{-2}	4.22×10^{-3}	1.6×10^{-3}	1.2×10^{-2}	3.6×10^{-2}

TABLE 4-4. COMPARISON OF MEASURED AND PREDICTED PEAK VECTOR PARTICLE MOTIONS AT TONOPAH CHURCH AND TONOPAH MOTEL, SCHOONER EVENT

An explanation for the lower level of peak vector particle motions recorded at the Tonopah stations from Schooner is related to differences in the seismic spectral composition for equivalent yield cratering and contained events and to the decreased seismic energy efficiency of cratering events as compared to normal contained events. Chapter 5 will compare the seismic energy efficiency of Schooner with other underground nuclear detonations.

CHAPTER 5

SEISMIC ENERGY EFFICIENCY

The objective of this chapter is to determine the amount of energy from underground nuclear explosions which goes to form elastic waves in the far-field radiation zone. This subject has been studied by other investigators for nuclear events, notably by Carder, et. al. (1958 and 1961), Berg , et. al. (1964), Lowrie and Mickey, (1965) and Trembly and Berg, (1966).

The approach taken in this study is to develop the analytic solution of the spherically symmetric Sharpe's problem into an energy equation. The parameters appearing in the equation are evaluated through a self-consistent method within the theory. In principal, once the elastic radius and pressure function acting at the elastic radius are determined, the seismic energy can be calculated with this model.

5.1 THEORY AND ANALYSIS

The displacement potential for wave motion produced by a spherically symmetric exponential pressure function acting in an ideally elastic medium has been derived by Sharpe (1942) and can be stated as

$$\phi = \frac{ap_0}{\rho r \left[(\omega_1/\sqrt{2} - \alpha)^2 + \omega_1^2\right]} \qquad (5\text{-}1)$$

$$\left\{-e^{-\alpha\tau} + e^{-\omega_1\tau/\sqrt{2}} \left[(1/\sqrt{2} - \alpha/\omega_1) \sin \omega_1\tau + \cos \omega_1\tau\right]\right\}$$

$$\text{for } \tau \geq 0$$

$$= 0 \qquad \text{for } \tau < 0$$

where the pressure function acting at the elastic radius (r = a), i.e., the radius at which the medium behaves elastically, is

$$p = p_0 e^{-\alpha\tau} \quad \text{for } \tau \geq 0 \qquad (5\text{-}2)$$

$$= 0 \qquad \text{for } \tau < 0,$$

p_0 is the peak pressure, α is the decay constant = $1/T_0$, T_0 is the time for the pressure to decay to $p_0 e^{-1}$, τ is the retarded time = $t - \frac{(r-a)}{c}$, $\omega_1 = 2\sqrt{2}\ c/3a$, c is the compressional velocity, r is the radial distance from the source, ρ is the density of the medium, and Lame's constants, λ and μ, are assumed equal (Poisson's ratio = 0.25). From the displacement potential ϕ, the displacement in the medium can be determined easily from the relationship $u = \frac{\partial\phi}{\partial r}$, where u is the displacement. The decay time, T_0,

is assumed proportional to the elastic radius, a. The decay constant may then be written as $\alpha = 1/T_0 = k\omega_0$, where $\omega_0 = c/a$. The parameter k, in general, may be a function of the shot point parameters, but, as will be shown later, is not expected to be very sensitive. With the above substitution, the displacement may be calculated to be

$$u = \frac{9ap_0}{4\rho c^2} \left(\frac{a}{r}\right) \left\{\left(\frac{a}{r} - k\right) \frac{e^{-k\omega_0\tau}}{(3-3k+9k^2/4)} - \frac{e^{-2\omega_0\tau/3}}{\sqrt{2(3-3k+9k^2/4)}}\right.$$

$$\left.\left[\left(\frac{a}{r}\right) \sin(\omega_1\tau+\theta_1) - \frac{2\sqrt{3}}{3} \sin(\omega_1\tau+\theta_1-\theta_2)\right]\right\} \qquad (5\text{-}3)$$

where

$$\theta_1 = \tan^{-1} \frac{\sqrt{2}}{1-3k/2}$$

$$\theta_2 = \tan^{-1} \sqrt{2}$$

Particle velocity, $v = \partial u/\partial t$, is

$$v = \frac{3p_0}{2\rho c} \left(\frac{a}{r}\right) \left\{-\frac{3}{2} k \left(\frac{a}{r} - k\right) \frac{e^{-k\omega_0\tau}}{(3-3k+9k^2/4)} + \frac{e^{-2\omega_0\tau/3}}{\sqrt{2(3-3k+9k^2/4)}}\right.$$

$$\left.\left[\sqrt{3} \left(\frac{a}{r}\right) \sin(\omega_1\tau+\theta_1-\theta_2) - 2 \sin(\omega_1\tau+\theta_1-2\theta_2)\right]\right\} \qquad (5\text{-}4)$$

It is to be noted in equation (5-4) that the velocity has a $1/r$ and $1/r^2$ dependence. The far field radiation zone consists of the $1/r$ term only, since the $1/r^2$ term becomes negligibly small at large distances. The far field part of the velocity may thus be written as

$$v_{ff} = \frac{3p_o}{2\rho c}\left(\frac{a}{r}\right)\left\{\frac{3}{2}k^2\,\frac{e^{-k\omega_o\tau}}{(3-3k+9k^2/4)}\right. \qquad (5\text{-}5)$$

$$\left. -\frac{\sqrt{2}\,e^{-2\omega_o\tau/3}\sin(\omega_1\tau+\theta_1-2\theta_2)}{\sqrt{(3-3k+9k^2/4)}}\right\}$$

The instantaneous kinetic energy density corresponding to the far field is $1/2\,\rho v_{ff}^2$. Assuming spherical divergence, the total seismic energy (assuming that the total energy is twice the kinetic energy) is

$$E = 4\pi r^2 \rho c \int_0^\infty v_{ff}^2\, dt \qquad (5\text{-}6)$$

where $r \geq a$. For convenience, r is chosen to be a. Thus,

$$E = 4\pi a^2 \rho c \int_0^\infty v_{ff}^2 \Big|_{r=a} dt \qquad (5\text{-}7)$$

Substitution of equation (5-5) in equation (5-7) and integrating gives the seismic energy,

$$E = \frac{\pi P_o^2 a^3}{2\mu} K \qquad (5\text{-}8)$$

where

$$K = \frac{12k^3 - 4k^2 + 16}{9k^4 + 8k^2 + 16}$$

and μ is the modulus of rigidity. This expression determines the seismic energy input at the elastic radius of underground explosions, assuming that most of the motion is radially compressional at that radius, which is a good approximation for tamped nuclear explosions (Ferret (1968b)).

For a step function, k = 0, giving a K value of 1, and the radiated energy is simply

$$E_{STEP\ FN} = \frac{\pi p_o^2 a^3}{2\mu} \qquad (5\text{-}8a)$$

which is a result that Latter, et.al. (1961a), have obtained for the case of a step function.

In order to evaluate the energy expression (equation 5-8), determinations of p_o, a, k and μ are required. It is assumed that the medium "on the large" has low tensile strength and that the limiting pressure, p_o, is therefore in the neighborhood of the overburden pressure (Latter, et.al., 1961, a and b; and Kisslinger, 1963), in order to keep the medium from going into tension and propagating cracks. Poisson's ratio is taken to be 0.25 and μ is thus equal to $c^2\ \rho/3$.

A determination of the elastic radius, a, can be obtained from the amplitude spectra of the particle velocities. The Fourier transform of the displacement for Sharpe's problem at a distance r, has been obtained by Latter, et.al. (1959), as

$$\hat{Z}(\omega) = \frac{\hat{p}a}{4\mu}\left(\frac{1}{r^2} + \frac{i\omega}{rc}\right)\frac{c^2}{\omega_o^2 + i\omega_o\omega - \beta\omega^2} \qquad (5\text{-}9)$$

where ω is the angular frequency, $\beta = (\lambda+2\mu)/4\mu$, $\hat{p}$ is the Fourier transform of the pressure function at a, and the other quantities have been previously defined.

For $r >> c/\omega$, the amplitude spectrum of the displacement is

$$|\hat{Z}| = \frac{a\omega c}{4\mu r} \left| \frac{\hat{p}}{(\omega_o^2 - \beta\omega^2) + i\omega_o\omega} \right| \qquad (5\text{-}10)$$

and the amplitude spectrum of the velocity is simply

$$|\hat{v}| = \omega |\hat{Z}|$$

The Fourier transform of the exponential pressure function is

$$p = \frac{p_o}{\alpha + i\omega}$$

and

$$|\hat{p}| = \frac{p_o}{\sqrt{\alpha^2+\omega^2}}$$

The velocity amplitude spectrum then becomes, with the substitution $a = k\omega_o$,

$$|\hat{v}| = \frac{ap_o}{4\mu r} \cdot \frac{\omega^2}{[\beta^2\omega^6+(\beta^2k^2-2\beta+1)\omega_o^2\omega^4+(k^2-2\beta k^2+1)\omega_o^4\omega^2+k^2\omega_o^6]^{1/2}} \quad (5\text{-}11)$$

Taking the derivative of $|\hat{v}|$ with respect to ω and equating to zero, gives the dimensionless equation

$$\beta^2\left(\frac{\omega_m}{\omega_o}\right)^6 - (k^2-2\beta k^2+1)\left(\frac{\omega_m}{\omega_o}\right)^2 - 2k^2 = 0 \quad (5\text{-}12)$$

$$\omega_o = c/a$$

which specifies the extreme points, ω_m, of the velocity amplitude spectrum. Figure 5-1 shows a plot of ω_m/ω_o versus k, for a Poisson's ratio = 0.25 ($\beta = 0.75$). Note that equation (5-12) only applies in the far field. Thus, if the frequency of maximum amplitude lies around 2 Hz and c = 5 km/sec, $r >> c/\omega_m$ or $r >> 400$ m ensures that the observation distance r, lies in the far field. In practice, to determine an elastic radius from equation (5-12), a value of k and ω_m are needed. If there is significant shear and/or surface wave motion, the frequency of maximum amplitude is determined from the compressional wave window (i.e., the time window on the

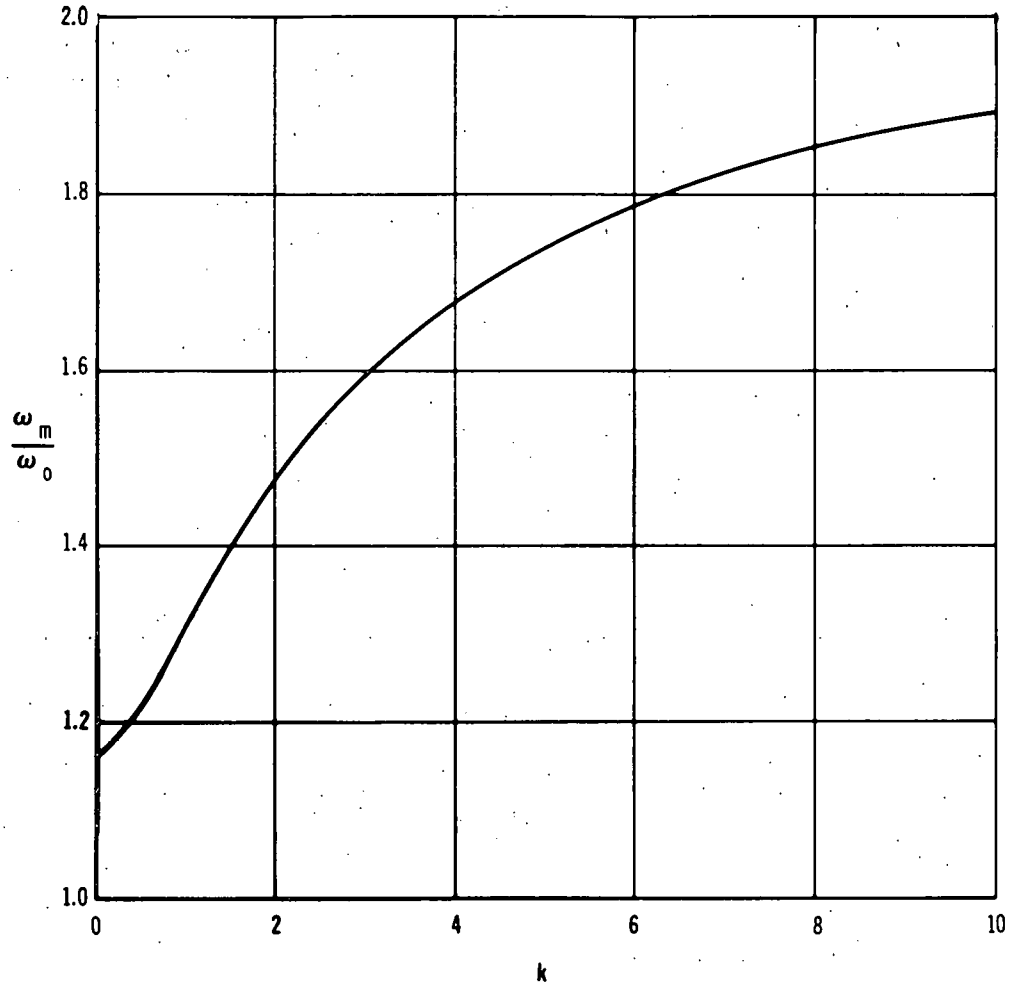

Figure 5-1. Ratio of the Frequency (ω_m) of Peak Spectral Amplitude and Resonant Cavity Frequency (ω_o) Versus the Parameter k

seismogram which is predominantly composed of longitudinal motion) since this model only holds for compressional waves. Although the observation distance must be in the far field, it must be small with respect to the differential attenuation effects of the earth. This would be a function of the dominant frequency content of the compressional waves.

In order to evaluate the constant k, equation (5-12) and the relation $\alpha = k\omega_o$ are used to give the relationship

$$\beta^2 \left(\frac{\omega_m}{\alpha}\right)^6 k^4 + (2\beta-1)\left(\frac{\omega_m}{\alpha}\right)^2 k^2 - \left(\frac{\omega_m}{\alpha}\right)^2 - 2 = 0 \qquad (5\text{-}13)$$

Figure 5-2 shows a plot of k versus (ω_m/α), for a Poisson's ratio of 0.25. It is seen that for a constant ratio of (ω_m/α), k is constant for a particular Poisson's ratio. In general, k is to be considered a function of the shot point parameters. However, k is not expected to vary significantly, since the ratio (ω_m/α) which is proportional to decay time of the pressure pulse at the elastic radius/dominant period of seismic motion should not vary significantly.

The parameter k can be evaluated from a combination of free-field data and far field seismic data. The free-field data give a determination of α, and seismic data determines ω_m.

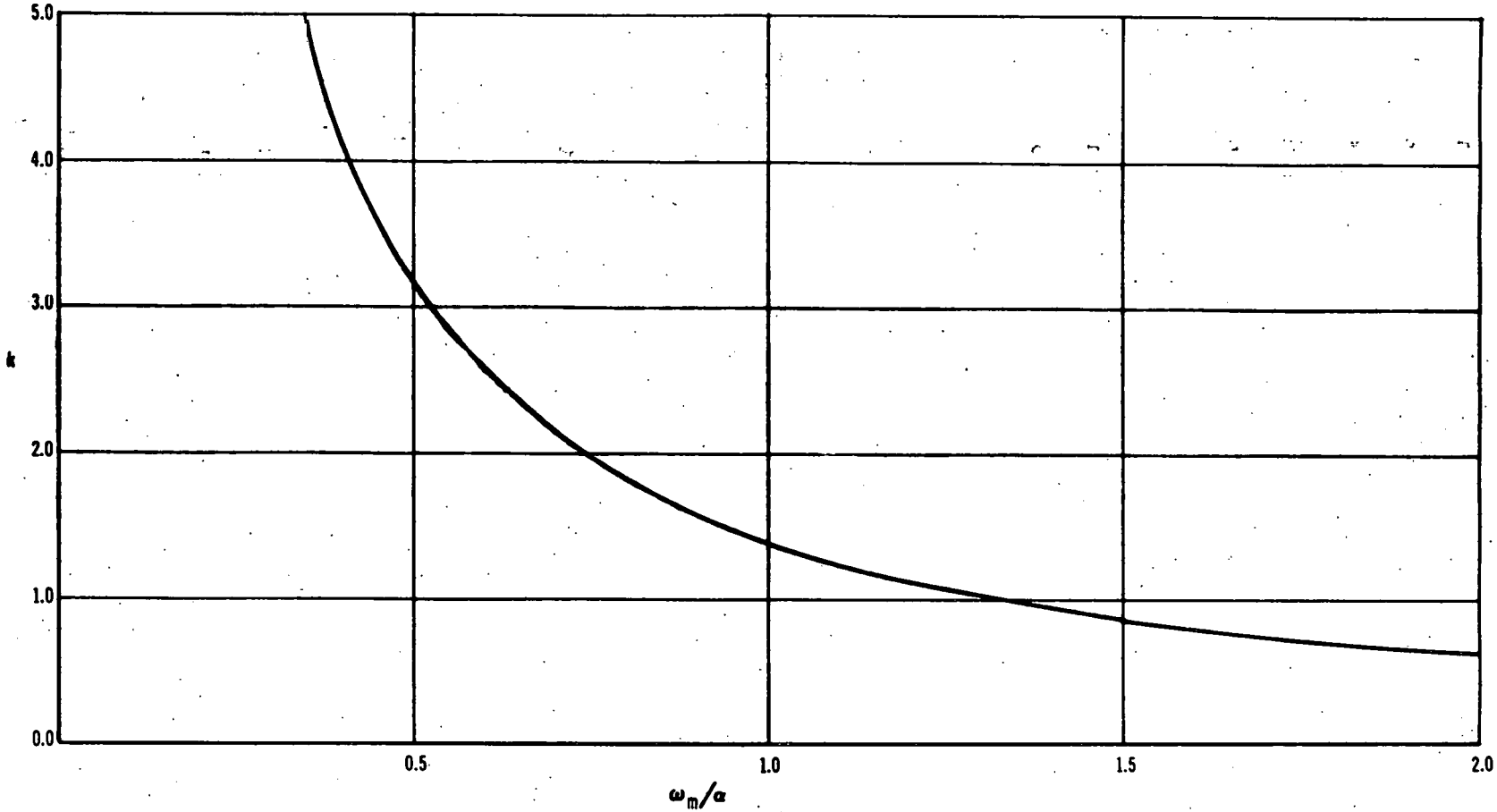

Figure 5-2. The Parameter k Versus the Ratio of the Frequency (ω_m) of Peak Spectral Amplitude and the Decay Constant (α)

5.2 EXAMPLES OF SEISMIC ENERGY EFFICIENCY COMPUTATIONS

The seismic energy efficiency was determined for four contained nuclear detonations (Shoal, Salmon, Boxcar, and Benham), a decoupled nuclear detonation (Sterling), and the nuclear cratering detonation (Schooner). These six events provide an adequate data sample, since they encompass a wide range of yields and physical conditions. Details of the computation performed for each detonation are given below.

Salmon. For the Salmon event (described in Table 5-1), free-field measurements from Perret (1968a) indicate a T_o = 20 msec, which gives α = 50/sec. The band-pass filter spectra which are approximations to Fourier amplitude spectra from the compressional wave windows of stations 10-South (18 km) and 20 South (31 km) are shown in Figures 5-3 and 5-4. Radial horizontal and vertical components of particle motion are shown. The frequency of maximum amplitude, f_m, is estimated to be about 4 Hz. This gives a value of (ω_m/α) of 0.50, and from Figure 5-2, a k value of 3.20. Figure 5-1 gives the relationship $\omega_m = 1.61\ \omega_o$, from which the elastic radius can be evaluated, $a = \frac{1.61c}{\omega_m}$. Using a compressional velocity of 4.67 km/sec gives a_{Salmon} = 299 meters, which corresponds to a peak shock pressure of 370 bars (Perret, 1968). The overburden pressure is 180 bars, which indicates that the limiting pressure p_o = 370 bars is 2.06 times the overburden pressure. Inserting these numbers into equation (5-8) for the seismic energy gives a seismic efficiency (seismic energy/initial energy available) of 5.8%.

TABLE 5-1. RESULTS OF SEISMIC ENERGY CALCULATIONS

Event	Shoal	Salmon	Boxcar	Benham	Schooner	Sterling
Shot Location	Sand Springs Range, Nevada	Tatum Salt Dome, Mississippi	Pahute Mesa, Nevada	Pahute Mesa, Nevada	Pahute Mesa, Nevada	Tatum Salt Dome, Mississippi
Type	Nuclear Contained	Nuclear Contained	Nuclear Contained	Nuclear Contained	Nuclear Cratered	Nuclear Decoupled
Yield (kt)	12.5	5.3	1200	1100	30	0.38
Depth of Burial (ft)	1205	2716	3822	4630	353	2716
Scaled Depth ($ft/kt^{1/3}$)	519	1552	354	447	107	3751
Medium	Granite	Salt	Rhyolite	Tuff	Tuff	Salt
Density(gm/cc)	2.55	2.2	2.1	2.25(av.)	2.23	2.2
Overburden Pressure (bars)	92	180	237	311	236	180
Compressional Velocity (km/sec)	5.55	4.67	3.84	3.66(av.)	3.41	4.67
f_m (Hz)	2.5	4.0	0.75	0.8	1.25	36.0
Seismic Energy Radiated (kt)	2.3×10^{-1}	3.1×10^{-1}	5.5×10^{-1}	6.7×10^{1}	9.5×10^{-2}	3.14×10^{-5} (1.3×10^{15} ergs)
Seismic Energy Efficiency (%)	1.8	5.8	4.6	6.1	0.32	0.008

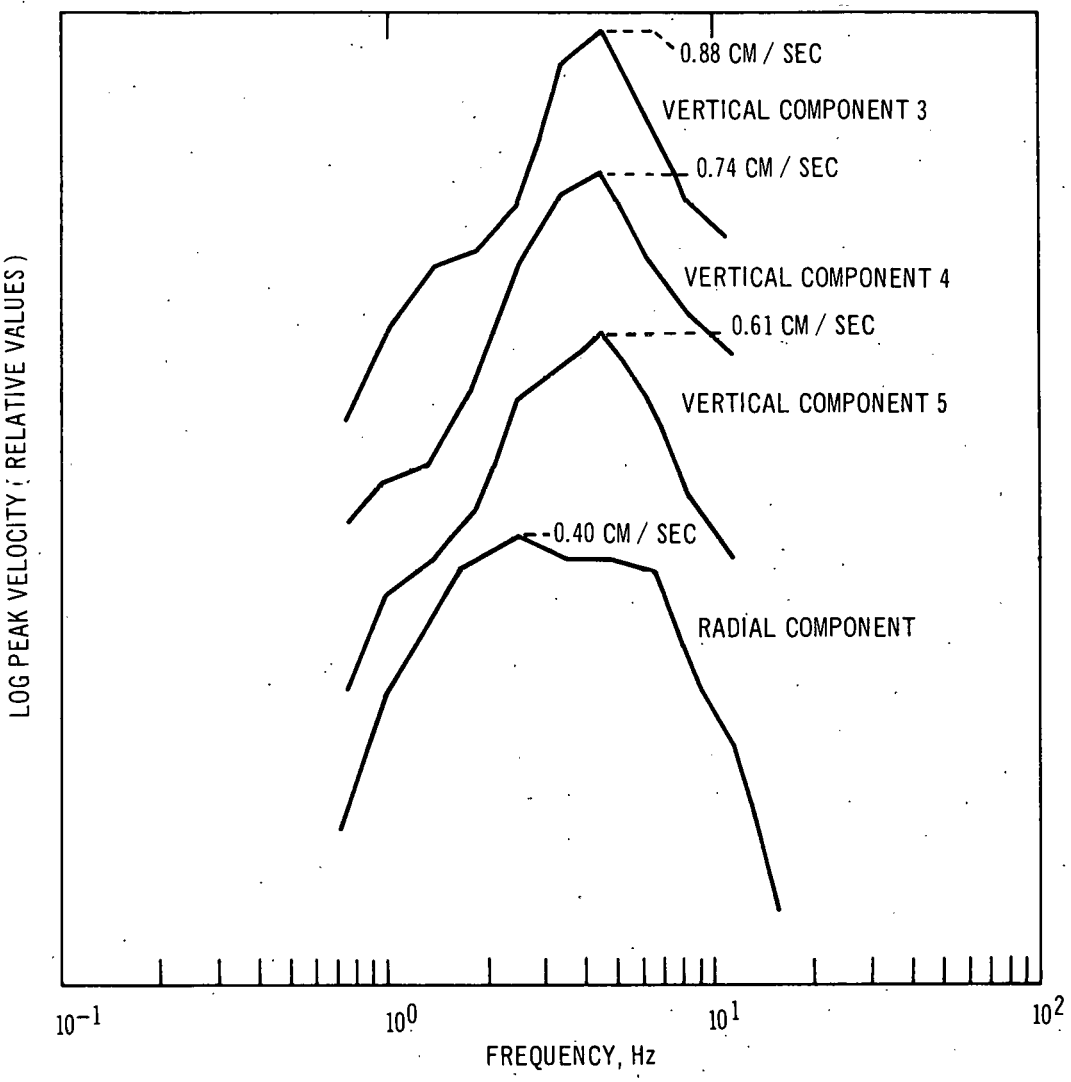

Figure 5-3. Particle Velocity Band-Pass Filter Spectra of the Compressional Wave Window, Salmon Event, Station 10-South (18 km)

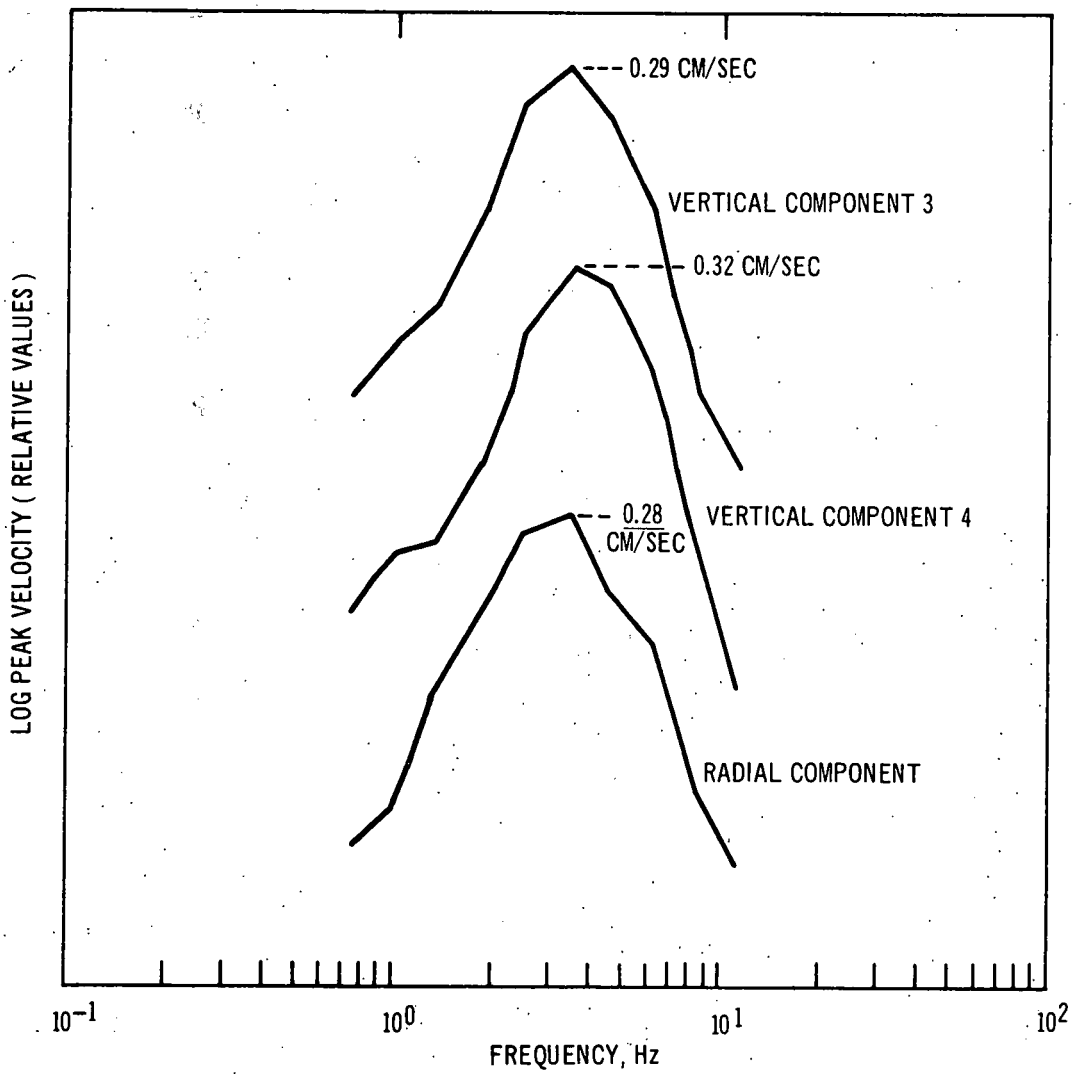

Figure 5-4. Particle Velocity Band-Pass Filter Spectra of Compressional Wave Window, Salmon Event, Station 20-South (31 km)

Shoal. For the Shoal event (described in Table 5-1), free-field measurements from Weart (1965) give an average T_o of 70 msec and α = 14.3/sec. The spectra (Perret, 1967 and Weart, 1965) are not very definitive. They give an estimate of f_m between 2.0 and 3.0 Hz or approximately 2.5 Hz. Thus, ω_m/α is 1.13 and k is 1.22. From Figure 5-1, $\omega_m = 1.35\ \omega_o$, and using a compressional velocity of 5.55 km/sec gives a_{Shoal} = 477 meters which corresponds to a peak shock pressure of about 145 bars (Weart, 1965) Overburden pressure is about 92 bars, and the limiting pressure is 1.58 times as great. Evaluation of the seismic energy gives a seismic efficiency of 1.8%. Trembly and Berg (1966) found a seismic efficiency of 0.7% from experimental observations of the Shoal event. Their theoretical model gave a seismic efficiency of approximately 2% in the southwestern quadrant. Also, they determined an average elastic radius of 510 meters which is comparable with the value of 477 meters determined here.

In general, to determine an elastic radius without free-field measurements, a value of k between 1 and 4 is appropriate. Using an average value of the ratio $\left(\frac{\omega_m}{\omega_o}\right)$ from Figure 5-1, gives the relationship $a = 1.5\ c/\omega_m \pm 13\%$. Although this uncertainty can be tolerated in determining the elastic radius, it would lead to a considerably larger uncertainty in the seismic energy, since the elastic radius appears as a^3. Also there would be uncertainty in the function K appearing in the energy formula. However, this difficulty can be effectively eliminated by rewriting equation (5-8) as

$$E = \frac{\pi p_o^2 c^3}{2\mu\, \omega_m^3} \left[K \left(\frac{\omega_m}{\omega_o} \right)^3 \right] \qquad (5\text{-}14)$$

where the function $K \left(\frac{\omega_m}{\omega_o} \right)^3$, plotted versus k in Figure 5-5, is seen to be relatively insensitive to k for the values of k between 0 and 4. Using an average value of 1.5 for the function gives

$$E = \frac{3\pi\, p_o^2\, c^3}{4\mu\, \omega_m^3} \pm 10\% \qquad (5\text{-}15)$$

and p_o is estimated by the average of Salmon and Shoal results, i.e., 1.8 times the overburden pressure.

Boxcar, Benham and Schooner. As described in Table 5-1, Boxcar and Benham were large yield, contained nuclear events detonated in Pahute Mesa, while Schooner was a nuclear cratering event detonated in the same area. Figures 5-6 through 5-8 show compressional wave amplitude spectra of the radial horizontal components of particle motion at surface stations for the particular events (Boxcar spectra were obtained from Hays (1969)). Equation (5-15) in combination with f_m and the elastic parameters was used to compute the seismic energies. Boxcar and Benham show seismic efficiencies of 4.6% and 6.1%, respectively, while Schooner shows a seismic efficiency of 0.32%. The comparison between contained events and the cratering event in Table 5-1 indicates that cratering events have significantly lower seismic efficiencies than contained events.

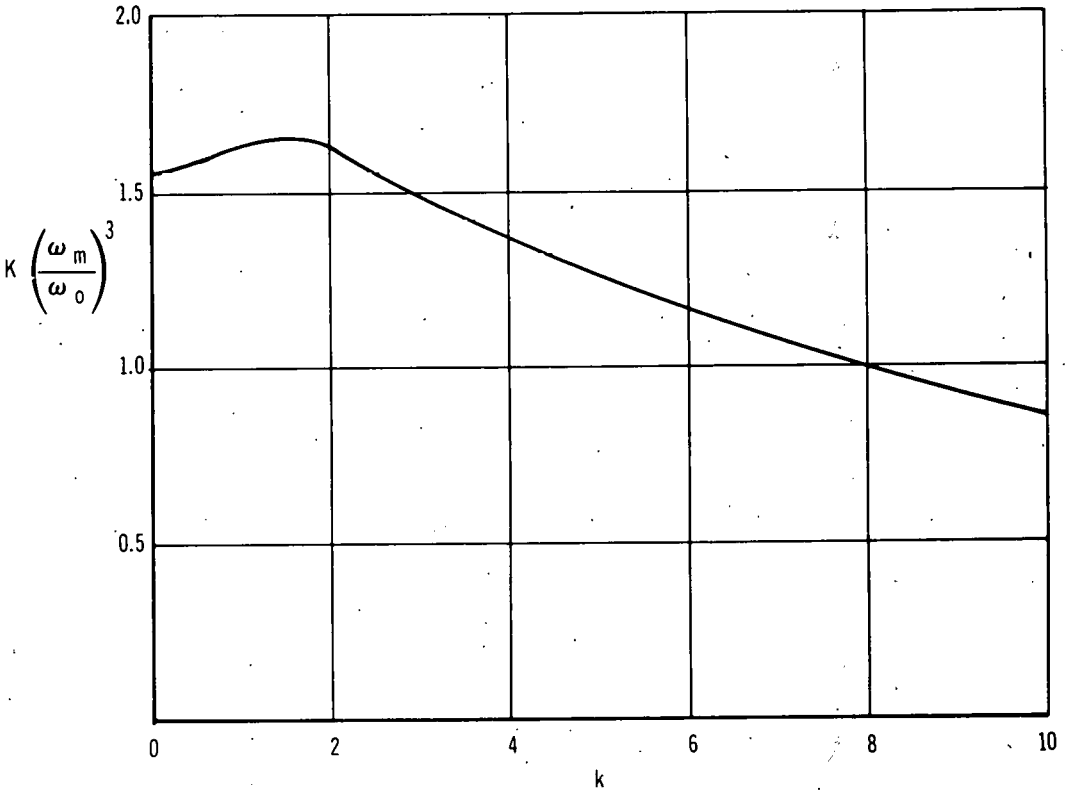

Figure 5-5. The Function K Times the Cube of the Ratio of the Frequency (ω_m) of Peak Spectral Amplitude and Resonant Cavity Frequency (ω_o) Versus the Parameter k

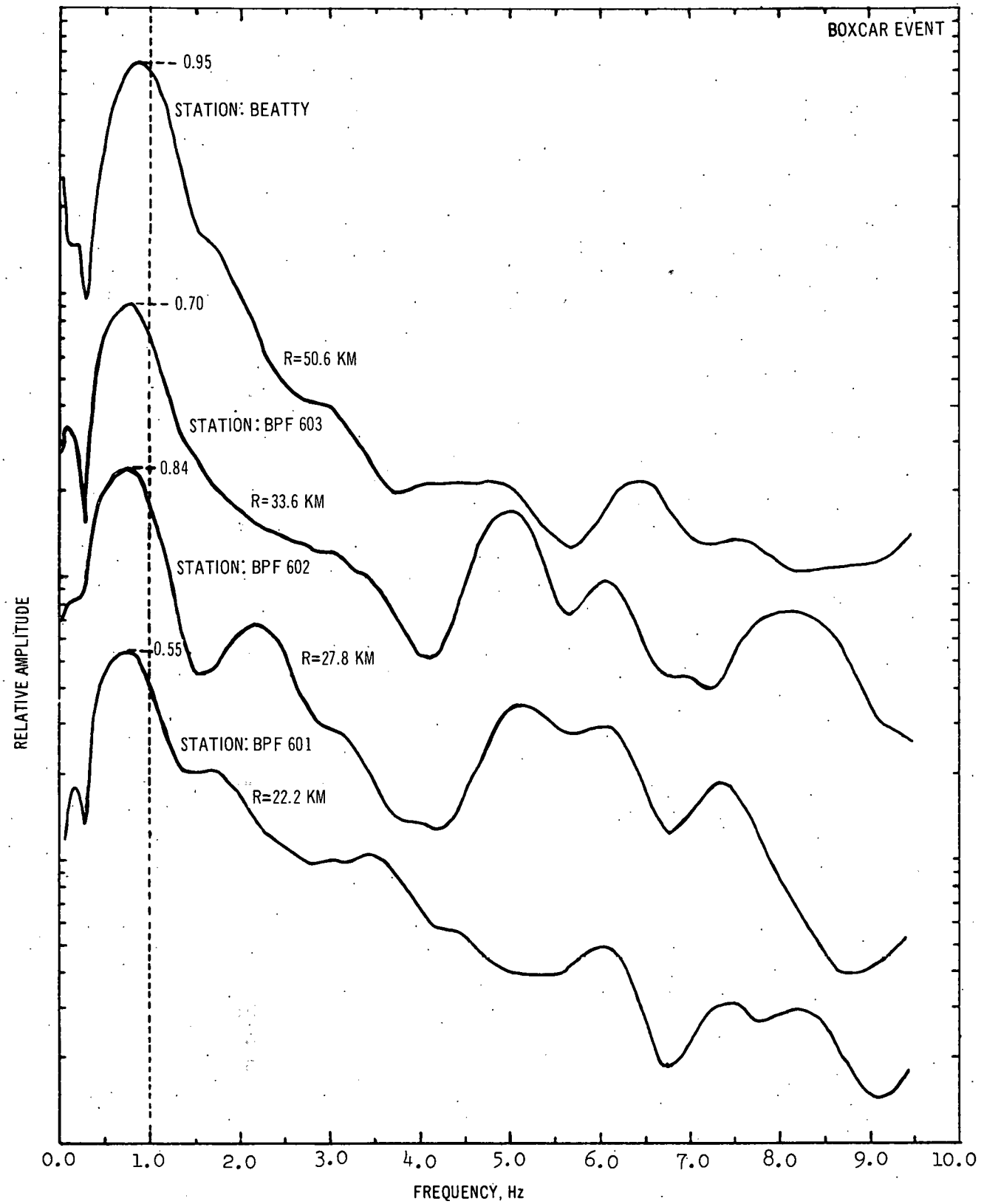

Figure 5-6. Smoothed Fourier Amplitude Spectra of the Compressional Wave Window, Radial Component, Boxcar Event

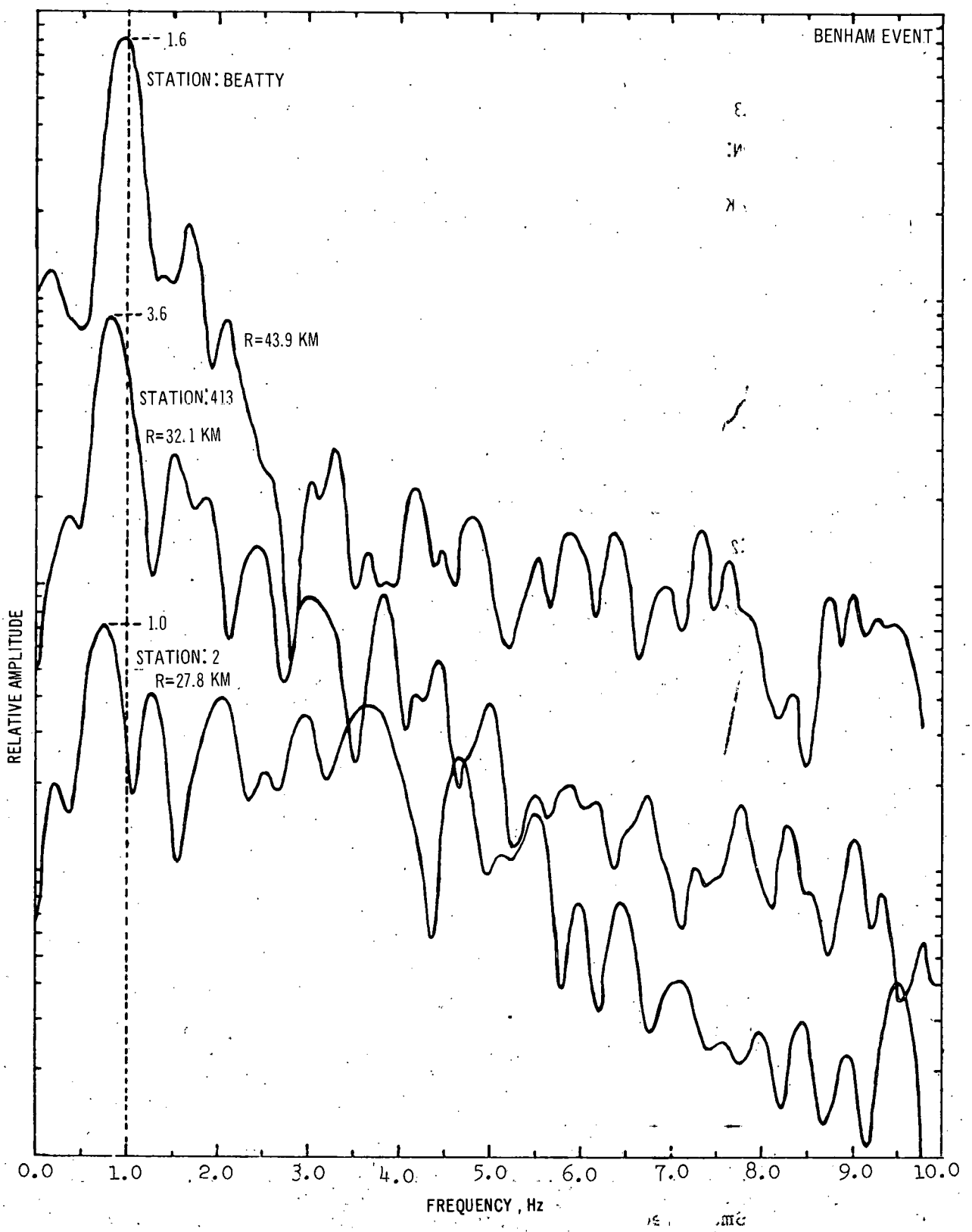

Figure 5-7. Smoothed Fourier Amplitude Spectra of the Compressional Wave Window, Radial Component, Benham Event

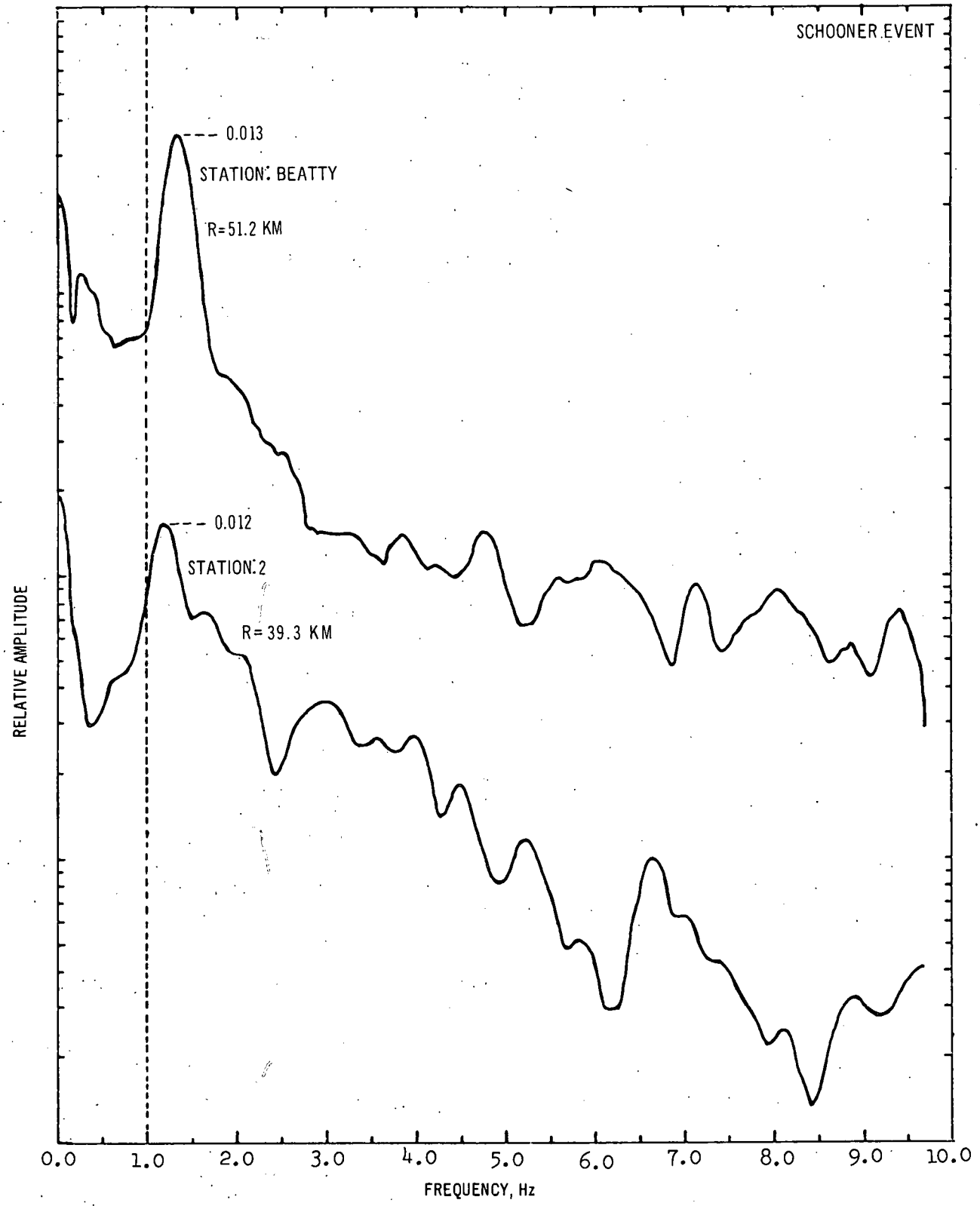

Figure 5-8. Smoothed Fourier Amplitude Spectra of the Compressional Wave Window, Radial Component, Schooner Event

Sterling. The Sterling event was a 380 ton nuclear decoupling shot detonated in the Salmon cavity of 17.4 meters radius. The pressure input at the walls of the cavity consists of a number of spikes oscillating about a mean pressure of about 160 bars. Band-pass spectra at surface stations between 1 and 2 km from the event show a frequency of maximum amplitude around 36 Hz (Davis, 1968). Using the value of (ω_m/ω_o) for a step pressure function (k = 0) from Figure 5-1 gives the relation

$$a = \frac{1.16c}{\omega_m}\Big|_{\text{STEP FN}}$$

which yields an elastic radius of 24 meters. This value of the elastic radius is probably large since the frequencies associated with the ground motion were very high and the differential attenuation effects considerably reduced f_m at 1 and 2 km. This is observed in the spectra obtained at 6 and 7 km where f_m reduces to values between 10 and 20 Hz (Davis,1968). The free-field data of Perret (1968) obtained at distances between 166 and 660 meters indicate f_m's larger than 40 Hz. This evidence indicates that the medium probably behaved elastically at the cavity wall for the step pressure of 160 bars.

Using equation (5-8a) for the seismic energy liberated by a step pressure function in conjunction with an a of 17.4 meters and p_o of 160 bars gives a radiated energy of 1.3×10^{15} ergs, and

a seismic efficiency of 0.0084%. Perret (1968) experimentally found a mean radiated energy of 3×10^{15} ergs which corresponds to a seismic efficiency of 0.019%. The difference in radiated energies may be due to the significant shear motions associated with the event. The ratio of seismic efficiencies of Salmon/Sterling is 690, or 305 if the higher value is used, which indicates a decoupling factor between 200 and 500 in the radiated energy, assuming that a 380 ton tamped event would have the same seismic efficiency as Salmon.

The conclusions to be drawn are that seismic energies determined by the analytic procedure of this chapter are reasonable estimates, and that, in particular, cratering and decoupled events display significantly lower seismic efficiencies than normal contained events.

CHAPTER 6

SUMMARY AND RECOMMENDATIONS FOR ADDITIONAL WORK

Seismic data were measured at 17 seismic stations for the nuclear cratering detonation, Schooner, and were analyzed and compared with corresponding data observed from other cratering and contained nuclear detonations. Peak vector particle velocities were determined for Schooner and compared with normalized data from other detonations. Measured band-pass filter spectra from Schooner were scaled to account for yield and device depth of burial differences and compared with band-pass filter spectra observed from cratering (Cabriolet) and contained detonations (Knickerbocker, Rex, and Duryea). A preliminary determination of the correlation of the amplitude and frequency characteristics of the ground motion generated by Schooner with specific elastic wave type (P, S, surface) time windows was made and compared with the equivalent correlation for the Cabriolet and Benham detonations. The seismic energy efficiency of Schooner was determined analytically and compared with the seismic energy efficiency of four contained nuclear detonations (Shoal, Salmon, Boxcar, and Benham) and one nuclear decoupled detonation (Sterling). The results of these analyses provide additional insight into the important characteristics of ground motion resulting from nuclear cratering detonations.

6.1 SUMMARY OF CONCLUSIONS

The basic conclusions which resulted from the analyses described above are summarized below:

1. Peak Vector Particle Motion - the peak vector particle velocities recorded at both alluvium and hard rock sites (and the derived peak vector accelerations and displacements) agree qualitatively with results obtained from other cratering events and are low relative to the mean value predicted for equivalent yield contained detonations on the basis of Nevada Test Site experience. The velocities observed from Schooner range from about 0.2 to 1.3 of the mean predicted value for alluvium sites and from 0.4 to 0.7 for hard rock sites. Derived accelerations range from 0.2 to 0.6 of the mean predicted value for alluvium stations and from about 0.1 to 0.5 for hard rock sites. Displacements range from 0.1 to 1.1 and from 0.35 to 0.7 for alluvium and hard rock sites respectively. These results agree qualitatively with spectral results on the basis of depth of burial scaling, as noted below.

2. Band-Pass Filter Spectra - band-pass filter spectra observed from Schooner agree, when scaled for yield and device depth of burial, with the spectra from Cabriolet, (cratering detonation) and Knickerbocker, Duryea and Rex (contained detonations). Before scaling for depth of burial, the band-pass filter spectra from cratering detonations are somewhat lower in magnitude than the mean spectra from equivalent parameter contained detonations and the dominant energy content is shifted to the low-frequency end of the spectrum. Thus, with respect to seismic motions, a cratering event may be considered as a contained event buried at a relatively shallow depth of burial. The relatively shallow depth of burial causes the high frequency spectral composition to be considerably reduced and the low frequency composition slightly reduced relative to that of contained detonations.

3. Amplitude and Frequency Characteristics of Elastic Wave Types - the peak vector and peak horizontal particle velocities observed from Schooner and Cabriolet correlate primarily (with two exceptions) with the surface wave time window. An analogous analysis performed for Benham, a contained detonation, does not lead to the same correlation,

for many of the peak particle velocity measurements occur in the P wave window. Insufficient data are available at this time to explain the apparent correlation of peak particle velocity with the surface wave time window as a physical phenomenon distinctly related to cratering detonations; although, it appears possible that the dominant low frequency spectral composition of cratering detonations may selectively enhance the surface wave generating mechanism. Band-pass filter and Fourier amplitude spectrum analysis of wave mode time windows on the radial component showed that the surface wave mode time window contributes the peak amplitude at the lowest dominant frequency (about 0.5 Hz) in all cases except at ETS-2, the S wave mode time window contributes the intermediate particle velocities (at a dominant frequency of about 0.8 - 1.2 Hz), and the P wave mode time window contributes the smallest particle velocities at the highest dominant frequency (about 1.2 - 4.5 Hz) for Schooner. The transfer function for the shallow layered system at Tonopah, Nevada, derived on the basis of the seismograms recorded at Tonopah Motel and Tonopah Church, verifies that the frequency dependent amplification of the layered system is independent of whether the input energy source is a nuclear cratering or a nuclear contained detonation. However, the peak vector particle motions (particle acceleration, displacement, and velocity) observed at Tonopah are significantly lower than the mean value predicted for equivalent yield contained detonations on the basis of Nevada Test Site experience. The lower level of peak particle motions is related to the diminished high frequency spectral composition and to the decreased seismic energy efficiency of cratering detonations, as is summarized below.

4. Seismic Energy Efficiency - the seismic energy efficiency (radiated energy/initial energy available) is significantly lower (about a factor of 0.1) for nuclear cratering detonations than for equivalent yield nuclear contained detonations. The lower seismic energy efficiency means that cratering detonations are significantly less efficient in forming elastic waves in the radiation field, than contained detonations. The lower seismic energy efficiency is related to the shallower depth of burial for cratering detonations.

On the basis of the results obtained for Cabriolet (Klepinger and Mueller, 1969) and for Schooner, the following guidelines seem

reasonable for making ground motion predictions for NTS cratering detonations:

- Preliminary peak vector motion predictions can be based on NTS experience with equivalent yield contained detonations for planning purposes. These predictions will be conservative for the relatively high frequency ground motions, the peak particle accelerations and velocities, and will need to be reduced by a factor which is related to the shallow depth of burial of cratering detonations relative to the standard scaled depth of detonation. The correction for shallow depth of burial is based on a scaling technique developed by Mueller (1969). The ratio of the scaled depth of detonation of the event under consideration to another event (or set of events) at a standard scaled depth of burial is defined as λ. From theoretical considerations, it can be shown that the peak vector particle acceleration needs to be corrected for depth of burial by the multiplicative factor $\lambda^{0.63}$ and the peak vector particle displacement by $\lambda^{0.48}$. The peak vector particle velocity is corrected on the basis of the characteristics of observed band-pass filter spectra. The multiplicative factor applicable at NTS for peak vector velocities is $0.5+0.5\lambda^{0.63}$.

- Spectral (Pseudo Relative Velocity (PSRV) predictions for planning purposes can also be based on NTS experience with equivalent yield contained detonations. These predictions will be conservative at the short period end of the spectrum, unless a correction for the shallow depth of burial of the cratering detonation is incorporated. This frequency dependent correction (Mueller, 1969) yields a multiplicative constant for each frequency. The magnitude of the constant is related to the ratio of the scaled depth of detonation of the event under consideration to another event (or set of events) at a standard scaled depth of burial. For cratering detonations, the correction for shallow depth of burial reduces the level of PSRV at the short period end of the spectrum while leaving the level at the long period end of the spectrum essentially unchanged.

6.2 RECOMMENDATIONS FOR ADDITIONAL WORK

Useful physical insight into the characteristics of ground motion of a nuclear cratering detonation has been obtained by the analyses contained in this report. However, additional data from cratering detonations are required in order to extend significantly the ability to predict accurately the ground motion characteristics of nuclear cratering detonations. Future Plowshare excavation projects (Yawl, Sturtevant, Phaeton, etc.) will provide the basic data needed to achieve this goal.

Specific recommendations of future work include the following:

1. Determine the similarities and differences of the amplitude and frequency characteristics of ground motion from cratering and equivalent parameter contained detonations.

2. Process and compile a representative ground motion data sample for cratering detonations on which to base statistically derived peak amplitude (acceleration, displacement, and velocity) and PSRV prediction equations.

3. Determine the experimental and theoretical correlation between wave modes, peak ground motion, and frequency dependent amplification for cratering detonations.

4. Determine the experimental and theoretical effect of the physical properties of the source medium on factors such as the amplitude and frequency characteristics, seismic energy efficiency, and wave mode generation of cratering detonations.

These activities will significantly improve the physical basis for making predictions of ground motion for future nuclear cratering detonations.

REFERENCES

Berg, Jr., J. W., L. D. Trembly and P. R. Laun (1964); Primary Ground Displacements and Seismic Energy Near the Gnome Explosions, Bull. Seism. Soc. Am.; 54, 1115-1126.

Carder, D. S., W.K. Cloud, L. M. Murphy and J. Hershberger (1958); Surface Motions for an Underground Explosion, Operation PLUMBOB; WT-1530; U. S. Coast & Geodetic Survey.

Carder, D. S., L. M. Murphy, T. H. Pearch, W. V. Mickey and W. K. Cloud (1961); Surface Motions from Underground Explosions, Operation HARDTACK, Phase II; WT-1741; U. S. Coast & Geodetic Survey.

Davis, A. H. and J. R. Murphy (1967); Amplification of Seismic Body Waves by Low-Velocity Surface Layers; Environmental Research Corporation; NVO-1163-130; AEC.

Davis, L. L. (1968); Analysis of Ground Motion and Containment, Sterling Event; VUF-1035, Environmental Research Corporation.

Diment, W. H., S. W. Stewart and J. C. Roller, (1961); Curstal Structure from the Nevada Test Site to Kingman, Arizona, from Seismic and Gravity Observations; Journal of Geophysical Research; Vol. 66, p. 201.

Hannon, W. J., (1964); An Application of the Haskell-Thomson Matrix Method to the Synthesis of the Surface Motion Due to Dilational Waves; Bulletin of the Seismological Society of America; Vol. 54, p. 2067.

Haskell, N. A., (1953); The Dispersion of Surface Waves on Multilayered Media; Bulletin of the Seismological Society of America, Vol. 43, p. 17.

Hays, W. W., (1969); Amplitude and Frequency Characteristics of Elastic Wave Types Generated by the Underground Nuclear Detonation, Boxcar, Bulletin of the Seismological Society of America, Vol. 59, No. 6 (in press).

Hill, D. P. and L. L. Pakiser, (1967); Seismic Refraction Study of Crustal Structure Between the Nevada Test Site and Boise, Idaho; Geological Society of America Bulletin; Vol. 78, p. 685.

REFERENCES
(Continued)

King, K. W., (1969); Ground Motion and Structural Response Instrumentation, Technical Discussions of Off-Site Safety Programs for Underground Nuclear Detonations, U. S. Atomic Energy Commission, Nevada Operations Office, NVO-40, Revision No. 2, Chapter 8.

Klepinger, R. W. and R. A. Mueller, (1969); Analysis of Ground Motion, Cabriolet Event; PNE-958, Environmental Research Corporation.

Latter, A. L., R. E. LeLevier, E. A. Martinelli and W. G. McMillan, (1961a); A Method of Concealing Underground Nuclear Explosions, Journal Geophysical Research, Vol. 66, 943-946.

Latter, A. L., E. A. Martinelli, J. Mathews and W. G. McMillan, (1961b); The effect of Plasticity on Decoupling of Underground Explosions, Journal Geophysical Research; Vol. 66, 2929-2936.

Lowrie, W. R. and W. V. Mickey, (1965); Strong-Motion Seismic Measurements, Project DUGOUT; PNE-605F; U. S. Coast and Geodetic Survey.

Murphy, J. R. and J. A. Lahoud, (1969); "Analysis of Seismic Peak Amplitudes from Underground Nuclear Explosions," Bulletin of the Seismological Society of America, Vol. 59, No. 6 (in press).

Murphy, J. R. and A. H. Davis, (1969); Amplification of Rayleigh Waves in a Surface Layer of Variable Thickness; Environmental Research Corporation; NVO-1163-175; AEC.

Orkild, P. P., (1968); "Report of Exploration Progress, Pahute Mesa-Period July 31, 1966 - January 31, 1968;" U. S. Geological Survey, TID-24290, DTIE.

Perret, W. R., (1963); Free-Field Ground Motion Studies in Granite - Operations Nougat-Shot Hardhat; POR-1803; Sandia Corporation.

Perret, W. R., (1967); Surface Motion Response Spectra, Project Shoal; SC-RR-66-696; Sandia Laboratory.

REFERENCES
(Continued)

Perret, W. R., (1968a); Free-Field Particle Motion from a Nuclear Explosion in Salt, Part I, Project Dribble, Salmon Event; VUP-3012; Sandia Laboratory.

Perret, W. R., (1968b); Shear Waves From a Nuclear Explosion in a Salt Cavity; Bull. Seism. Soc. Am. 58; 2043-2051.

Sharpe, J. A., (1942); The Production of Seismic Waves by Explosion Pressures. I; Theory and Empirical Field Observations, Geophysics 18; 144-154.

Stuart, D. J., J. C. Roller, W. H. Jackson, and G. B. Mangan, (1964); Seismic Propagation Paths, Regional Traveltimes, and Crustal Structure in the Western United States; Geophysics; Vol. 29; p. 178.

Sutton, G. H., W. Mitronovas and P. W. Pomeroy, (1967); Short-Period Seismic Energy Radiation Patterns from Underground Nuclear Explosions and Small-Magnitude Earthquakes; Bull. Seism. Soc. Am. 57; 249-267.

Tewes, H. A., (1969); Memorandum-UOPKG 69-18; To: Schooner Distribution; Subject: Schooner Scientific Reports; Lawrence Radiation Laboratory; K-Division, T-105, L-41.

Trembly, L. D. and J. W. Berg, Jr., (1966); Amplitudes and Energies of Primary Seismic Waves Near the Hardhat, Haymaker, and Shoal Nuclear Explosions; Bull. Seism. Soc. Am. 56; 643-653.

Weart, W. D., (1965); Free-Field Earth Motion and Spalling Measurements in Granite, Project Shoal, VUF-2001; Sandia Corporation.

PROJECT SCHOONER REPORTS

Report No.	Agency	Author	Title
PNE-520	LRL	H. A. Tewes	Schooner Summary
PNE-521	Sandia	L. Vortman	Close-In Air Blast
PNE-522	ERC	W. W. Hays R. A. Mueller C. T. Spiker, Jr.	A Contribution to the Analysis of Seismic Data from Cratering and Contained Events
PNE-523	ESSA/ARL		Weather and Radiation Predictions, Schooner Event
PNE-524	USPHS		Off-Site Surveillance, Schooner Event
PNE-525	REECo		On-Site Radiological Safety, Schooner Event
PNE-526	EG&G	H. Nishita W. A. Rhoads	Ecological and Environmental Effects from Local Fallout from Schooner. 1. Soil Thermoluminescence in Relation to Radiation Exposure Under Field Conditions

DISTRIBUTION LIST
(TID-4500, Category UC-35)

No. Copies	
1	AEC ALBUQUERQUE OPERATIONS OFFICE
1	AEC BETHESDA TECHNICAL LIBRARY
1	AEC DIVISION OF BIOLOGY AND MEDICINE
25	AEC DIVISION OF PEACEFUL NUCLEAR EXPLOSIVES
1	AEC LIBRARY, WASHINGTON
1	AEC MISSION TO THE IAEA
10	AEC NEVADA OPERATIONS OFFICE
1	AEC NEW YORK OPERATIONS OFFICE
1	AEC PATENT OFFICE
5	AEC SAN FRANCISCO OPERATIONS OFFICE
1	AEC SAVANNAH RIVER OPERATIONS OFFICE
1	AEC SCIENTIFIC REPRESENTATIVE, ARGENTINA
1	AEC SCIENTIFIC REPRESENTATIVE, BELGIUM
1	AEC SCIENTIFIC REPRESENTATIVE, ENGLAND
1	AIR FORCE AERO PROPULSION LABORATORY (APE)
1	AIR FORCE AIR UNIVERSITY LIBRARY
1	AIR FORCE INSTITUTE OF TECHNOLOGY
1	AMES LABORATORY (AEC)
1	ARGONNE NATIONAL LABORATORY (AEC)
9	ARMY ABERDEEN PROVING GROUND
1	ARMY CONSTRUCTION ENGINEERING RESEARCH LABORATORY
1	ARMY ELECTRONICS COMMAND
3	ARMY ENGINEER NUCLEAR CRATERING GROUP
6	ARMY ENGINEER WATERWAYS EXPERIMENT STATION
1	ARMY LETTERMAN ARMY INSTITUTE OF RESEARCH
1	ARMY MATERIEL COMMAND
1	ARMY MEDICAL FIELD SERVICE SCHOOL
1	ARMY MEDICAL RESEARCH & DEVELOPMENT COMMAND
1	ARMY MOBILITY EQUIPMENT RESEARCH AND DEVELOPMENT CENTER
1	ARMY OFFICE, CHIEF OF ENGINEERS
1	ARMY PICATINNY ARSENAL
1	ARMY WALTER REED MEDICAL CENTER
1	ATOMIC POWER DEVELOPMENT ASSOCIATES, INC. (AEC)
1	ATOMICS INTERNATIONAL (AEC)
1	AUSTRAL OIL COMPANY (AEC)
2	BATTELLE MEMORIAL INSTITUTE (AEC)
3	BATTELLE-NORTHWEST (AEC)
1	BROOKHAVEN NATIONAL LABORATORY (AEC)
1	BUREAU OF MINES, BARTLESVILLE (INT)
1	BUREAU OF MINES, LARAMIE (INT)
1	CER GEONUCLEAR CORPORATION (AEC)
1	DEPARTMENT OF AGRICULTURE NATIONAL LIBRARY
1	DASA LIVERMORE
1	DASA WASHINGTON
1	DU PONT COMPANY, AIKEN (AEC)
1	DU PONT COMPANY, WILMINGTON (AEC)
1	EBERLINE INSTRUMENT CORPORATION (AEC)
1	EG&G, INC., ALBUQUERQUE (AEC)
1	EG&G, INC., LAS VEGAS (AEC)
5	EL PASO NATURAL GAS COMPANY (AEC)
8	ENVIRONMENTAL RESEARCH CORPORATION (AEC)
1	ENVIRONMENTAL RESEARCH CORPORATION, LAS VEGAS (AEC)
1	ENVIRONMENTAL SCIENCE SERVICES ADMINISTRATION, LAS VEGAS (COMM.)

No. Copies	
1	ENVIRONMENTAL SCIENCE SERVICE ADMINISTRATION, MARYLAND (COMM.)
1	GENERAL DYNAMICS/FORT WORTH (AF)
1	GENERAL ELECTRIC COMPANY, CINCINNATI (AEC)
1	GENERAL ELECTRIC COMPANY, SAN JOSE (AEC)
1	GEOLOGICAL SURVEY, FLAGSTAFF (INT)
1	GEOLOGICAL SURVEY, MENLO PARK (INT)
3	GEOLOGICAL SURVEY, PECORA (INT)
2	GULF GENERAL ATOMIC INCORPORATED (AEC)
2	HOLMES AND NARVER, INC. (AEC)
1	IDAHO NUCLEAR CORPORATION (AEC)
1	INSTITUTE FOR DEFENSE ANALYSIS (ARMY)
1	JET PROPULSION LABORATORY (NASA)
1	JOHN A. BLUME AND ASSOCIATES (AEC)
1	LAWRENCE RADIATION LABORATORY, BERKELEY (AEC)
1	LAWRENCE RADIATION LABORATORY, LIVERMORE (AEC)
1	LIBRARY OF CONGRESS
2	LOS ALAMOS SCIENTIFIC LABORATORY (AEC)
1	LOVELACE FOUNDATION (AEC)
1	MASON AND HANGER-SILAS MASON CO., INC. AMARILLO (AEC)
1	MUTUAL ATOMIC ENERGY LIABILITY UNDERWRITERS (AEC)
1	NASA JOHN F. KENNEDY SPACE CENTER
1	NATIONAL BUREAU OF STANDARDS (COMM.)
1	NAVY ATOMIC ENERGY DIVISION
1	NAVY OFFICE OF NAVAL RESEARCH (CODE 422)
2	NAVY ORDNANCE LABORATORY
1	NAVY POSTGRADUATE SCHOOL
1	NAVY SHIP SYSTEMS COMMAND HEADQUARTERS
2	NUCLEAR ENERGY LIABILITY INSURANCE ASSOCIATION (AEC)
4	OAK RIDGE NATIONAL LABORATORY (AEC)
1	PENNSYLVANIA STATE UNIVERSITY (AEC)
3	PUBLIC HEALTH SERVICE, LAS VEGAS (HEW)
1	PUBLIC HEALTH SERVICE, MONTGOMERY (HEW)
1	PUBLIC HEALTH SERVICE, ROCKVILLE (HEW)
1	PUBLIC HEALTH SERVICE, WINCHESTER (HEW)
1	PUERTO RICO NUCLEAR CENTER (AEC)
1	PURDUE UNIVERSITY (AEC)
1	RADIOPTICS, INC. (AEC)
1	REYNOLDS ELECTRICAL AND ENGINEERING CO. INC. (AEC)
1	SANDIA CORPORATION, LIVERMORE (AEC)
1	SOUTHWEST RESEARCH INSTITUTE (AEC)
1	STANFORD UNIVERSITY (AEC)
1	SYSTEMS, SCIENCE & SOFTWARE (DASA)
1	TEXAS A AND M UNIVERSITY (AEC)
1	TEXAS NUCLEAR CORPORATION (AEC)
1	UNION CARBIDE CORPORATION (ORGDP) (AEC)
2	UNITED NUCLEAR CORPORATION (AEC)
1	UNIVERSITY OF CALIFORNIA, DAVIS, TALLEY (AEC)
1	UNIVERSITY OF ROCHESTER (KAPLON) (AEC)
1	UNIVERSITY OF TENNESSEE (AEC)
1	UNIVERSITY OF UTAH (AEC)
1	UNIVERSITY OF WASHINGTON (AEC)
1	WESTINGHOUSE ELECTRIC CORPORATION, (WAL) (AEC)
27	AEC DIVISION OF TECHNICAL INFORMATION EXTENSION
25	CLEARINGHOUSE FOR FEDERAL SCIENTIFIC AND TECHNICAL INFORMATION